Matériaux pour la Géologie de la Suisse

GEOPHYSIQUE
N° 32

Publiés par la Commission Suisse de Géophysique
Organe de l'Académie Suisse des Sciences Naturelles,
Subventionnée par la Confédération

THE MAGNETOTELLURIC SURVEY OF THE PENNINIC ALPS OF VALAIS

P.-A. Schnegg

ISSN 0253-1186

Imprimeries Centrales Neuchâtel S.A. - CH-2001 Neuchâtel
1998

Editor's preface

The present publication entitled "The Magnetotelluric Survey of the Penninic Alps of Valais" is Report Nr. 32 of the "Contribution to the Geology of Switzerland - Geophysical Series", published by the Swiss Geophysical Commission.
This report is the accomplishment of eight years of work done at the Observatoire Cantonal and at the University of Neuchâtel by many scientists and initiated by the author. It describes the basic principles of the MT method and the specific technique used in the frame of the project. A special attention is paid to the petrography, mineralogy and electrical conductivity of the some rocks encountered in deep sounding available in this region. MT and GDS models in two and three dimensions are presented and a geological interpretation is suggested based on the results of these modelisations.
The Swiss Geophysical Commission is very grateful to Dr. P.-A. Schnegg for having produced this monograph which is an important contribution to the knowledge of the deep structure of the Swiss Alps.
Special thanks are due to the Swiss National Academy of Natural Sciences for its financial support of this publication.

Zurich, August 1998

In the name of the
Swiss Geophysical Commission
The President:

Prof. Emile Klingelé

PREFACE

The magnetotelluric (MT) sounding method was introduced in Switzerland by Prof. Gaston Fischer in the middle of the Seventies. As a new co-director of the Observatoire Cantonal of Neuchâtel, Gaston Fischer was in charge of proposing original geophysical methods as a novel scientific project to replace the then-declining research in astronomy. This was the start of original work in geomagnetism done at our institute. Our group pioneered many "standard" features of the MT technique, bringing substantial contribution to the development of MT in fields such as instrumental design, field practice, basic electromagnetic induction theory, data processing and data modelling. Many MT campaigns have been organised all over the country. However, due to a rather high level of man-made perturbations, very little was published so far. We found much better conditions in foreign countries, where large, less densely populated areas could be studied with our new method. Hence the bulk of our MT surveys was done abroad. But some areas in Switzerland, mainly those resting on lithologies of low resistivity, are still favourable to MT studies. We must point out, however, that this situation is deteriorating with the advent of new dams, more power lines, railways, and the overall increase of electric energy consumption. New acquisition and processing techniques (controlled-source MT, remote reference MT) have been developed to cope with higher levels of cultural noise. We used such techniques. However, they soon appeared to become insufficient. We believe, therefore, that it is urgent to complete the MT survey of Switzerland within the next 15-20 years, otherwise the advantages of the method (complementarity with seismics at reduced cost) will be definitely lost.

An exploratory MT campaign in the lateral valleys of the canton of Valais immediately drew our attention to the anomalous behaviour of the apparent resistivity curves. These curves displayed a pronounced down-going trend at lower periods, instead of the usually observed rise, as seen in the Swiss Molasse basin or in the Jura. At the same time, seismic lines of the National Research Program 20 (PNR/NFP) were made available. Although irreplaceable, seismic information can be helpfully complemented with MT. Knowledge of the electrical resistivity of the rocks at depth permits the removal of some uncertainties about the nature of the reflectors seen in the seismic lines. It was decided to systematically explore all the areas of Valais which were accessible by car (the measuring equipment weights more than 100 kg). To avoid having large sectors without measurements, nine MT sites had to be set up with helicopters.

The author is grateful to Messrs J. Ma, R. Costa, Dipl. phys. A. Jornod, Dipl. geophys. M. Gurk , Dr. W. Stiefelhagen, Dr. N. Smiljanic, Dr. P. Weibel, and Dr. W. Masero for their helpful contribution during the field work; Prof. Dr. M. Burkhard for critical review of the geology and suggestions for geological models; Dipl. geol. C. Lambelet for mineralogical information; Dr. G. Losito for laboratory measurements of rock conductivity; Dr. C. Vitti for S.E.M. images; Dr. P. Glover for comments on the rock conductivities; Prof. Dr. I. Müller for providing VLF instrumentation; Dr. J.-P. Gisiger of Electrowatt AG, for providing access to cores from two boreholes; The Swiss Federal Office of Topography for making maps available; Special thanks to Prof. Dr. G. Fischer who launched the MT research in Switzerland, for numerous fruitful discussions, help during field work and for critical review of the manuscript. This research was carried out as a joint project with the support of the Swiss National Science Foundation (PhD salaries) and the Swiss Geophysical Commission (field expenses).

P.-A. Schnegg
May 1998 - University of Neuchâtel

TABLE OF CONTENTS

SUMMARY

Between 1988 and 1996 the Geomagnetism Group of the Institute of Geology of the University of Neuchâtel acquired magnetotelluric (MT) and geomagnetic depth sounding (GDS) data at 34 sites spread out over the Penninic part of canton Valais. A number of alternative field and laboratory techniques were used to complement at a smaller scale the information gained at depth by the MT and GDS methods. By sampling artificial and natural electromagnetic signals at frequencies ranging from 180'000 to 10^{-3} Hz and carrying out data modelling, a 3D distribution of the electric conductivity of the rocks was obtained, ranging from the surface to depths in excess of 10 km. Soon after the first few soundings, it became obvious that the high-resistive gneiss at the surface were underlain by an extremely good conductor. The following measurements immediately confirmed the presence of a thick dipping conductor and allowed more precise determination of its geometry.

The availability of newly acquired seismic lines right through our MT survey area helped identify the lithology responsible for the enhanced conductivity (Zone Houillère). Fortunately, this layer crops out at the surface, making it possible to check in the laboratory the reality of this remarkable electric behaviour. Electron microscope investigations revealed the mechanism of the electrical conductivity (carbon film at the grain boundaries).

The slope discrepancy between the conducting slab and the seismic reflectors is interpreted as due to a major shear zone dragging the lithological contacts downward to the south. The shear zone itself does not show up as seismic reflector.

The results of the 3D modelling clearly show that the shape of the conducting slab strongly departs from a cylindrical geometry and closely matches the uppermost crustal boundary. The general trend of the conducting body displays the same curvature as the Alpine arc and shows a marked depression matching the large scale geometry of the Rawil saddle and the Insubric backfold.

1. Introduction

From 1988 until 1996 magnetotelluric (MT) and geomagnetic deep sounding (GDS) investigations were conducted in canton Valais within the frame of the projects of the Swiss Geophysical Commission. It appeared very soon that we were faced with a major regional anomaly in the resistivity structure within the Penninic nappe structure. A low resitivity zone was identified over several tens of kilometers of lateral extent, dipping southward in apparent accord with the large scale geometry of the frontal/basal Penninic thrust contact.

From 1986 to 1993, the NRP20 acquired three deep reflection seismic profiles across the Alps of Western Switzerland (Pfiffner et al., 1997). While this survey provided new insight into the crustal geometry at depth, the interpretation of many geometric features such as a major NW-ward dipping reflectors at mid-crustal depths remain controversial. The interpretation of reflectors is hampered by the fact that the deeper reflectors cannot be tied unambiguously with any rocks and structures observed at the earth's surface. The MT method provides an alternative means to constrain geological cross sections, by revealing the conductivity/resistivity rather than seismic velocity contrasts of rock masses. Furthermore, MT soundings are not restricted to 2D profiles, but can be conducted easily to cover large areas in map view. MT soundings have been successfully applied in different geodynamic contexts like subduction zones (Jones, 1993; Winckler et al., 1998), old suture zones (Stanley, 1989), crustal scale shear zones (Mareschal et al., 1995), active collision, crustal extension, (ERCEUGT-Group, 1992).

Our current knowledge of the electrical conductivity structure of the earth's crust is provided essentially by the MT and GDS methods. While many regional anomalies have been identified in various geodynamic contexts, at depths ranging practically from the surface down to the base of the crust, (Jones, 1992; Mareschal et al., 1992; Masero et al., 1997) the reasons for the anomalously high conductivity is not easily identified (Glover and Vine, 1994; Jödicke, 1992). Subtle mineralogical changes, especially their carbon and/or sulphide content, rock texture (mylonite- and cataclasite-lined fault zones), as well as the presence or absence of fluids and/or melts are variously held responsible for lateral variations in the conductivity of the crust. The most prominent high conductivity anomalies are caused by fine grained, carbon rich schists and mylonite zones. Ore minerals, mostly sulphides, can also play an important role. Both carbon and sulphides (and other opaque material) may be a primary cause of high conductivity, or a secondary one when introduced into shear zones during deformation by the advection of mineralizing fluids. The presence of saline fluids or melts are another potential cause, albeit much debated, for high conductivity zones in the middle and lower crust (Jödicke, 1992).

Our study in the Valais Alps is unique because it concerns layers which extend from the earth's surface down to depths in excess of 10 km. This provides the opportunity to study the electric conductivity structure of the upper tier of this young Alpine crust. Excellent outcrop conditions in deeply eroded Alpine valleys together with the fact that the entire nappe sequence has been tilted and eroded during late Alpine folding, we have the possibility to identify the petrographic nature of various rock masses involved. In the present situation, high electrical conductivity could be tied to high carbon contents within metasedimentary rocks of carboniferous age of the Zone Houillère.

This work can be understood as a Swiss contribution to the central segment of the EGT, in the field of the electrical properties of the crust. In their compilation of MT and GDS measurements along the European Geotraverse, the authors (ERCEUGT-Group, 1992) point to the ubiquitous existence of a highly conductive layer in the upper crust. We shall investigate the possibility that this layer might be of the same origin as our conducting slab.

Like many other geophysical techniques, MT and GDS data must be subjected to modelling to extract the geological information. This operation in general proves to be difficult. The reasons for this are: 1) occurrence of non-uniqueness problems, particularly when the signal to noise ratio is poor. This trouble can sometimes be bypassed by using other techniques that constrain the model. 2) lack of computing power. For multidimensional models, computing time increases with a power of the mesh size. The advent of new modelling schemes and of more powerful computers will certainly allow faster and more accurate model determination to be made in the near future. But there is little hope that our successors will be able to collect data of better quality. Current coils and amplifiers already show noise figures smaller than the external cultural noise. Man-made electromagnetic perturbations are likely to increase. This phenomenon has been observed by the author during more than 10 years of field work. We are therefore confident that our data will be subjected to other modelling efforts in the future. Hence, to ease data access for later investigators, we have clearly separated the measured data and their interpretation in the two main Chapters 2 and 3: *Database*, and *Data modelling*. Chapter 4, on the other hand, is devoted to a *Geological interpretation* .

Chapter 2 shows plots of apparent resistivity and phase (MT), and plots of real and imaginary induction arrows (GDS). Results of auxiliary methods are also available: very low frequency (VLF) and laboratory measurements of rock electrical conductivity.

In Chapter 3, the data set is submitted to various modelling schemes, ranging from 1D to 3D. A tentative geological explanation is then proposed in Chapter 4, taking into account that the mineralogy of the conductor is known from our sample analyses.

It appeared very soon that the N30°W axis, which is perpendicular to the Rhone river at the city of Sion, was a preferred direction for the GDS induction vectors and consequently a major structural axis. To ease the construction of the electrical conductivity model we have represented all the maps of this report within the same rotated frame, keeping the origin of the coordinate system constant. The geographic coordinates of the lower-left frame corner are fixed to

Latitude: 45° 42' 39" N Longitude: 7° 14' 49" E

1.1. Geological background

The study area is located in the central Penninic part of the Western Alps, almost entirely in canton Valais, Switzerland (Fig. 1.1). The Rhone valley represents a natural separation between the external, "Helvetic" and internal "Penninic" zone of the Central Alps. Our MT survey is confined to the Penninic domain. The separation between Helvetic and Penninic domains is based on paleogeographic considerations. The Helvetic domain corresponds to the south-eastern edge of the former European continent, and involves a late variscan basement, exposed in the external crystalline massifs (Fig.1.1) . This basement is covered by a sedimentary passive margin series which ranges from Triassic to Oligocene in age. During

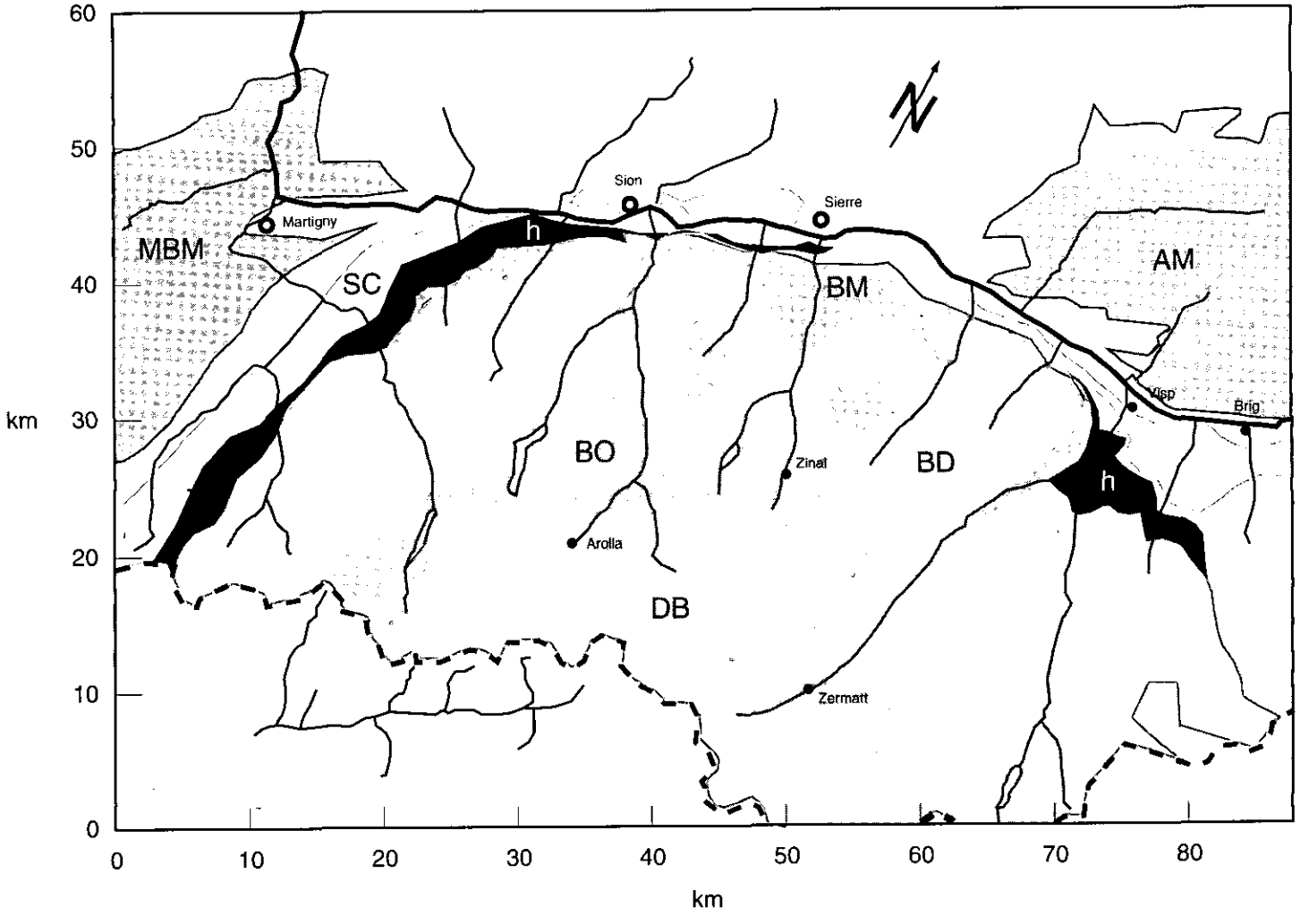

Figure 1.1 Geotectonic map of the studied area. The origin is at 45° 42' 39" N 7° 14' 49" E. The frame is rotated 30° to the W. SC: Sion-Courmayeur zone h: Zone Houillère and Stalden zone BM: Mesozoic of Gd. St-Bernard nappe and Zone houillère BD: Crystalline of Gd. St-Bernard nappe BO: Bündnerschiefer DB: Dent Blanche nappe MBM: Mt. Blanc massif AM: Aar massif

Oligocene Alpine collision, the more internal Helvetic cover series have been detached along shaly horizons (Triassic, Aalenian, lower Cretaceous) and transported tens of km's to the NW, where today they form the famous Helvetic cover nappes (from top to bottom: Wildhorn-, Diablerets- and Morcles nappes). The Penninic zone, on the other hand, consists in a complex stack of basement and cover nappes, which are found tectonically above the highest (ultra)-Helvetic units. In terms of paleogeography, « Penninic » encompass all domains which, during Mesozoic times, occupied the mobile area between "stable" Europe in the north and « stable » Apulia in the south. In other words, the Penninic nappes comprise both oceanic and continental units including a microcontinent named "Briançonnais". From north to south (bottom to top) the most important paleogeographic areas are as follows : Valais ocean, Briançonnais micro-continent, Piemont-Ligurian Ocean (Escher et al., 1997):

1) The lowermost Penninic units of the study area belong to the so-called Sion-Courmayeur zone, made up of mesozoic sedimentary rocks issued from the former Valais ocean. In the older literature, this entire rock suite, dominated by calc-schists, has been called « Bündnerschiefer » in German and « schistes lustrés » in French. Recent investigations have made it possible to identify many individual formations and tectonic sub-units (Jeanbourquin and Burri, 1989) and the term « schistes lustrés » should not be used anymore without adding a tectonic provenance i.e. « schistes lustrés Valaisans ». The limit between Ultrahelvetic and Valaisan (Penninic) is somewhat gradual and depends on interpretations. In any case, the frontal / basal Penninic thrust is decorated by the presence of evaporite series of Triassic age. While anhydrite and gypsum are ubiquitous at the outcrop (a major open pit mine near Sierre), rock salt is also present at depth as documented by an underground mine near Bex.

2) The next higher unit is the « Grand St. Bernard nappe », made up of an intricate stack of basement and cover units, issued from the so-called « Briançonnais » continental domain. Of particular interest to our study is the deepest, northernmost « Zone Houillère ». Its high carbon content, makes this « nappe » a good candidate for a geoelectric anomaly. This unit is characterised by its pre-Triassic basement which comprises a thick metasedimentary series of carboniferous age, rich in coal (anthracite) layers and generally of a dark grey colour due to an abundant carbon pigment. The Zone Houillère, albeit somewhat disrupted by later faults, can be followed laterally over about 200 km SW-ward into the Western Alps, where this zone is punctuated by now abandoned coal mining operations. The rest of the Grand St. Bernard nappe is composed of mostly granitic basement overlain by thick metasedimentary series of Permian to Tertiary age. In terms of electrical conductivity, it is worth mentioning that all these units are either dominated by a quartz-feldspath composition (granites, orthogneiss, metaconglomerates, sandstones) or thick platform carbonate series (Triassic limestones and dolomites). Potential electric conductors such as black shales, or greenschists are not regionally abundant, nor do they form laterally continuous horizons.

3) Units issued from the Liguro-Piemontais Ocean and its border are found today in what is called the Zermatt-Saas Fee Zone and the Nappe du Tsaté. Both units are characterised by the presence of ophiolite series together with calc-schists (« schistes lustrés liguro-piémontais »).

4) The Dent Blanche nappe, riding above the Tsaté nappe is again a continental crystalline basement unit, made up essentially of an orthoseries (gabbro to granite) with only a very minor remnant of sedimentary cover. The Dt. Blanche nappe is thought to be issued from the southern Apulian plate and is therefore correlated with the lower Austroalpine units of eastern Switzerland and Austria.

The present day geometry of the Valais Alps is characterised by a large scale elliptical basin shape, where the highest tectonic unit, the Dt. Blanche nappe is preserved as a Klippe in the

centre. This « basin » is surrounded by dome shaped antiforms on three sides. The south-eastern limit corresponds to a major late Alpine (Oligo-Miocene) « back » fold which runs all along the southern, internal limit of the Central Alps. To the west and north-west, the Penninic nappes of the Valais area are limited by the external crystalline Mt. Blanc-Aiguilles Rouges massif, a huge dome-like antiform which affects all tectonic contacts (Helvetic and Penninic thrusts). Similarly, to the north and north east, the Aar-Gotthard massif forms a natural boundary to the basal Penninic thrust. Note, however, that the Penninic nappes, prior to erosional disruption, had an extension which reached at least 50 km further to the north, as testified by the presence of the prealpine Klippen nappes. The formation of the external crystalline massifs and consequently the basin shape of the Penninic nappes, as well as the external crystalline massive domes is a major late Alpine feature which came into existence during thick skinned thrusting deformations starting in early Miocene, and probably continuing today. While most of the nappe stacking, including backfolding and doming of the external crystalline massifs, can be explained by NW directed convergence and collision between Apulia and Europe, considerable out-of-plane movements and resulting deviations from cylindricity have been recognised. One of the more prominent oblique features within the western Alps is known as the Simplon-Rhone line (Steck et al., 1989). Late Alpine, i.e. mostly Miocene movements along this line, are NE-SW oriented extensions in the Simplon area, with an estimated horizontal extension in excess of 15 km and concomitant exhumation of the Lepontine dome to the east (Mancktelow, 1992). Further west, the Simplon normal fault zone is thought to continue in a SW-NE oriented zone of dextral strike slip, with a total dextral offset of more than 10 km (Burkhard, 1988). Note that the Simplon-Rhone line is not a vertical fault, however; the precise geometry of this zone at depth and its projection below the Penninic nappes of Valais remain uncertain.

1.2. The magnetotelluric and geomagnetic deep sounding methods

Magnetotelluric prospecting is a technique of geophysical exploration that makes use of the natural fluctuations of earth's geomagnetic field, or pulsations, and the induced electric field variations. The small amplitude time variations of the magnetic field arise from magneto-hydrodynamic waves propagating in the magnetosphere. These fields can be measured at the surface of the earth. These electric (sometimes called telluric) and magnetic fields are related to each other by a surface impedance that is a function of the conductivity structure of the earth's substrata.

The tensor relationship between the E (electric) and H (magnetic) fields at any given frequency can be expressed as

$$\begin{bmatrix} Ex \\ Ey \end{bmatrix} = \begin{bmatrix} Zxx & Zxy \\ Zyx & Zyy \end{bmatrix} \begin{bmatrix} Hx \\ Hy \end{bmatrix}$$

where field components along two perpendicular axes have been indicated. This tensor impedance Z, a function of frequency and space coordinates, depends upon the conductivity of the earth in the surrounding area. If the horizontal wavelengths of the incident fields are sufficiently long, Z assumes time and source independence. Hence, Z is a useful measure of the conductivity structure of the earth.

In the simplest case of a homogeneous 1D geological substratum the impedance reduces to a scalar Z

$$Z = \sqrt{\frac{i\omega\mu}{\sigma}}$$

with $\omega=2\pi\nu$, where ν is the frequency, μ and σ the permeability and conductivity of the half space. The resistivity $\rho = 1/\sigma$, the inverse of the conductivity, is in fact more frequently used. A very useful parameter is the so-called skin depth δ, the depth at which the wave is attenuated by a factor 1/e of its surface magnitude:

$$\delta = \sqrt{\frac{2}{\omega\mu\sigma}}$$

The following table illustrates typical investigation depths δ of the method:

ν / ρ	1 Ωm	1000 Ωm
1 Hz	0.5 km	16 km
0.01 Hz	5 km	158 km

Resistivities as low as 1 Ωm are often associated with graphite, sulphides or crustal liquids, sea water or brines. At the other end, high resistivities in excess of 1000 Ωm are found over crystalline basements, shields or dry limestone sediments. The range of resistivity values which have been observed on the earth spans over 8 orders of magnitude.

The available frequency range begins in the audio part of the spectrum (10^4 Hz) and ends up at 10^{-5} Hz (corresponding to periods of 100'000 seconds).

A very common treatment of the earth's conductivity is to consider a horizontally layered structure, where the layers assume constant lateral conductivity. This simplistic representation rarely leads to real models of the earth and must be regarded as a preliminary step. However, it makes possible the creation of initial models which can be used at the beginning of multidimensional approaches. At the surface of the earth the impedance is no longer constant but varies with the frequency of the field. The impedance is a complex number and therefore, somewhat intuitively challenging. The resistivity and phase, two handier parameters are favourcd. Thcy are related to the impedance by

$$\rho_a = \frac{1}{\omega\mu}\left|Z(\omega)\right|^2 \qquad \varphi = Phase\ (Z)$$

The *a* in ρ_a stands for "apparent", since this resistivity is no longer the true resistivity of any material, but the complicated influence of several layers of different resistivities. In MT practice, the sounding results are presented most of the time as plots of the decimal logarithm of ρ_a and of the phase against the decimal logarithm of the period.

The above description gives no indication related to possible azimuthal variation of the parameters. Actually, as long as the geological substratum fulfils perfect 1D geometry, there is no azimuthal variation at all. So any magnetic field component combined with the electric field component measured at right angle should always produce the same value of ρ_a. But this is not likely to occur in the real world. Practically, the magnetic and electric fields are recorded simultaneously along two orthogonal directions which are kept constant during the whole campaign. These directions may be aligned with the surface geology for convenience, but often the north direction is chosen. The resulting impedance matrix Z can be mathematically rotated to maximise the difference between off-diagonal elements Z_{xy} and Z_{yx}.

In ideal 2D cases, the diagonal elements Z_{xx} and Z_{yy} should tend towards zero. This rotation brings the new reference axes in concordance with the geological strike. Unfortunately, static effects may affect the electric voltage measured on one of the lines, or even on both, adding frequency-independent offsets of unknown magnitude. The geological strike is more safely obtained by measuring the vertical component of the magnetic field. This constitutes the principles of the GDS (geomagnetic deep sounding) technique. This kind of data is obtained simultaneously with the MT data, by using a third magnetic field sensor. The vertical component of the inducing magnetic field is close to zero. Moreover, on a 1D substratum, there is no vertical component of the induced magnetic field at all. This is no longer true when the substratum displays significant lateral conductivity variations. The induced H_z field is related to the inducing field by

$$H_z = AH_x + BH_y$$

where A and B are complex functions of the frequency. The real part of these functions are of great interest. They represent the components of induction vectors which point towards more resistive areas of the substratum. Hence their directions, which are less affected by static effects, safely indicate the geological strike (or rather, a direction perpendicular to strike).

As soon as the true geological strike is known, 2D MT fields can be split into two independent modes, TE and TM. In the first mode, the electric currents flow in the strike direction whereas in the TM mode, the currents cross the strike at right angle. Obviously, the apparent resistivity and phase computed for each mode can vary considerably with the site location. Generally, the results of a full MT and GDS campaign are presented as curves of the apparent resistivity and phase, and surface plots of the induction arrows. The modelling work consists in looking for simple, geometric distributions of conductive and resistive blocks. The calculated responses of the model must fit the measured curves and plots within a given accuracy.

The reader who is willing to go deeper into the knowledge of the MT/GDS methods can read a compilation of basic articles edited by K. Vozoff (Vozoff, 1986).

1.3. Very low frequency (VLF) sounding method

A small fraction of the field work was spent deploying alternate techniques, namely VLF (a radiofrequency variation of MT). There is no difference of principle between VLF and MT. Here however, the data quality relies on the existence of powerful public radio transmitters. Their transmitting frequency (VLF: very-low-frequency) must cover a band of 1-2 decades so that enough depth span can be studied (Actually, the original classification of the electromagnetic spectrum allocates to VLF frequencies between 3 and 30 kHz). As dictated by the relationship linking the skin depth to the frequency, only targets a few tens of meters deep can be detected. Moreover, the method is limited to scalar impedance since the signal of only one transmitter can be used at a time.

1.4. Electrical conductivity of rock samples

Selected rock samples from two boreholes have been measured for electrical conductivity. Small rock cylinders are cut from 3-inch cores. Their electrical conductivity is measured under simulated physical conditions:

Temperature : 20° to 150°C;
Hydrostatic pressure : 9 to 39 MPa;
Internal fluid pressure : 3 to 33 MPa;
Frequency of the electric current : 0.005 to 200 Hz

Due to the small original size (3" diameter) of the available samples, the 2-electrode set-up was used on two short cylinders, whereas the more accurate 4-electrode set-up was used on a larger one.

2. Database

Because data modelling methods and computers are continuously improving, it was decided to make a sharp separation between the part which regards the measured data (this Chapter) and the effectively somewhat subjective part describing its use in the construction of geological models (Chapter 3). We think that drawing a very clear dividing line between these two research aspects can ease the task of investigators who, in the future, may attempt new data modelling of our database. Tables of the original data can be found in the Appendix. The impedances and induction coefficients are given in the measuring axes and have been corrected for instrumental response.

2.1. Practical aspects of data acquisition

Choosing a convenient site to perform MT/GDS soundings requires some experience. Inhabited areas and power lines must be kept at least 2-3 km away. Distance to railway lines should be even larger, particularly for DC trains. We have observed perturbing fields from such trains at distances up to 30 km. This range strongly depends on the ground conductivity, however. In areas where the cover shows a low resistivity (e.g. 5 Ωm, Po Valley near Ferrara), the critical distance reduces to a few km. In the Swiss Alps, the main cultural noise source is caused by the activity related to the electric power production. During the night, an additional noise source is generated by the pumps used to fill the water reservoirs. The AC trains did not significantly perturb our soundings, except in the area of the Simplon pass, the Lötchental and in the Rhone valley. This was not the case in the mountains which constitute the border between the cantons of Valais and Berne. The culprit is the DC train network of the MOB (Montreux-Bernese Oberland). DC current leakage prevented us from carrying out MT soundings in the whole area, even when the trains were not running since the line voltage could never be switched off.

Besides the concern for electrical noise, a good MT site must be protected against weather effects like wind and direct heat from the sun. It must be set-up at least 200 m away from a road, since trucks would generate noticeable variations of the magnetic field at shorter distances.

MT /GDS sites can be completely installed in some 90 minutes, making possible 3-site set-ups a day. The simultaneous operation of several MT acquisition sites is a known technique used to minimise the effect of noise, particularly the part of it which shows no geographic correlation from one site to the other. The method is dubbed *Remote reference MT*. The equipment required for 3 stations can be easily transported in a 4x4 van along with a crew of 3. Fig. 2.1 shows an MT/GDS set-up. Three magnetic sensors and three current electrodes constitute the EM field probes. The electric field sensors are Ag-AgCl electrodes designed for ocean studies (Filloux, 1973). We have fitted them for use in field work on dry ground. A Plexiglas tube terminated with a porous tip and filled with a 28 g/l NaCl solution houses the electrode (Fig. 2.2). The electrodes are driven into the earth in 30-cm holes filled with salted bentonite mud. Electrode separation is generally set to 48 m, but can vary between 15 and 100 m, according to the level of man-made perturbations and to soil resistance. One local electrode acts as a signal reference. Two other electrodes are used at the N and E ends of the dipoles, usually to magnetic north and east of the local electrode. Sometimes, depending on space availability in the field, the orthogonal dipole system must be rotated.

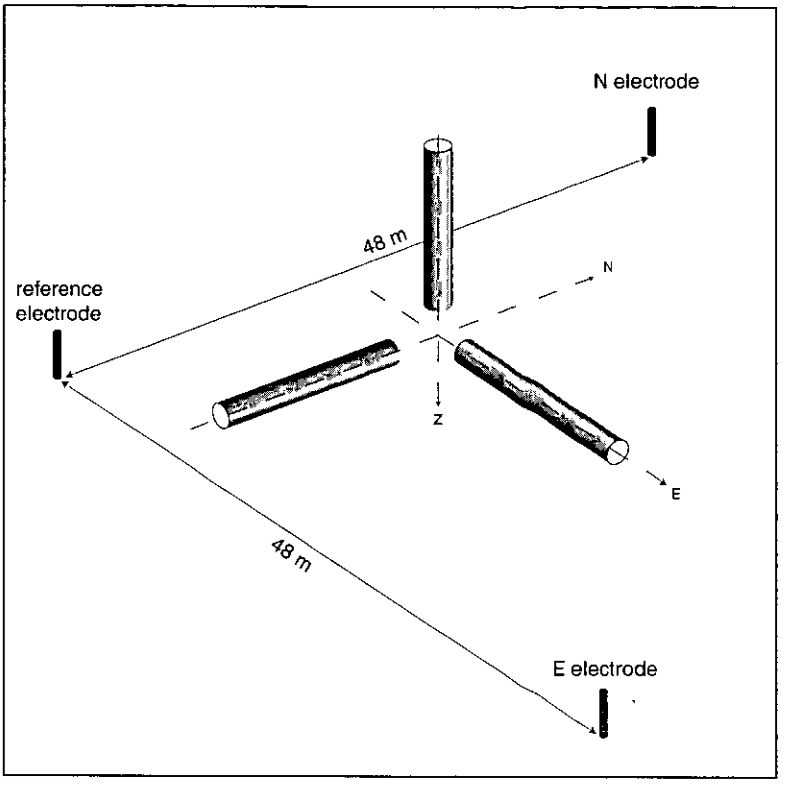

Fig. 2.1 Magnetotelluric set-up showing three induction coils aligned toward the north, the east and vertically. The electric field is measured as potential differences between electrode pairs, using a single electrode as reference.

Ten meters away from the local electrode a flat area is selected for the magnetic sensor set-up. These sensors are CM11E iron-core induction coils built by ECA, Paris (Andricux et al., 1974). Two of them are laid horizontally on the ground in the N and E directions, i.e., parallel to the telluric lines. They are held firmly on the ground by two stands equipped with 10-cm aluminium spikes. The third coil is maintained vertically in a 50 cm-deep hole dug into the earth. All the sensors connect to a datalogger hosted in a water-resistant box located near the local electrode. An accurate clock provides the signals required for synchronisation of several stations within 0.1 s per day. A block diagram of the amplifier/filters is given in Fig. 2.3.

Uninterrupted time series of the 5 components E_x, E_y, H_x, H_y and H_z were sampled at a frequency of 2 Hz during 24 hours. Some recordings have been repeated to secure the data when problems were suspected. When the time schedule permitted, we tried to start the data acquisition in 2-3 sites at the same time, which made it possible to process the data with the 'remote reference' method. Table 2.1 shows the listing of the MT/GDS sites (see Fig. 2.4 for site location). Not all the sites gave useful results. This was due, sometimes, to excessive cultural noise (LOE, SIM, PFY), or site disturbance by animals (DON). At site GAS, only 3 components of the magnetic field were measured, due to the lack of space to deploy the telluric lines in a steep forest. Sites PRA and SAL located in the Val Ferret, are likely to display large effects caused by the nearby DC railway of Martigny-Châtelard. At site MAU, finally, only the magnetic field data was found of sufficiently good quality.

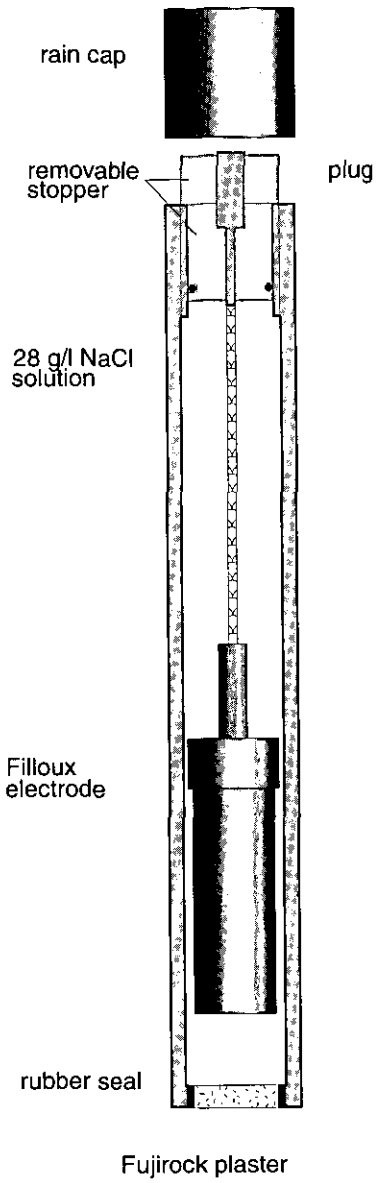

Figure 2.2 Unpolarisable Ag-AgCl telluric electrode with plexiglas housing and porous tip. Overall length with weather cap: 32 cm.

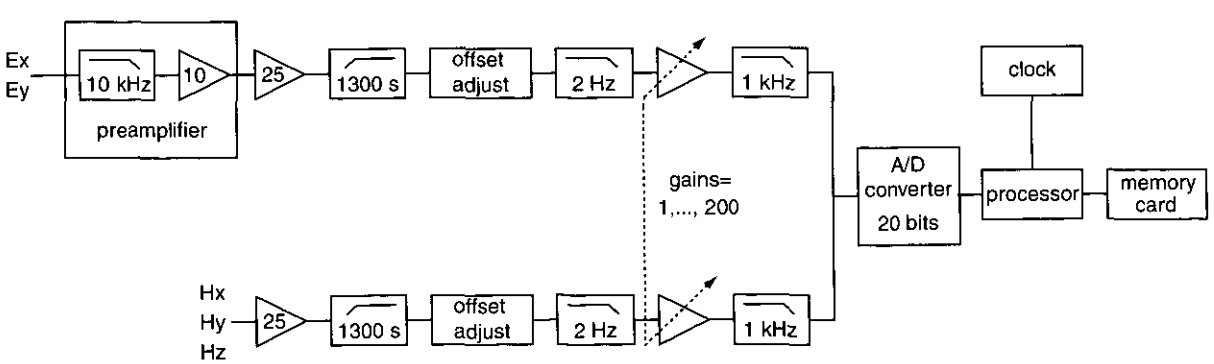

Figure 2.3 Block diagram of the MT/GDS data acquisition system

Nr	Date	Abbr.	East m	North m	X rel. km	Y rel. km	Elevation m	Site name	Data avail. gds/both	Telluric azimuth	Remote ref. with site Nr
1	08.06.88	ZIN	614'890	106'780	48.27	23.84	1723	Zinal	both	0	
2	09.06.88	BOS	619'960	115'370	56.96	28.74	1901	Turtmanntal	both	0	
3	10.06.88	LOE	632'190	142'770	81.25	46.36	1788	Loetschental	-	0	
4	20.09.88	MOY	610'790	105'890	44.28	25.12	2350	Moiry	both	0	
5	21.09.88	MAU	592'800	92'910	22.21	22.87	2420	Mauvoisin	gds	0	
6	22.09.88	CLE	589'990	109'060	27.85	38.26	1989	Cleuson	both	0	
7	02.08.90	TRI	594'900	107'745	31.44	34.67	2282	Combe de la Rosette	both	0	8
8	02.08.90	LOU	605'397	113'295	43.31	34.23	2700	Louché	both	0	7
9	02.08.90	DON	594'620	130'030	42.34	54.11	2400	Donin	-	0	
10	06.08.91	ARO	600'770	96'000	30.66	21.56	2500	Montagne d'Arolla	both	0	11
11	06.09.91	OLE	590'100	100'920	23.88	31.16	2420	Louvie	both	0	10
12	30.09.92	TOU	615'410	116'200	53.43	31.74	2507	Tsa du Touno	both	0	13
13	30.09.92	LUS	600'680	105'000	35.08	29.40	2205	La Luesse	both	0	12
14	06.09.93	COL	604'030	94'730	32.84	18.83	2070	Les Collons	both	0	
15	06.09.93	FER	608'790	99'880	39.54	20.91	1960	Ferpècle	both	0	
16	07.09.93	DIX	596'530	99'560	28.76	26.76	2400	Dixence	both	30	
17	07.09.93	NOU	600'710	107'100	36.15	31.20	2310	La Nouva	both	0	
18	06.09.94	VER	584'260	108'025	22.37	40.23	2140	Verbier	gds	34	
19	07.09.94	MAV	594'090	88'310	21.03	18.24	2015	Sud Mauvoisin	both	30	
20	09.09.94	PRA	574'790	88'760	4.54	28.28	1609	Prayon	gds	0	
21	09.09.94	SAL	574'720	92'500	6.35	31.55	1265	Saleina	gds	40	
22	05.09.95	ZER	618'260	94'630	45.12	11.63	2218	Zermatt	both	0	23
23	05.09.95	TAS	629'340	100'210	57.50	10.92	2218	Täschalp	both	15	22
24	06.09.95	BUR	631'290	124'280	71.23	30.79	1780	Bürchen	both	0	25
25	06.09.95	GAS	629'650	113'440	64.39	22.23	1680	Gasenried	gds	0	24
26	11.09.95	NAN	640'810	117'990	76.33	20.59	2250	Nanztal	both	0	27
27	11.09.95	NES	642'520	122'780	80.20	23.88	2470	Nesseltal	both	0	26
28	12.09.95	SIM	646'660	116'860	80.83	16.68	1600	Simplon	gds	0	
29	12.09.95	PFY	612'000	127'800	56.28	43.49	564	Pfyn	-	0	
30	04.06.96	MAS	601'000	116'800	41.25	39.46	1840	Mase	both	0	31
31	04.06.96	REC	605'575	118'725	46.18	38.84	1580	Réchy	both	0	30
32	09.10.96	THO	594'380	75'820	15.03	7.28	1095	Thoules	both	0	33
33	09.10.96	BAR	589'280	80'050	12.73	13.49	1580	Barlia	both	0	32
34	09.10.96	OYA	596'890	78'790	18.69	8.60	1538	Oyace	gds	0	
Origin & rotation angle:			585'000	62'000	30						

Table 2.1 MT / GDS sites listed in the chronologic order. Columns 4 and 5 give site coordinates in the Swiss system. Columns 6 and 7 are coordinates in a rotated (30 ° counter-clockwise) system with lower-left corner at 585 /62 km. Column 10 shows the data availability: gds=only GDS data, both=both MT & GDS. Column 11 gives the azimuth of telluric line 1 in the experimental set-up. Column 12 indicates station Nr available for remote reference processing.

A typical example of time series recorded simultaneously at two remote sites is shown in Fig. 2.5. The sites are located 18 km apart. This figure illustrates the fact that the horizontal magnetic field is laterally homogeneous over large distances, whereas H_z and the telluric fields are quite dependent on the geological substratum.

The geological information contained in the time series is completely contained in the tensor impedance Z (see Chap. 1), which, in the frequency domain, links temporal variations of the electric and magnetic fields. The evaluation of Z was done with the technique of the robust transfer function estimation pioneered by Egbert (Egbert and Booker, 1986). The principle invoked in this method relies on the observation that outlying data generally obey a different statistics than the normally distributed data. The method gives satisfactory results even in the presence of short segments of bad data, but cannot improve significantly soundings severely affected by noise. This scheme can be applied to data from 'remote reference' site pairs with additional improvement. The induction vectors can be obtained in the same programme run, but we preferred to use our own technique which gives additional points at longer periods.

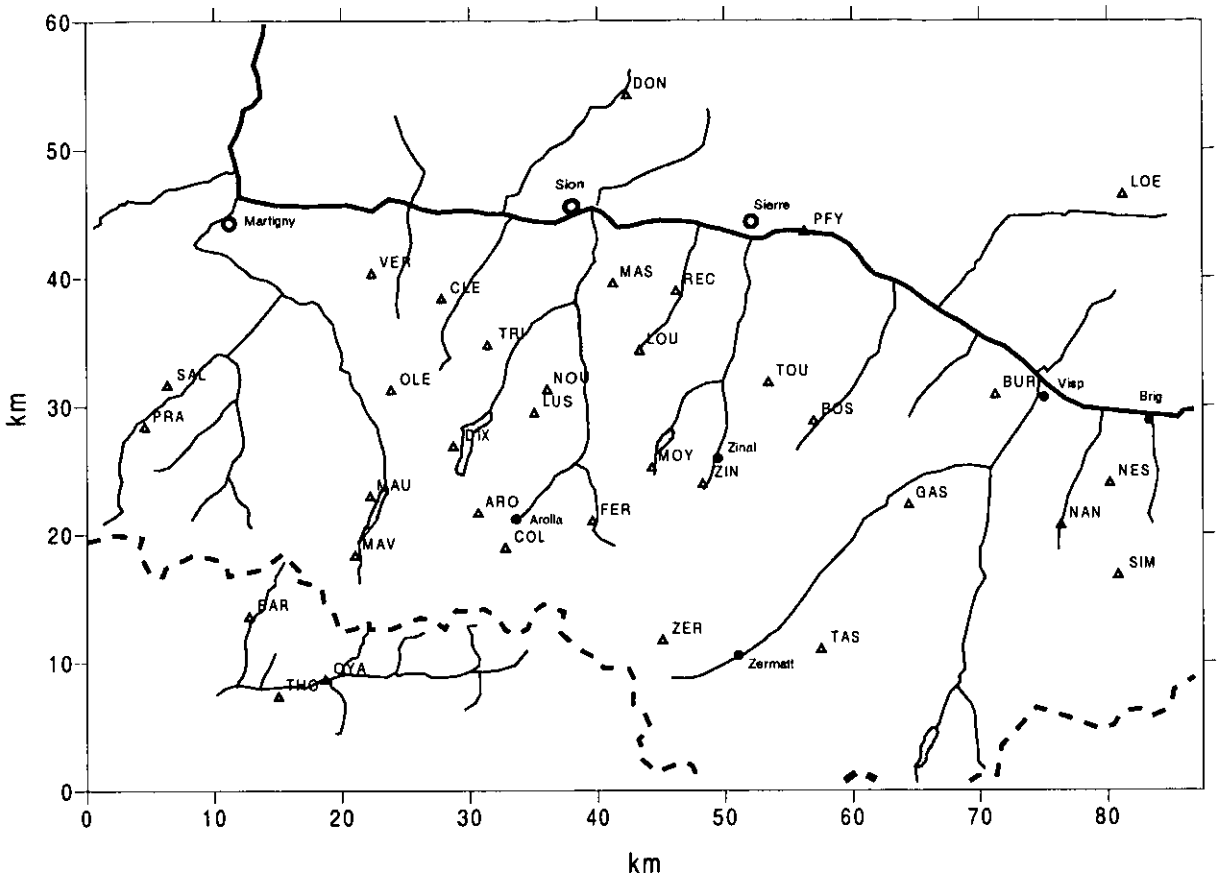

Figure 2.4 Magnetotelluric and GDS site location

2.2. Uninterpreted results

2.2.1. GDS and MT

Plots of the real and imaginary parts of the vertical magnetic field induction coefficients (induction arrows) are shown in Fig. 2.6 as functions of the logarithms of the periods. The axes of the figure are orientated N-S and E-W. A spatial representation of the arrows is shown in Fig. 2.7 at six periods (here the axes are NNW-SSE). Concentrating on the real part of the induction coefficients (the imaginary part is of little use because of its low, error prone level) we observe a homogeneous and constant distribution of the arrow directions over periods and locations. Induction arrows point in directions opposite to good-conducting regions. Thus, we can readily deduce from this that a conducting body must be plunging toward the SSE (in the Fig. 2.7 axes). The homogeneity of the arrow directions with lateral distance indicates that the shape of the body can be approximated by an elongated 2D prism of cylindrical symmetry. Obviously, a few sites (SAL, PRA, VER, only Fig. 2.6) indicate opposite directions. This is not surprising since these sites are located on the NW edge of the conducting body. For these sites, it is not clear whether some part of the vertical magnetic field originates from the nearby DC railway (Martigny-Châtelard line).

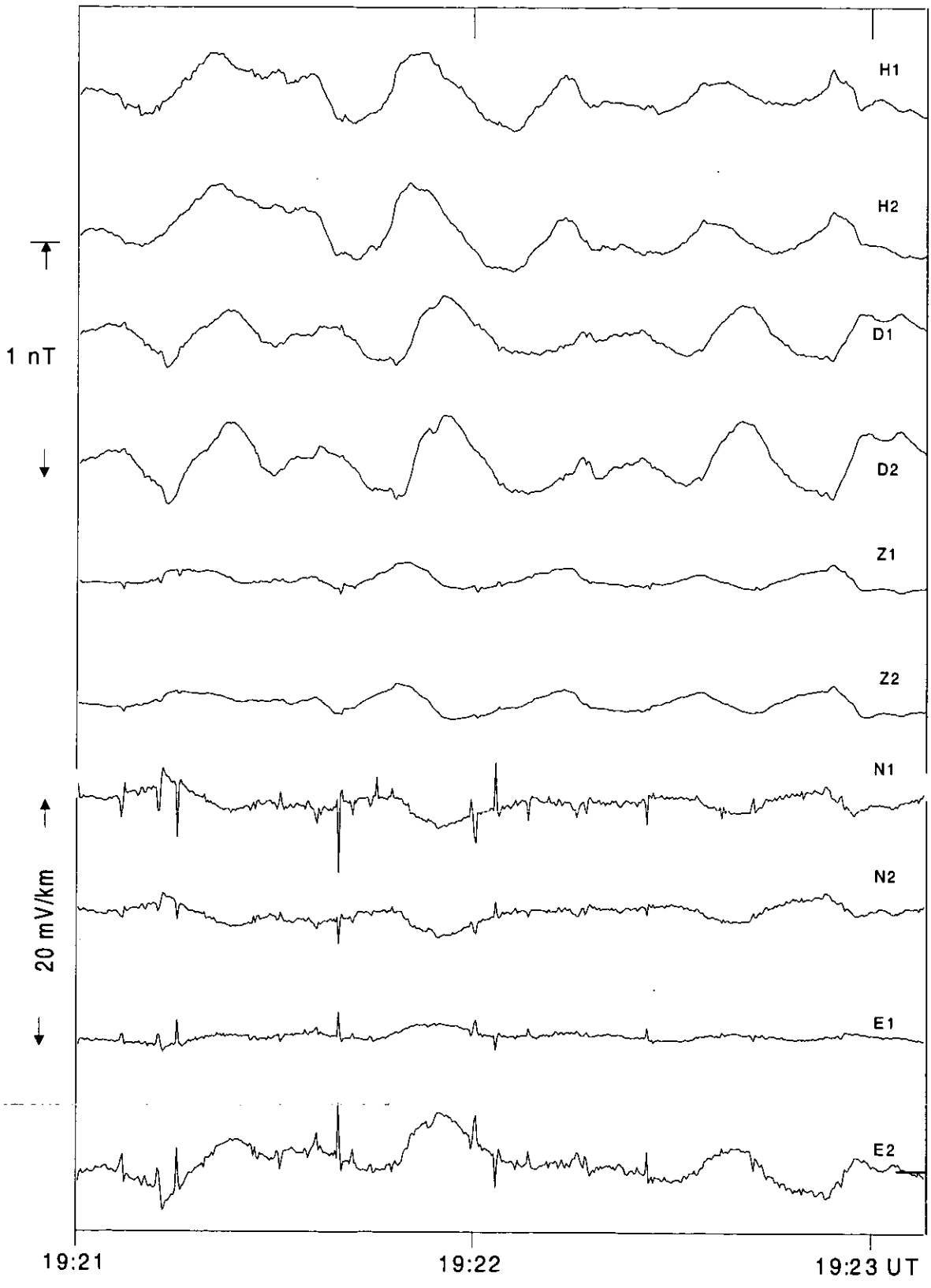

Fig. 2.5 Magnetic and telluric signals, simultaneously recorded at sites TOU (1) and LUS (2) in the interval 19:21-19:23 UT on 30 September 1992. H, D, Z components refer to magnetic north, east and vertical respectively, whereas N and E components refer to north and east telluric fields.

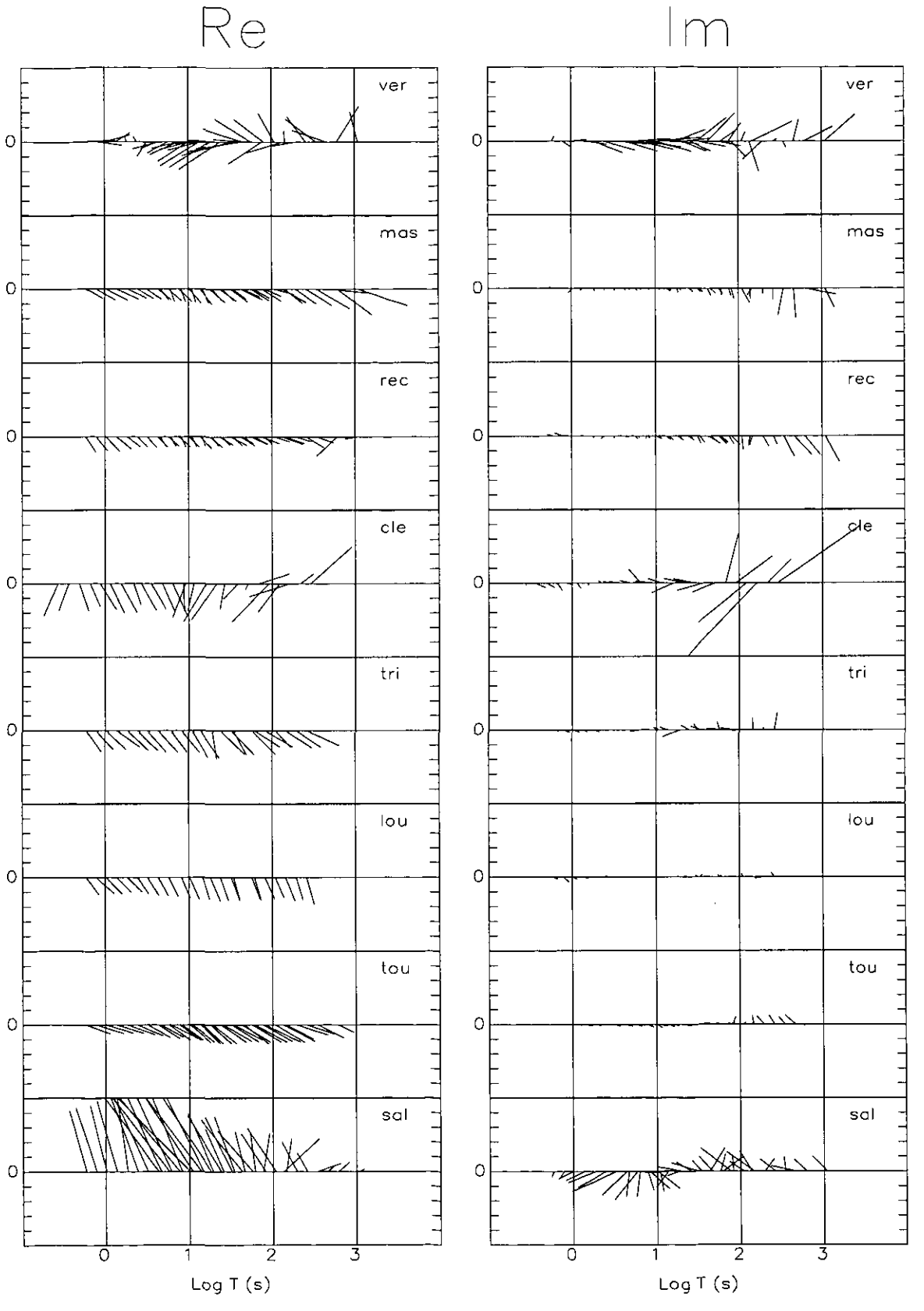

Figure 2.6 Measured induction arrows vs. signal period

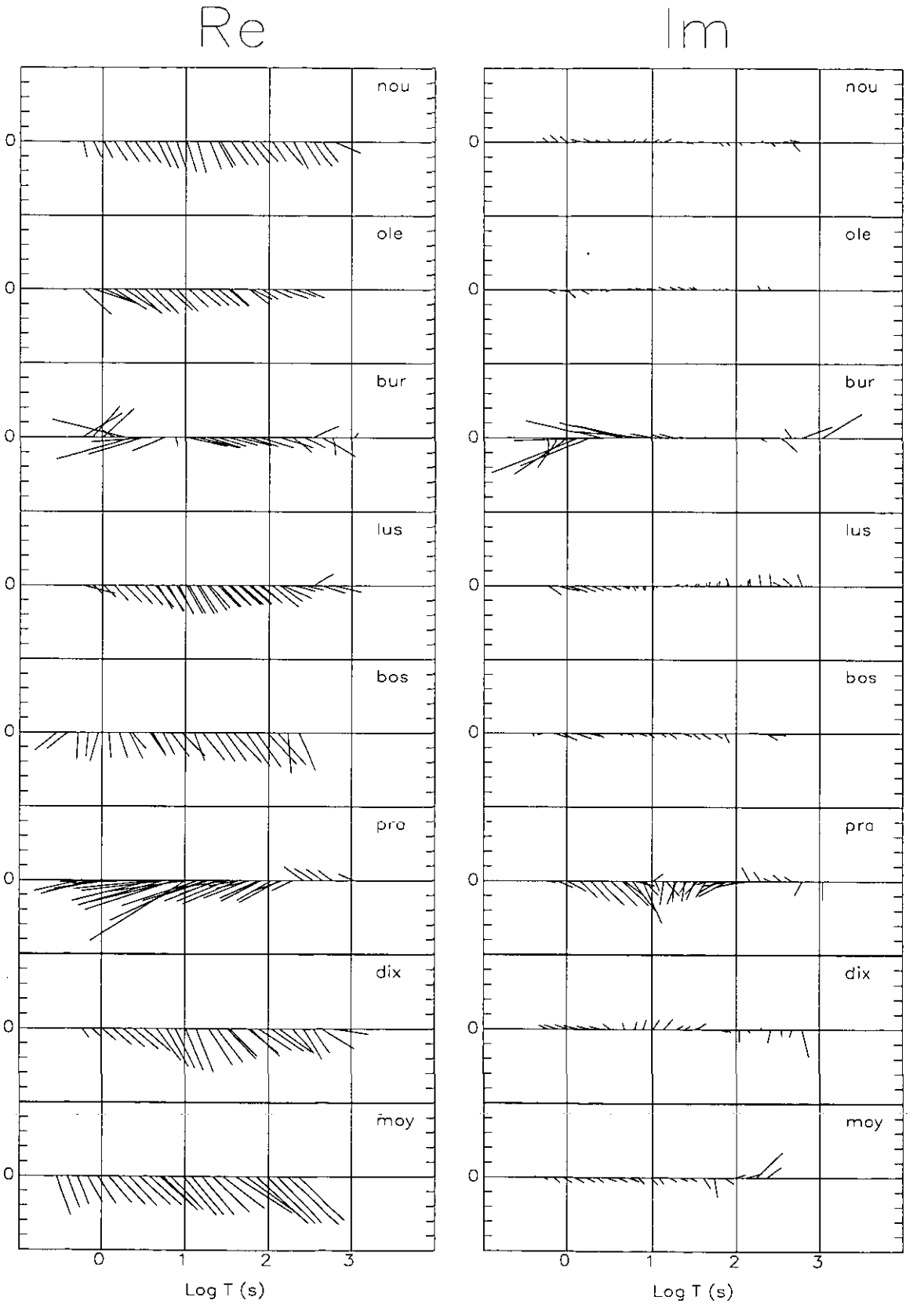

Figure 2.6 (cont.): Measured induction arrows vs. signal period

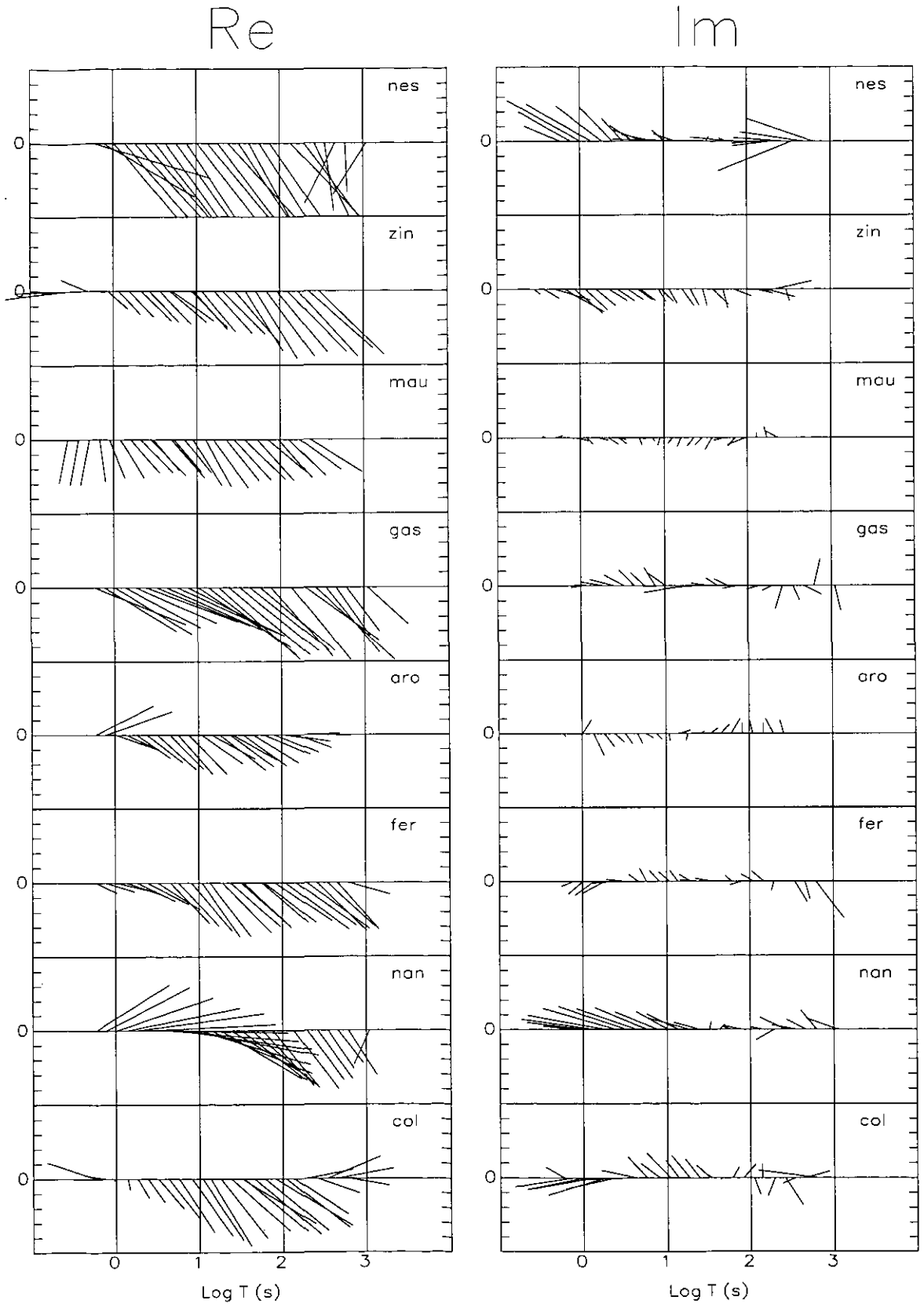

Figure 2.6 (cont.): Measured induction arrows vs. signal period

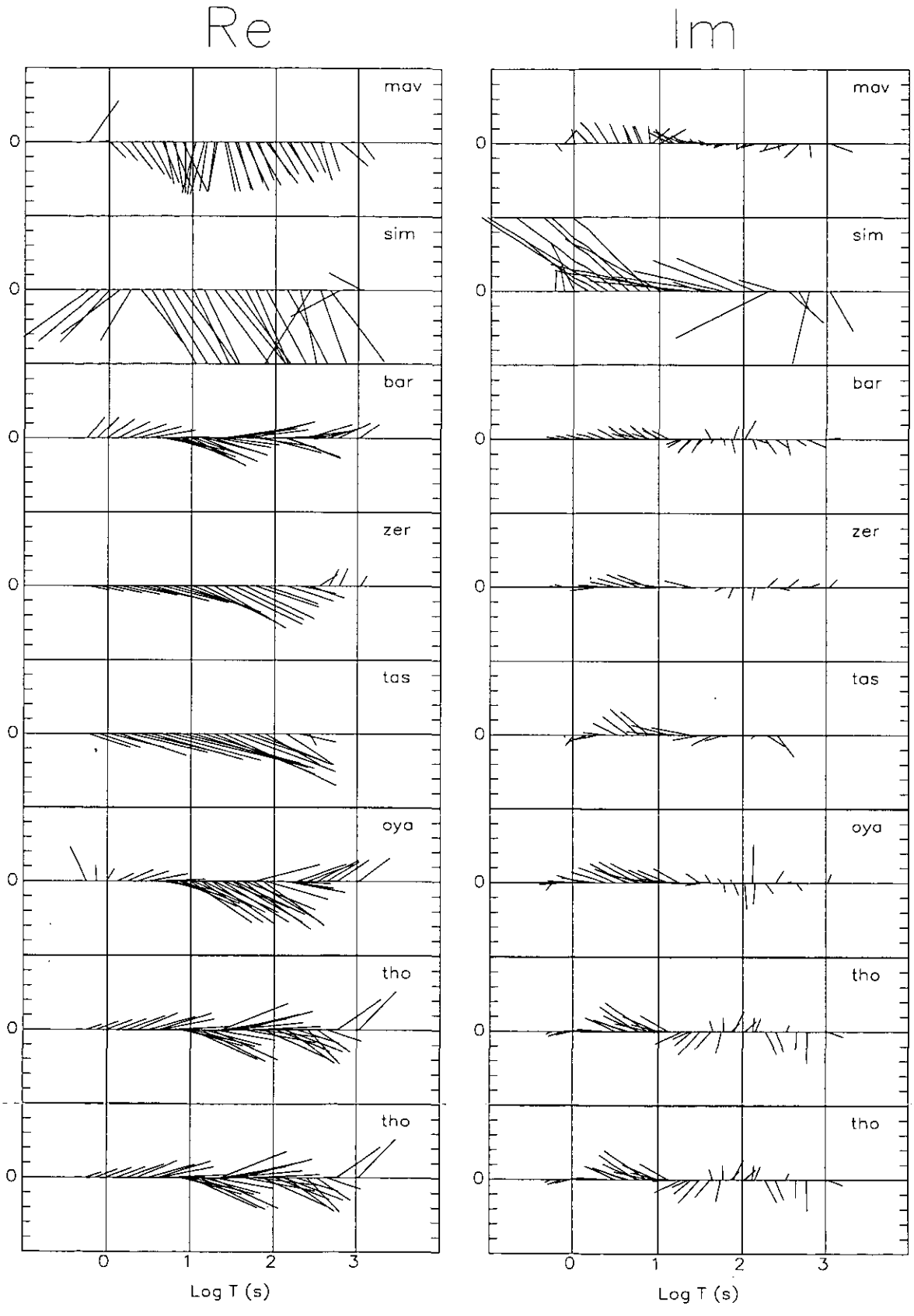

Figure 2.6 (end): Measured induction arrows vs. signal period

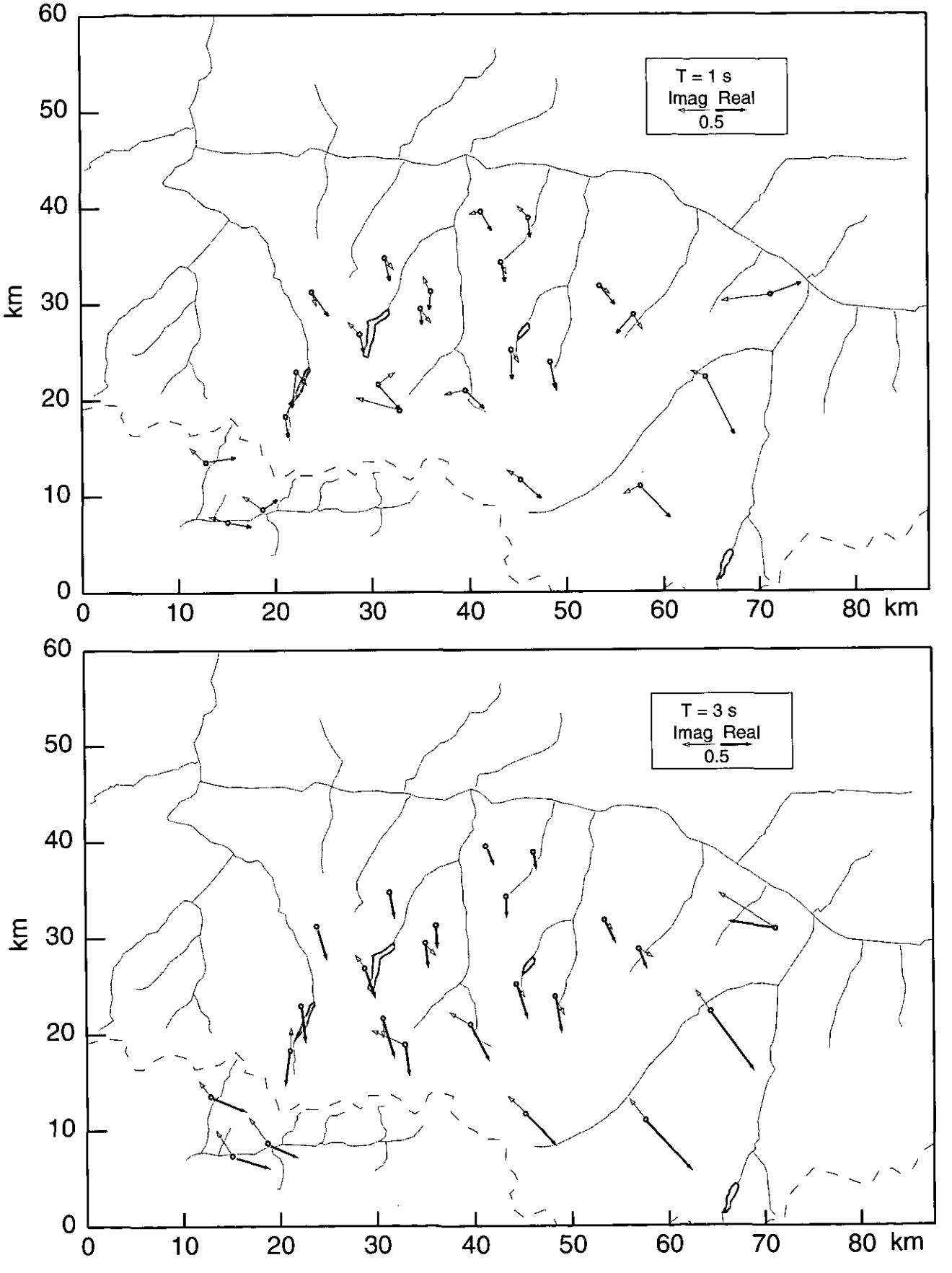

Figure 2.7 Measured real and imaginary induction arrows at 2 periods

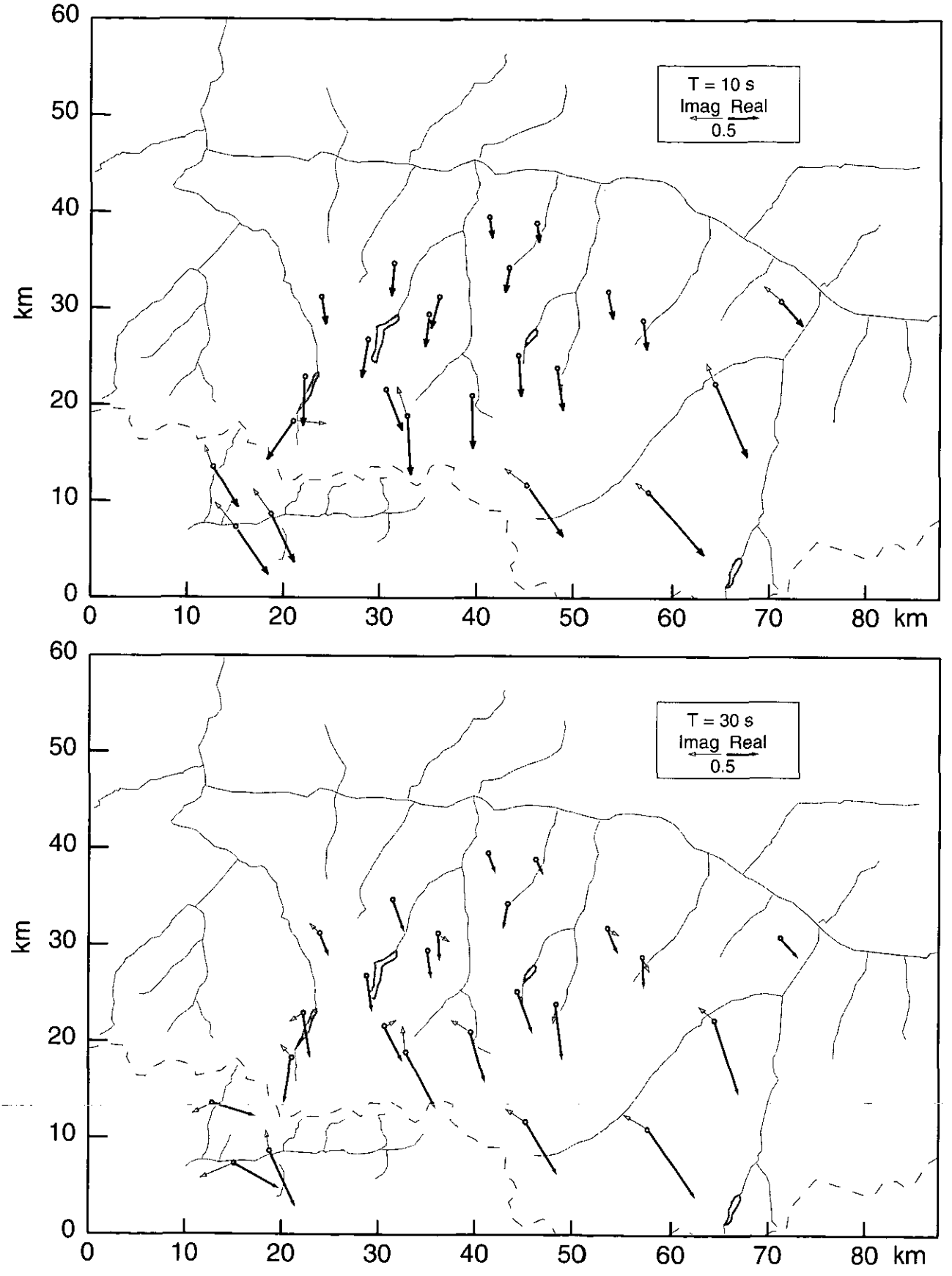

Figure 2.7 (cont.) Measured real and imaginary induction arrows at 2 periods

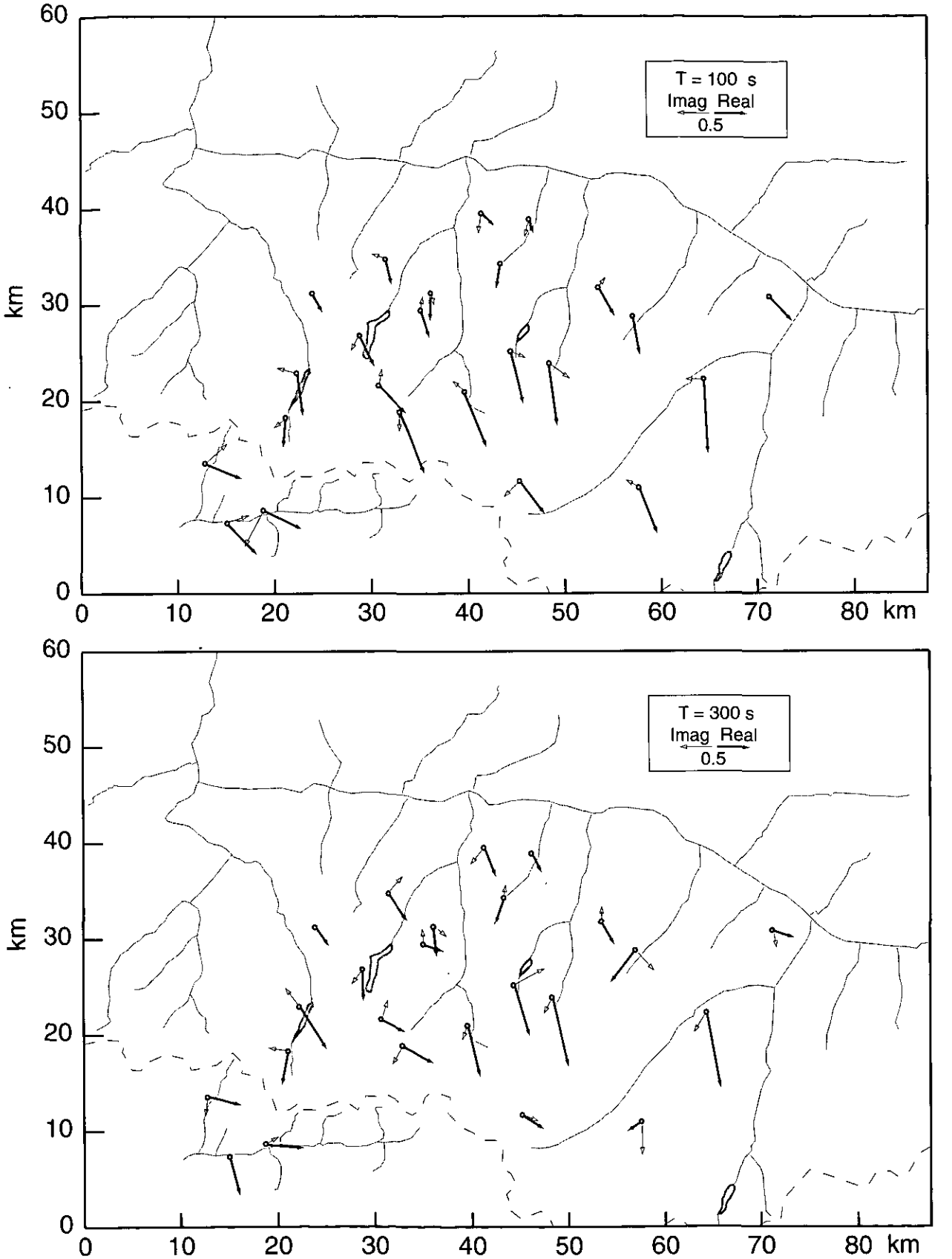

Figure 2.7 (end) Measured real and imaginary induction arrows at 2 periods

As was said in Chapter 1, the magnetotelluric impedance is not a convenient parameter for the final display of MT results. Plots of the apparent resistivity and phase must be preferred. Before computing these parameters, the measuring axes are rotated into the average direction (N30°E) suggested by the induction arrows. A rotation by a fixed angle makes sense here, since obviously the GDS data indicate a strong regional trend. Fig. 2.8 shows the apparent resistivity and phase computed for the major Z_{xy} and minor Z_{yx} axes of the rotated impedance tensor.

2.2.2 Very low frequency (VLF)

Soon after the beginning of the MT and GDS campaigns, it appeared clearly that a conducting body was plunging in the direction of the SSE. In the opposite direction, probability was high that the body would crop out at the surface. Proof of this was brought by the conductivity measurements of cores sampled in two nearby boreholes. VLF profiles have been conducted in the neighbourhood of one of the boreholes, where the surface geology indicated the presence of carbon in the rocks at the surface. The method has a limited depth of investigation of a few tens of meters. However, provided there is no strong lateral variation of the conductivity, the results of VLF are very reliable, since they suffer little from man-made perturbations. Three profiles about 500 m long have been measured, using each time the signals of three public radio transmitters at 183, 77.5 and 12.1 kHz. The results of these soundings are given in the form of apparent resistivity and phase as functions of the profile distance (Fig. 2.9).

2.2.3. Electrical conductivity of rock samples

We were given access to the drill core collection from two boreholes located 4-5 km to the north of Verbier, on the NE flank of the Pierre Avoi peak. Both boreholes are drilled into the Zone Houillère.

Borehole	Abbr.	Coordinates	Elevation	Sample depth	Total Depth
Les Etablons	CH5	584'209/108'481	2048	318 m	400 m
Som de Pro window	SOM7	583'066/110'186	1457	31.5 m	199 m

The two rock samples analysed were chosen according to their dark colour, suggesting elevated carbon content. Both are dense, black, fine-grained, slightly silty slates. The mineralogy is dominated by quartz and various sheet silicates (illite, muscovite, chlorite). The rock texture is characterised by an extremely well developed slaty cleavage or rather schistosity. Locally, this first schistosity is affected by a second and third phase of crenulation cleavage, almost absent in our test samples, however. Because conductivity measurement require cylindrical samples of 40 mm diameter and length, it proved difficult to cut the original 3" drill core cylinders into crack-free consolidated samples, particularly in the direction of the schistosity. The sample machining and measurement was performed at the rock physics laboratory of the University of Florence, Italy. Due to their small length, two samples were measured in the 2-electrode configuration (using same electrodes for current injection and potential measurement). A third sample was measured with 4 electrodes, but there was not noticeable improvement. An automatic measurement programme performs successive runs, varying temperature and hydrostatic pressure. The results of these tests are shown in Fig. 2.10. From the SOM7 graph, we see that the electrical resistivity of the rock is very low (0.6 Ωm), a value that can only be obtained in the presence of good electrical

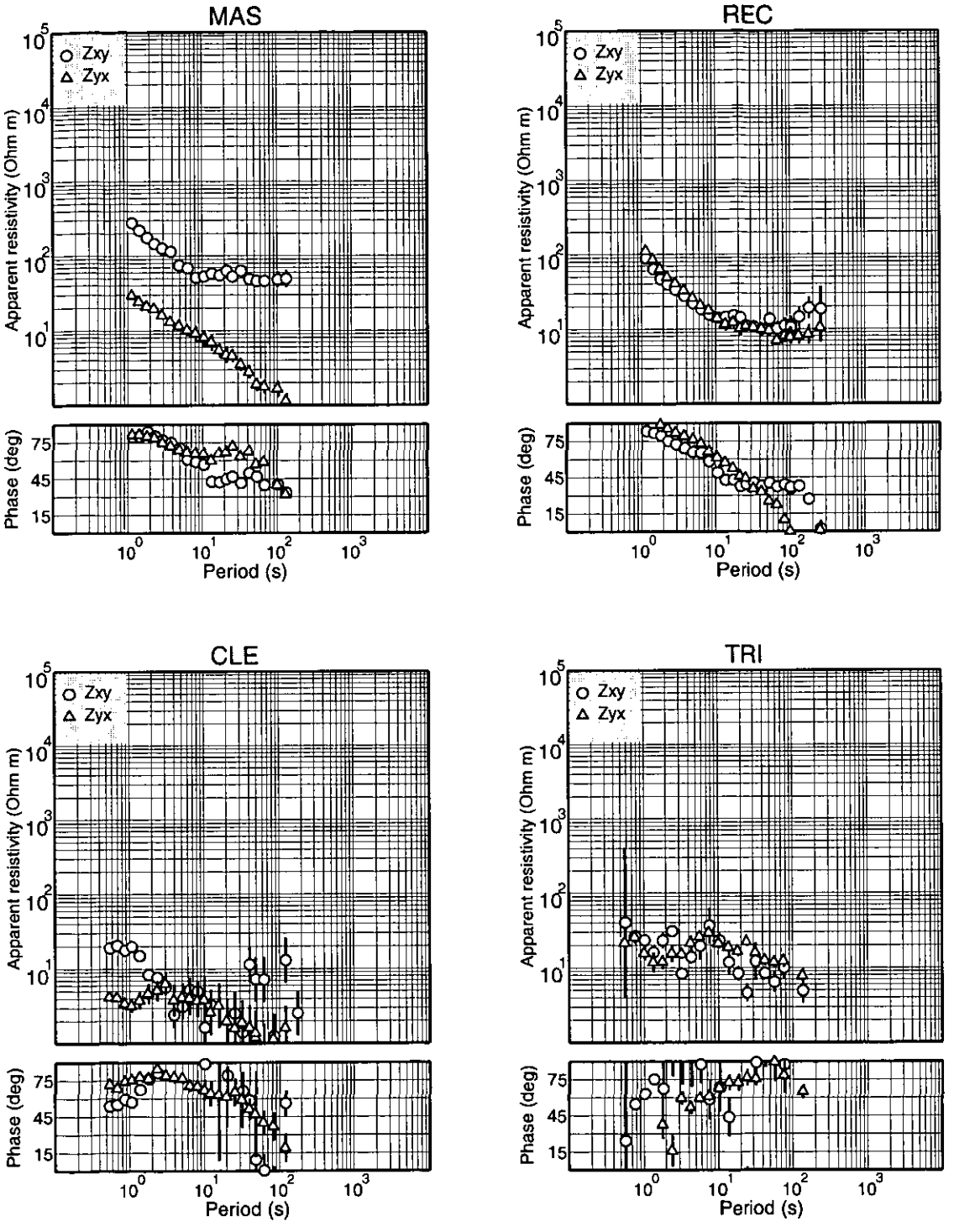

Figure 2.8 Apparent resistivity and phase computed for the rotated (30° West of N) impedance tensor.

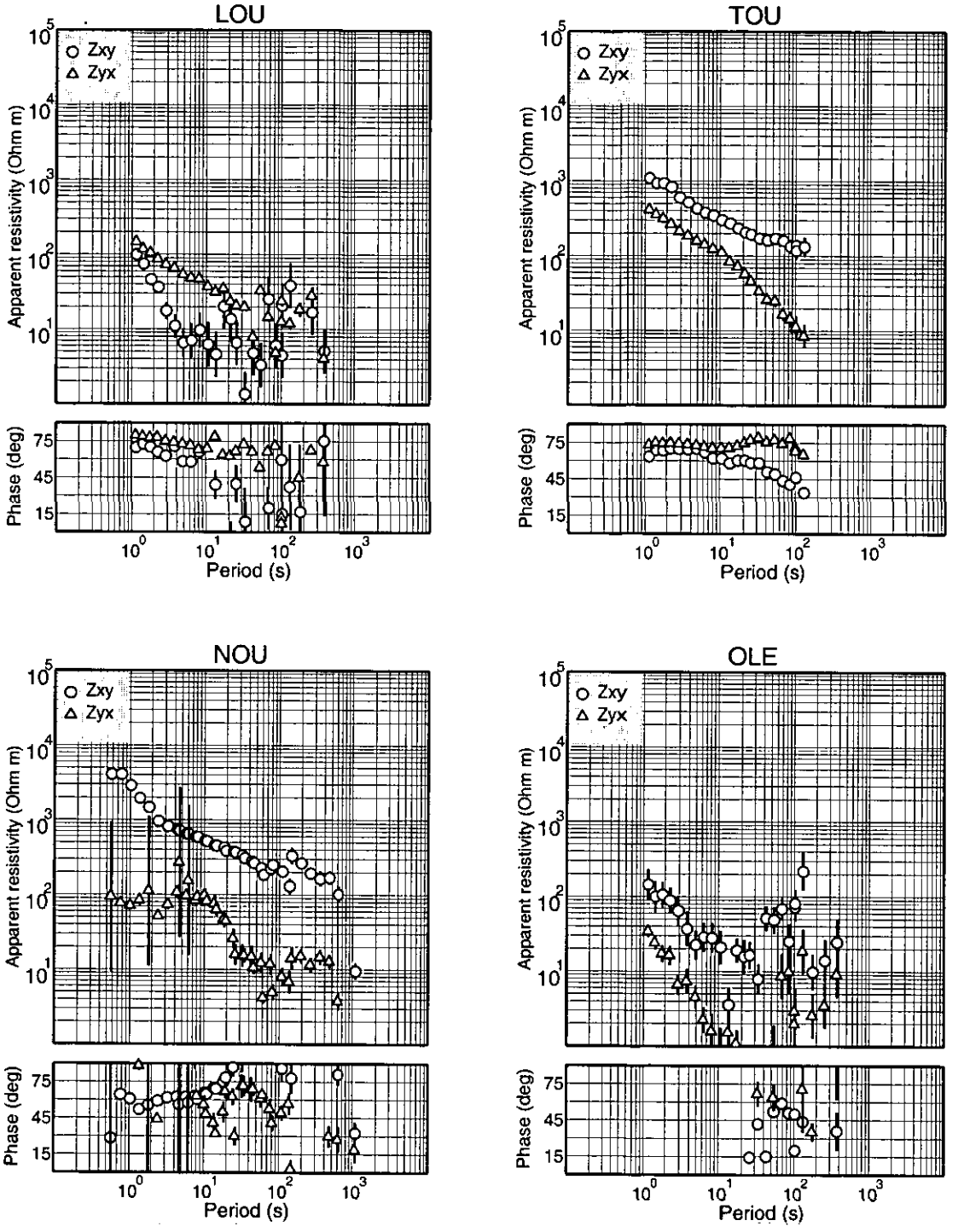

Figure 2.8 (cont.) Apparent resistivity and phase computed for the rotated (30° West of N) impedance tensor.

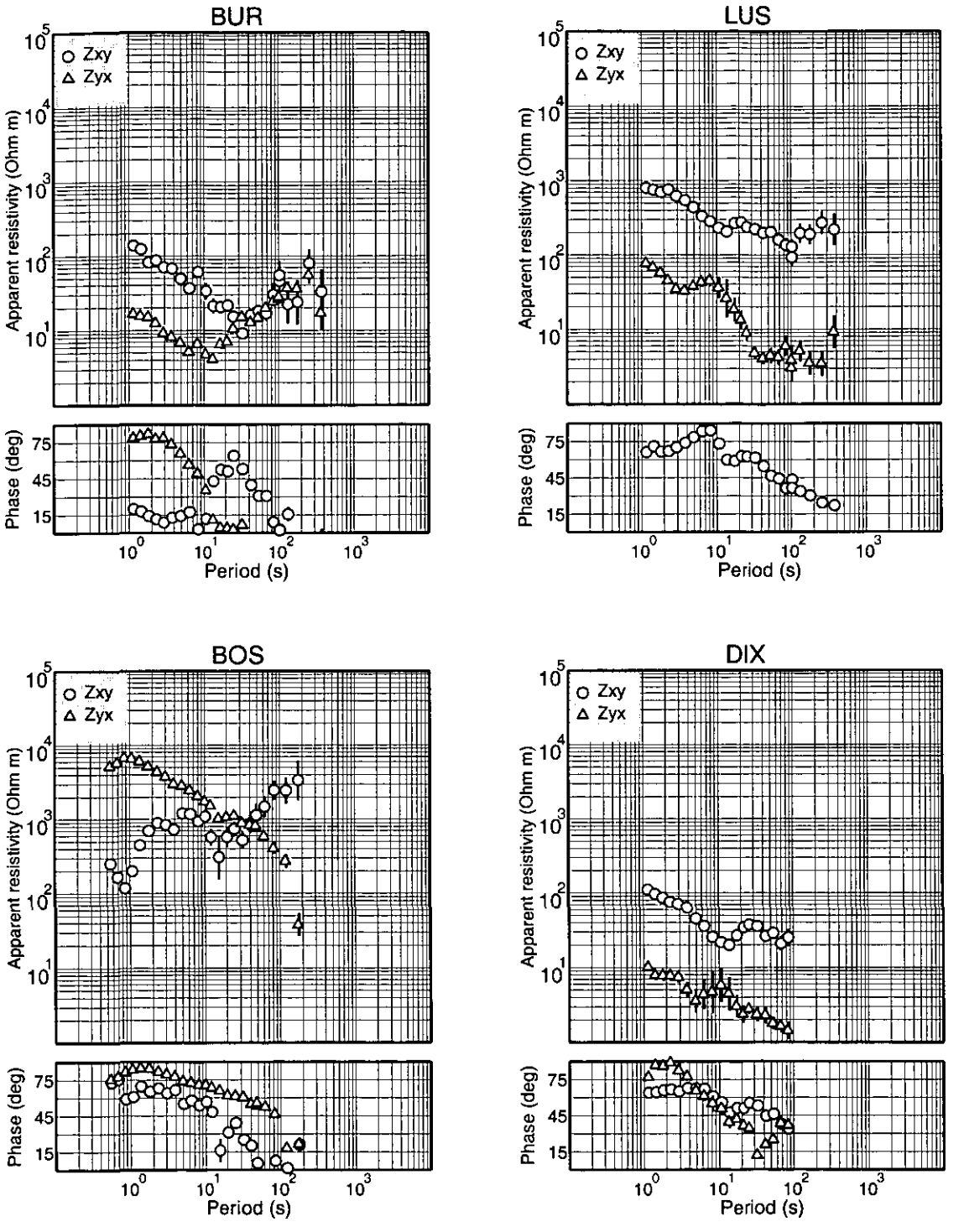

Figure 2.8 (cont.) Apparent resistivity and phase computed for the rotated (30° West of N) impedance tensor.

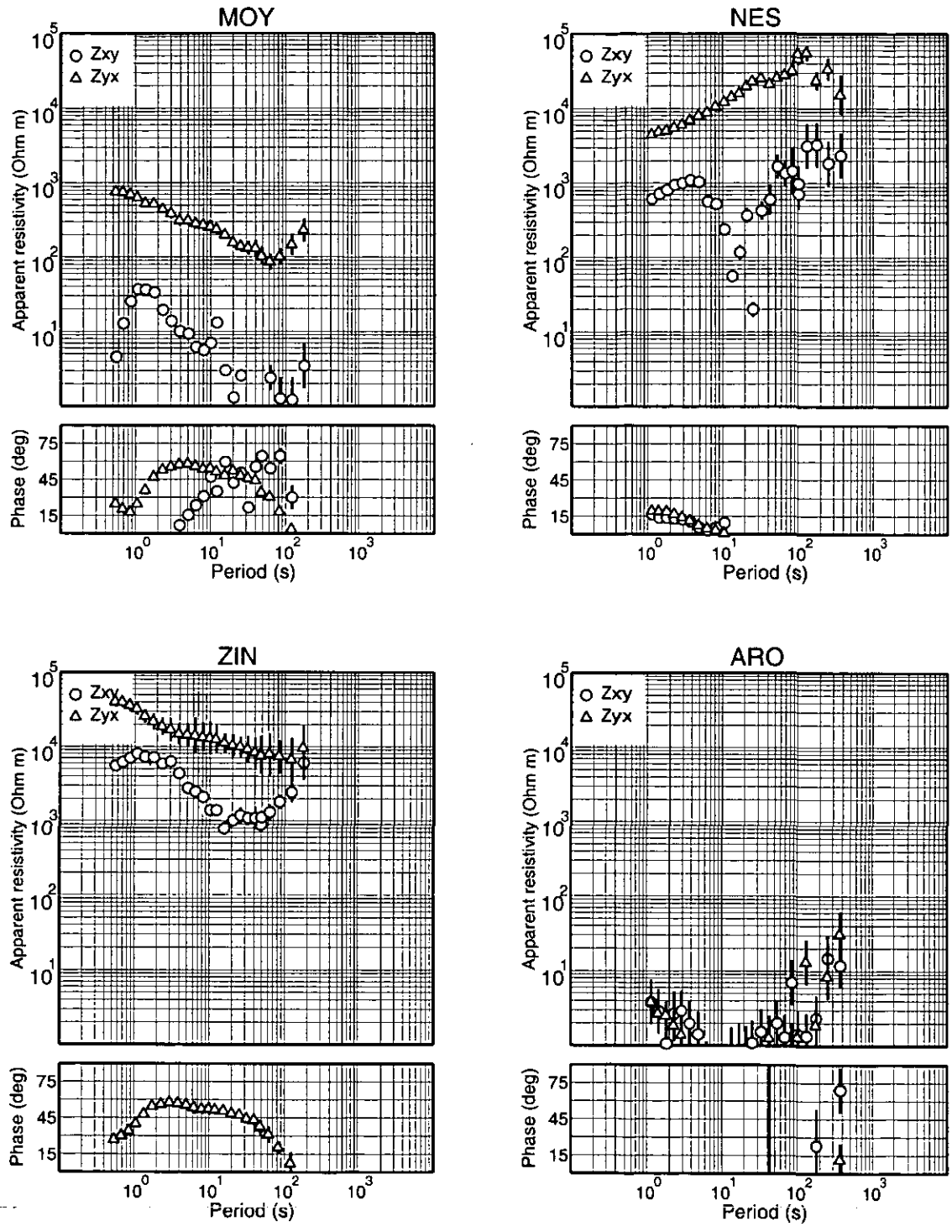

Figure 2.8 (cont.) Apparent resistivity and phase computed for the rotated (30° West of N) impedance tensor.

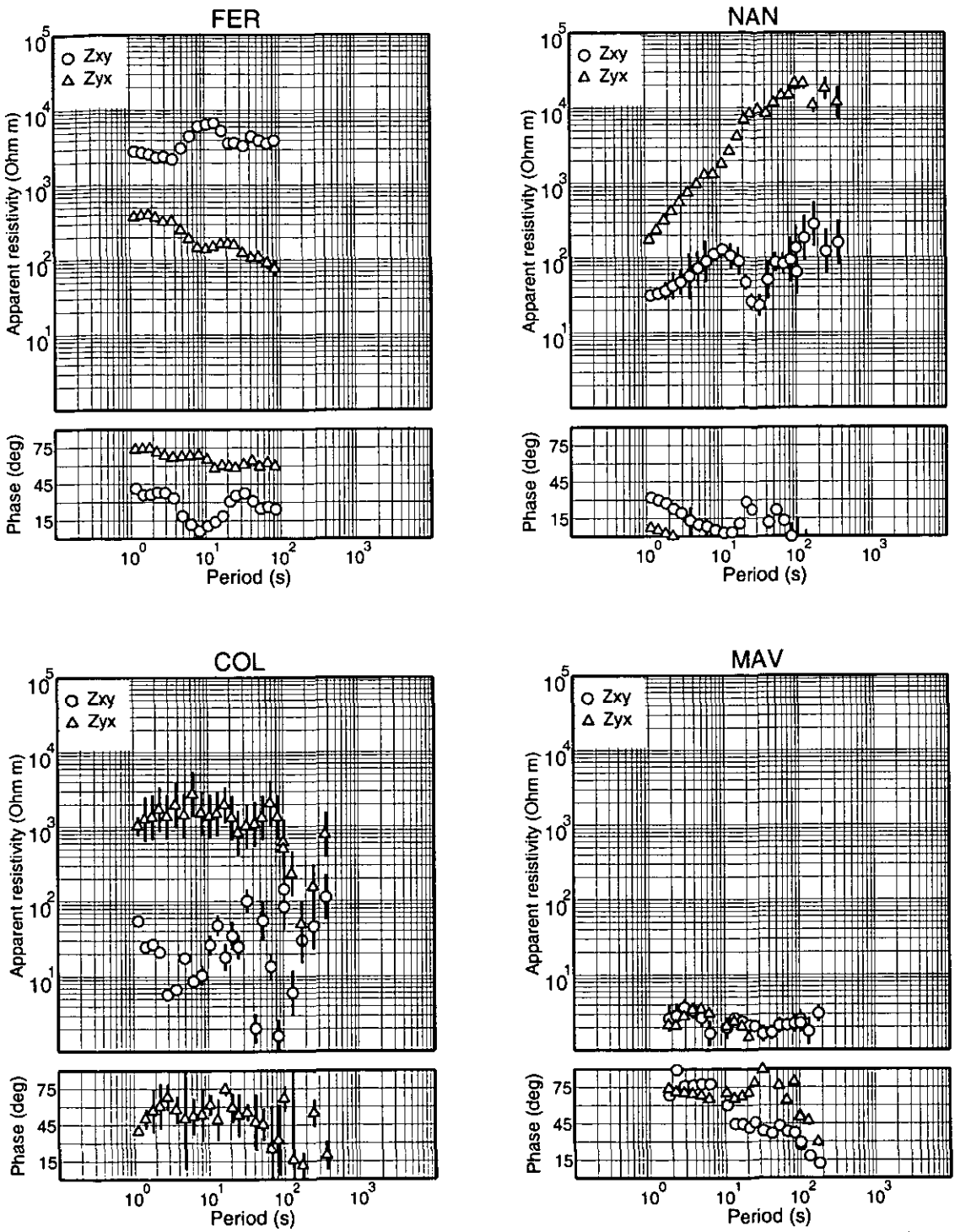

Figure 2.8 (cont.) Apparent resistivity and phase computed for the rotated (30° West of N) impedance tensor.

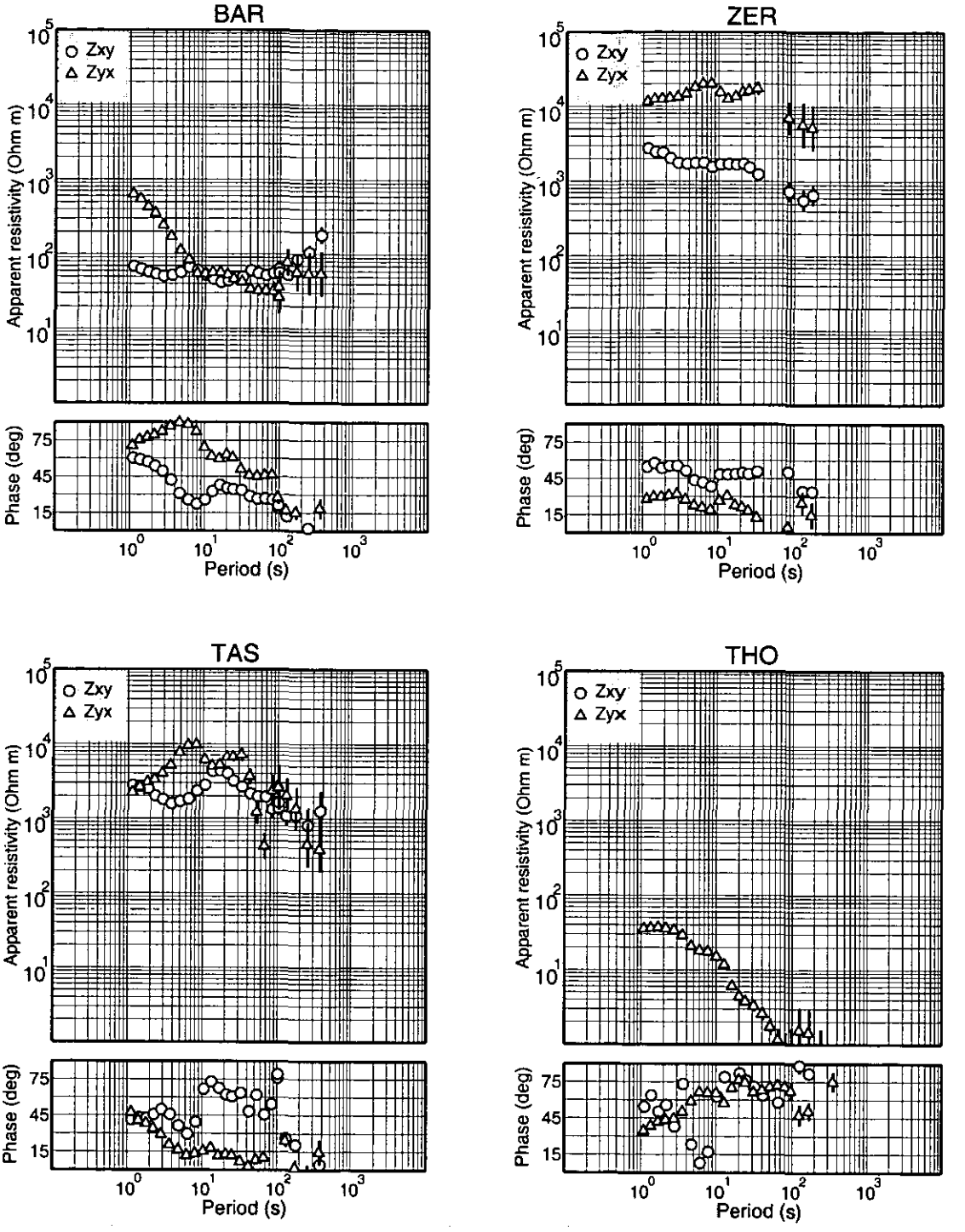

Figure 2.8 (end) Apparent resistivity and phase computed for the rotated (30° West of N) impedance tensor.

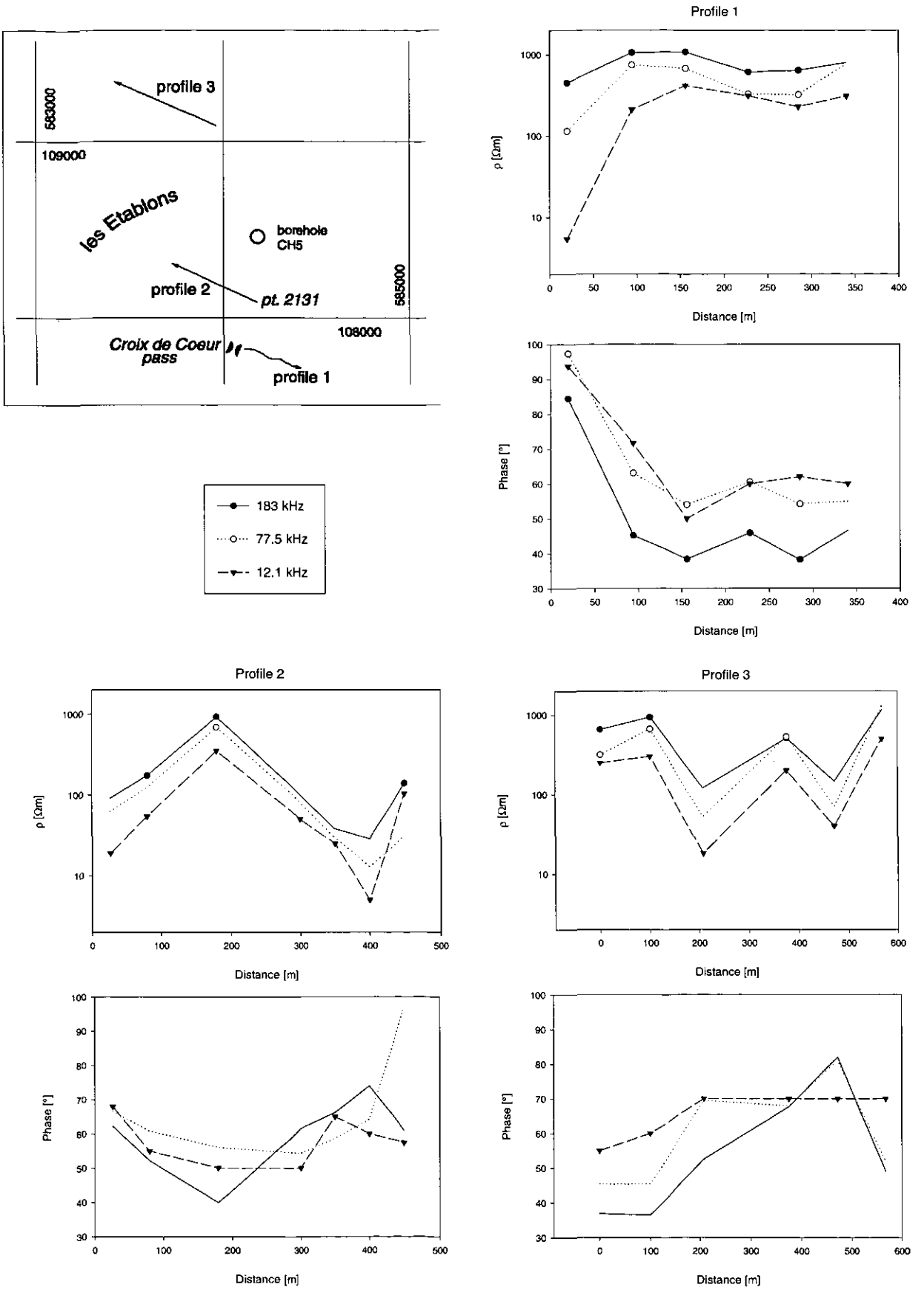

Figure 2.9 Map of the VLF profile location. Apparent resistivity and phase along the profiles.

conductors like graphite, or at least high-grade anthracite, or sulphides. It is remarkable that, although the CH5 samples look very similar to the SOM7 ones at first glance, they display a much higher resistivity (by a factor of 10^3).

In an auxiliary test, we tried to determine the nature of the fine-grained black pigment. Silicate minerals were removed by dissolution in concentrated hydrofluoric acid. Expected insoluble constituents are carbon of initially organic origin together with HF-insoluble ore-minerals. For SOM7 the proportion of insoluble residual powder amounted to 12-15%. XRD analyses did not reveal any significant mineral phase (opaques) other than ill-crystallised pre-graphite. Under hydrostatic pressure of 150 MPa, the resistivity of this powder was found to be as low as 0.003 Ωm. This is still 300 times the resistivity of pure, monocrystalline graphite, but 10^3 to 10^4 less than lignite and coal.

2.2.4. Petrography and mineralogy

Various laboratory methods have been applied on a series of samples from CH5 and SOM7 boreholes in an attempt to explain their dissimilar electrical properties which occur despite of their macroscopic resemblance. These methods are:

- optical microscopy
- x-ray powder diffractometry
- scanning electronic microscopy and spectroscopy
- transmission electronic microscopy and local spectra

Optical microscopy shows a typical slate texture with felsic, silt-sized quartz-rich ribbons alternating with very fine-grained (<10 μm) bands rich in mica, chlorite and dark non-identified pigment. The following paragenesis is observed and confirmed by XRD analyses: chlorite, white mica (illite), quartz, K-feldspar, albite, opaque minerals (mostly pyrite).

X-ray powder diffractometry was conducted on non-oriented whole rock (w.r.) powders as well as on oriented preparations of nominal grain size fractions 16-2 μm and < 2 μm. Whereas w.r. analyses confirmed the above-mentioned, optically determined mineral paragenesis, the clay size preparations revealed the dominance of chlorite over well crystallised illite (muscovite) among the abundant phyllosilicates, which, according to w.r. analyses, make up more than 50% of the samples. No graphite could be identified in these samples, however. Even after removal of silicates from the clay size fractions (16-2 μm), XRD analyses did not reveal any sizeable peak within the dark residue, other than a broad shoulder centred roughly at 3.34 Å, corresponding to the expected main peak of graphite.

Scanning electronic microscopy provided the key to understanding the dissimilar electric conductivity behaviour. This technique clearly shows that three parameters are very important for conductivity enhancement: rock texture, grain size and carbon content, although there is no need for very high C concentration. Intrusion of a conducting carbon film at grain boundaries into the phyllosilicates should play a determinant role as a path for electronic conduction in sample SOM7 (Fig. 2.11, courtesy of Dr. C. Viti, Univ. Siena). Conductivity increases with rising pressure (Fig. 2.10 c) at all temperatures studied. This is exactly what one would expect if the rock contains free reconnecting carbonaceous material (Glover and Vine, 1992). In CH5 however, local carbon enrichment results in large clusters without electrical connectivity due to the coarser granulometry.

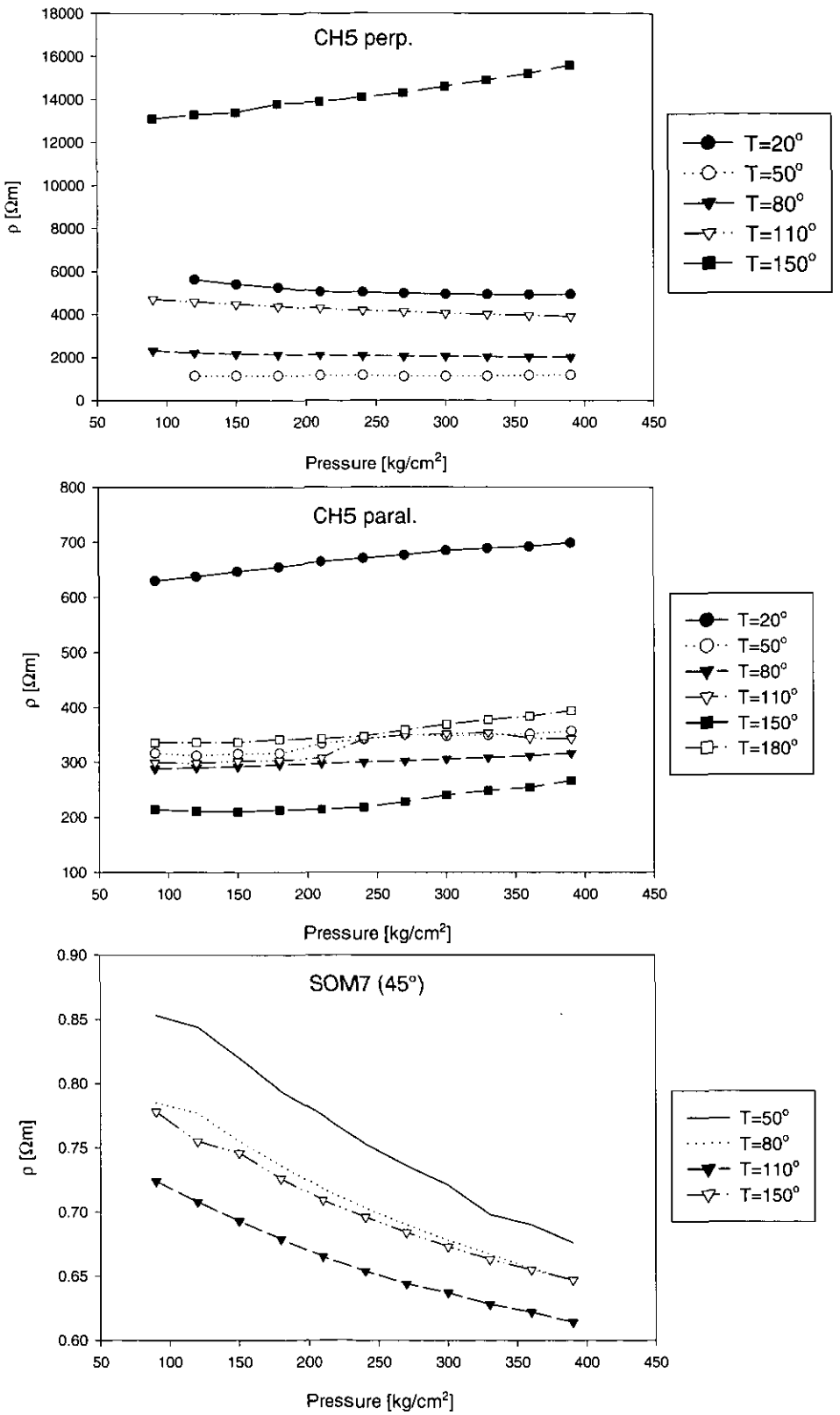

Figure 2.10: Electrical resistivity of 3 rock samples from boreholes CH5 and SOM7 vs. hydrostatic pressure at different temperatures. Samples from CH5 are cut perpendicularly and parallelly to schistosity. Sample from SOM7 is cut at an angle of 45 °.

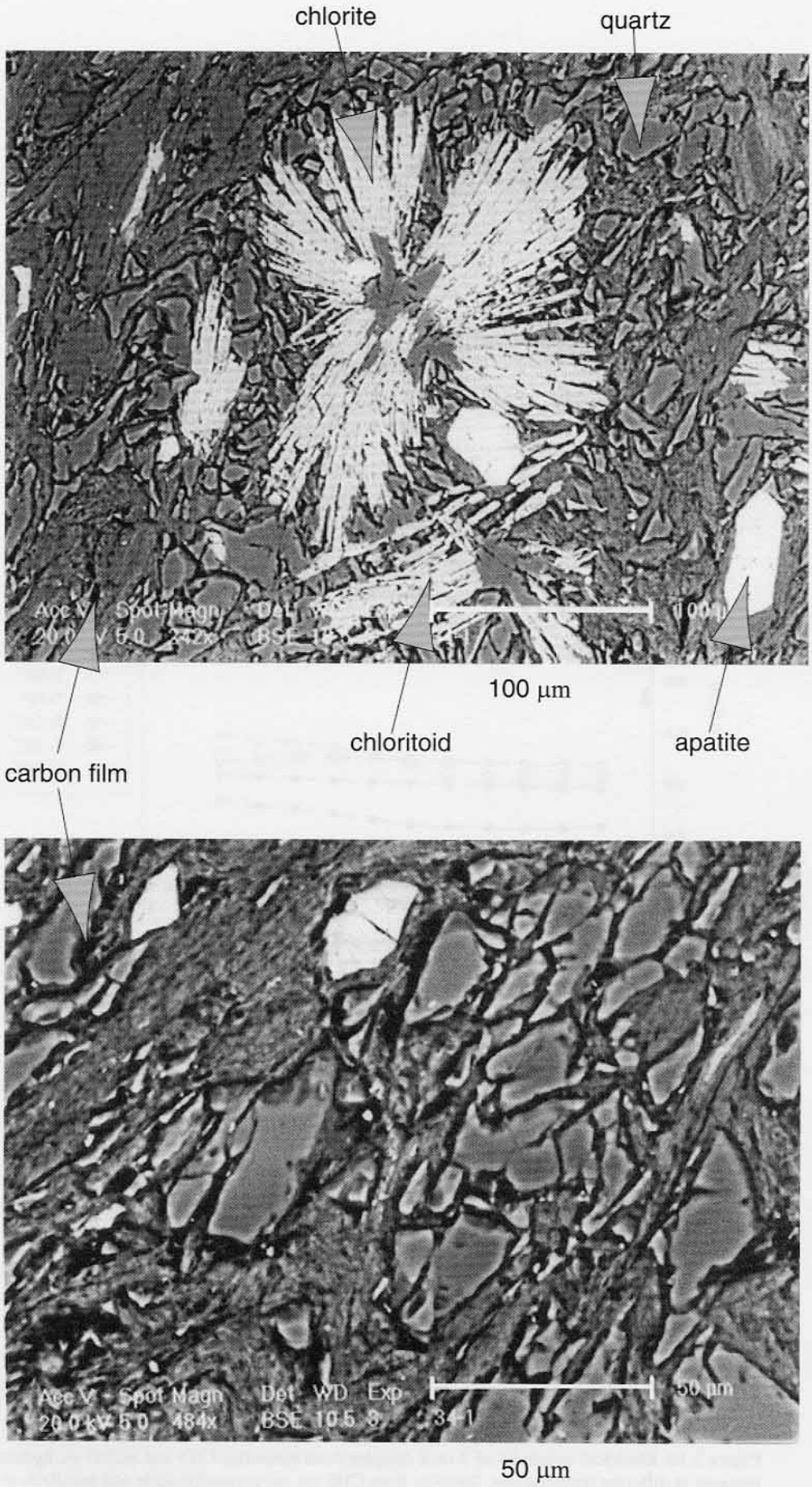

Figure 2.11 Scanning electron microscope images of highly conducting sample from borehole SOM7.

3. Data modelling

3.1 MT and GDS modelling

Generally, a first step toward MT data interpretation consists in computing 1D models at each site and then to proceed to higher-degree geometries. Eventually, a 2D model may be proposed from the distribution of the 1D models which serves as an initial model for more elaborate schemes. In the case of our data, however, this proved not to be very useful as many clues, like the direction of the induction arrows and availability of seismic data, could be used as valuable guidelines. Moreover, the 2D modelling methods which were employed proved extremely robust, regardless of the initial model. Two- and three-D modelling were carried out, but topographic information could not be used because of complexity limitations in the computing methods.

3.1.1 2D modelling

Ideally, 2D modelling of magnetotelluric and GDS data requires that measuring sites either are distributed along a line crossing the geological strike at right angle, or that the structure is perfectly 2D, in which case the exact location along strike becomes unimportant. Here there is no ambiguity relative to the strike direction in the dataset. The induction arrows point toward a very constant direction, with little period or location dependence. However, topographic roughness did not allow the deployment of MT sites along straight profiles. Instead, stations were fairly evenly distributed over the whole area, a 30 x 70 km rectangle.

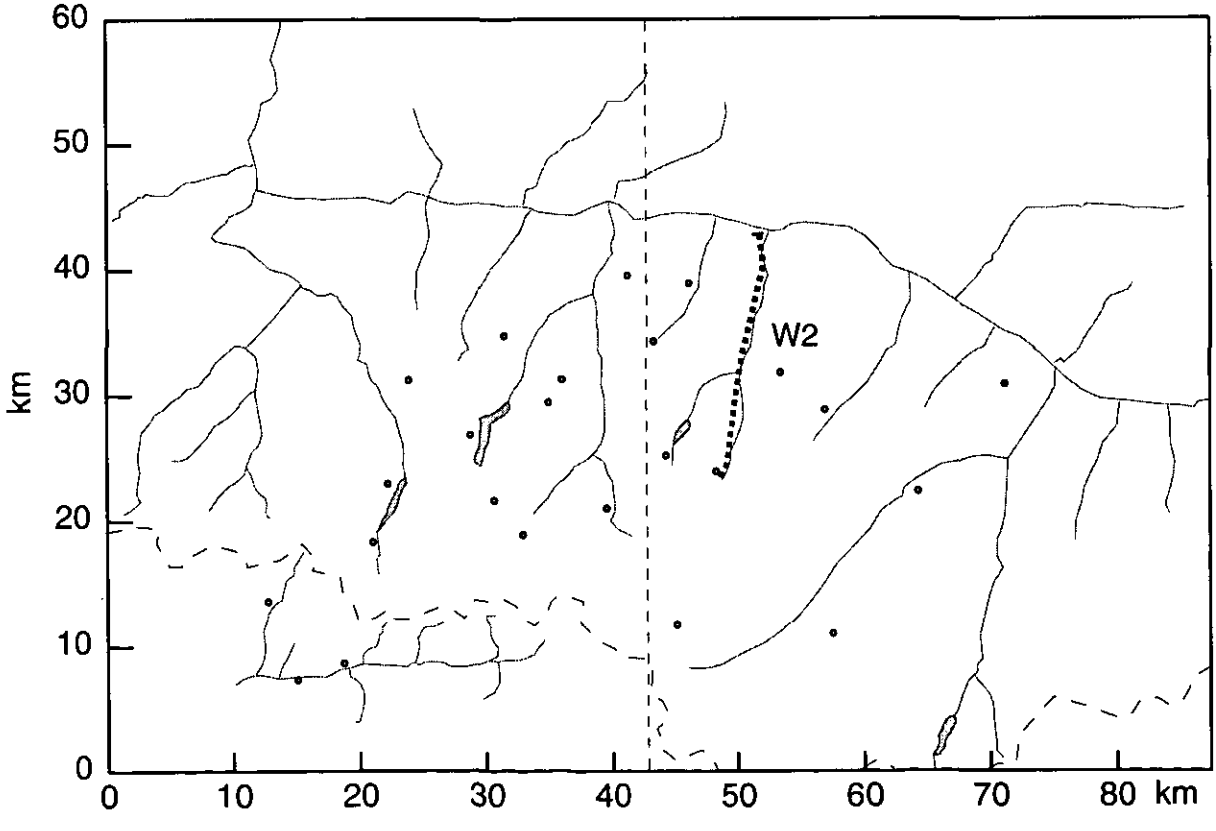

Figure 3.1 Map showing the 2D model profile axis (dashed line) and the location of seismic line W2.

To allow for future comparisons of the MT/GDS resistivity distribution with the seismic reflectors we selected a virtual cross-section along which all the MT parameters were calculated by 2D interpolation. This profile runs a distance of 42.8 km from the rotated frame origin, parallel to the vertical axis. This choice allows us to take full advantage of the nearby existing seismic line W2 which runs almost parallel to the profile at a distance of 7 km (Fig. 3.1).

Multidimensional modelling is a time-consuming task which rerquires lengthy finite-element computations. To keep computing time within manageable limits all the data parameters (apparent resistivity, phase, induction coefficients of TE and TM modes) were decimated, using only periods of 1, 3, 10, 30, 100 and 300 seconds. Since these periods did not appear in the original period list derived from the computation of the apparent resistivity and phase curves, the required data were derived through interpolation for these periods.

An 87.5 x 60 km rectangle was drawn such that its lower-left corner coincides with the origin of the rotated frame. Its sides are subdivided to produce a regular grid of 49 x 30 small rectangular cells (the grid itself comprises 50 x 31 nodes). Taking the data from each MT site, values of MT/GDS parameters were computed at the grid nodes and gridding was done with the kriging method. A virtual profile of simulated MT sites is chosen among the vertical lines of the grid. In the present study, line # 24 was used, because this line is ideally located in the middle of the site distribution, not too far from seismic line W2. Its abscissa, therefore, is located at 24*87.5/49 = 42.8 km. Along the virtual profile, interpolated values are available at all nodes with a 2 km spacing.

The 2D modelling method employs an automatic scheme based upon low-order polynomials (Schnegg, 1993; 1996). The results from the seismic profiles indicate that the target geology consists of dipping layers, the shape of which can be approximated very well by simple polynomials. To allow individual resistivity variations of the layers, this parameter is also expressed by a polynomial development. Moreover, because MT is known to suffer from low resolving power, the model searched for was kept as simple as possible: a four-layer structure. Hence, 4 resistivities and 3 thicknesses were controlled by 7 polynomials with degree 3 for the resistivity and degree 2 for the thickness (higher degrees would have led to oversized models in terms of computing time). Actually, the polynomials searched for were the decimal logarithms of resistivity and thickness to avoid negative value excursions of the parameters. The polynomials do not appear directly in the model (continuous distribution of the conductivity). Rather, the model is discretized as a set of rectangular boxes whose resistivities and heights are controlled by the polynomials (their width is fixed). The modelling scheme uses a steepest descent algorithm to minimise the misfit between measured data and model response. Taking all the polynomial coefficients into account, as many as 25 parameters are controlled simultaneously by the modelling programme.

A first modelling attempt uses the full MT information spread over 36 km along the virtual NNW-SSE profile. This computation shows that a very good conducting slab is plunging toward the SSE into a much more resistive rock matrix. The conductor takes up the northernmost part of the profile only. Computing time considerations limit the model size to a finite-element grid of 100 x 100 nodes. To increase the resolution of the slab image, a second run was carried out, limiting the profile to the conducting part of the slab. The final 2D model is shown in Fig. 3.2. It consists of a very high-conducting slab plunging into a quite homogeneous, resistive matrix. Of course, the real conducting slab probably assumes a smooth, continuous shape, well approximated by polynomials, but since our scheme can only handle rectangular boxes, we prefer to show this more direct representation. Table 3.1 gives

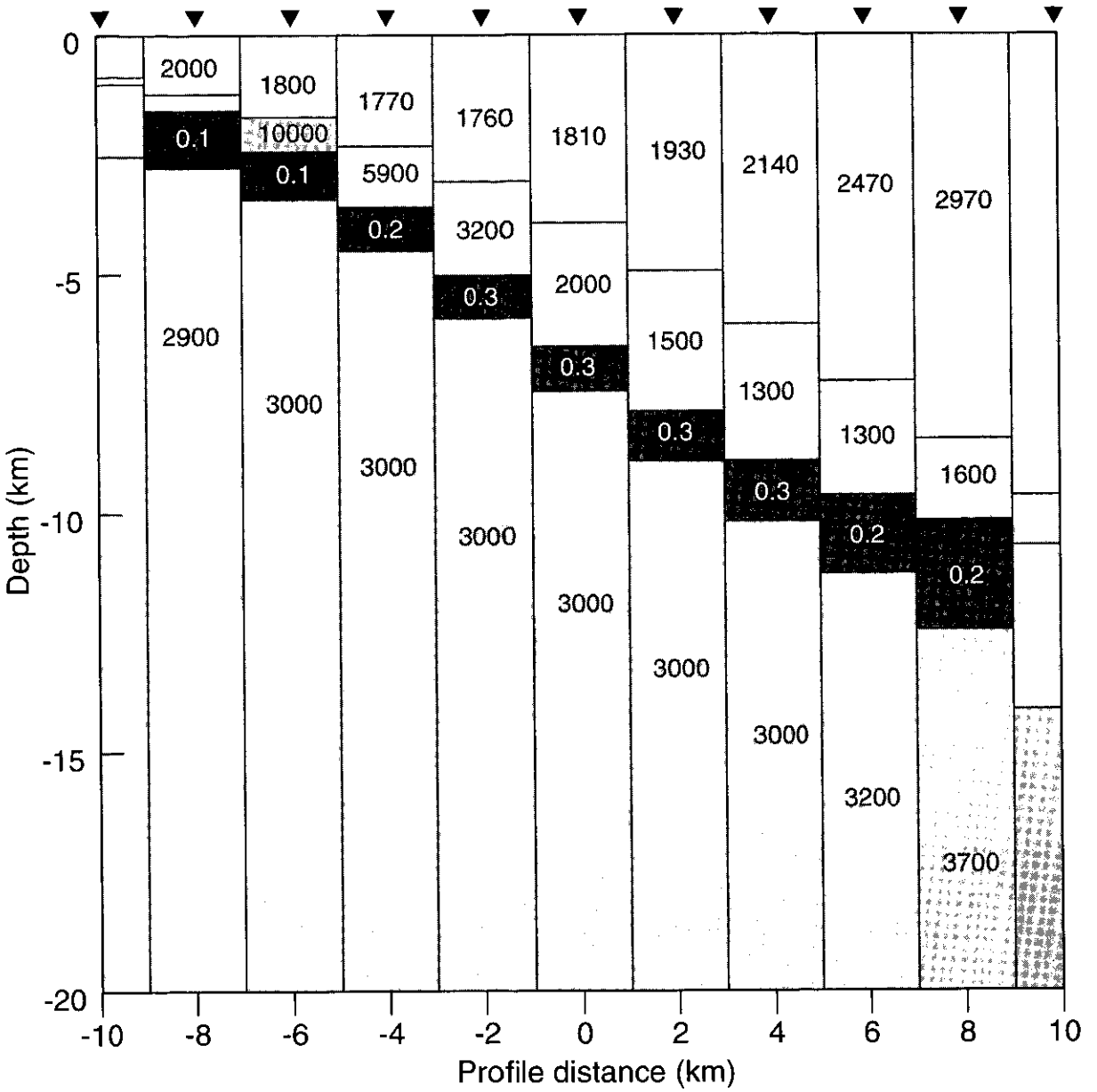

Figure 3.2 Magnetotelluric and GDS 2D model along virtual profile located 42.8 km from the rotated frame origin (dashed line on Fig. 3.1). The filled triangles indicate location of virtual MT sites. Resistivity values are given in Ωm.

the polynomial coefficients of the parameters ρ_i, h_i, for a coordinate origin located in the rotated frame at Y_0=32 km.

	A	B	C	D
ρ_1	0.325707E+01	0.100856E-01	0.204364E-02	0.794044E-05
h_1	0.572723E+00	0.515811E-01	-0.207974E-02	
ρ_2	0.331061E+01	-0.862720E-01	0.785408E-02	0.168859E-03
h_2	0.585052E+00	0.103525E+00	-0.111558E-01	
ρ_3	-0.439344E+00	0.133895E-01	-0.826619E-02	0.197352E-03
h_3	-0.139648E+00	0.273515E-01	0.454939E-02	
ρ_4	0.346896E+01	-0.396116E-02	0.813629E-03	0.164795E-03

Table 3.1 Polynomial coefficients of final 2D model. Decimal logarithm of each element ρ_i, h_i is a polynomial of the form $A+By+Cy^2+Dy^3$.

A comparison of model responses with interpolated measured data is shown in Fig. 3.3 for MT and Fig. 3.4 for GDS. Note that virtual sites 1 and 2 are located to the north of the northernmost MT station; their data may therefore be biased by extrapolation effects, due to a lack of information. Their misfit contribution has not been included in the modelling and this explains why they display a large misfit with respect to the model response.

3.1.2 3D modelling

Although the induction arrows of the Penninic Alps of Valais indicate only a small departure from cylindrical geometry (Fig. 2.7), results obtained by 2D modelling can barely be extrapolated laterally over distances larger than 10 kilometers. Other 2D modelling attempts could have been carried out along parallel profiles. They would have been less accurate however, because of a decreasing density of measuring sites. Instead, a 3D global modelling was preferred. In this modelling attempt, the data at every site was used directly, without spatial interpolation. As for 2D modelling, parameter values for every sites were interpolated at the same fixed periods.

The 3D modelling scheme employs a forward calculation based upon the integral form of Maxwell's equations (Mackie et al., 1993; 1994), where accelerated conjugate gradient relaxation is used to solve for H_x, H_y and H_z. To automate the search for the best model this scheme was incorporated into a control loop which optimizes the data-model misfit in a steepest descent algorithm (Schnegg, 1998).

The region of interest (a rectangle within the rotated frame with lower-left and upper-right corners at coordinates (10;0) and (82;42)) is subdivided into 24 x 14 x 20 rectangular boxes of size 3 x 3 x 0.5 km. Three columns and three rows are appended to each external side of the model, with increasing width of 6, 12 and 24 km, thus dividing the space into 30 x 20 x 20 blocks. Each vertical slice of this model is embedded in a larger 2D model which extends the regional features. A 1D structure (a half-space in this case) is added at the bottom.

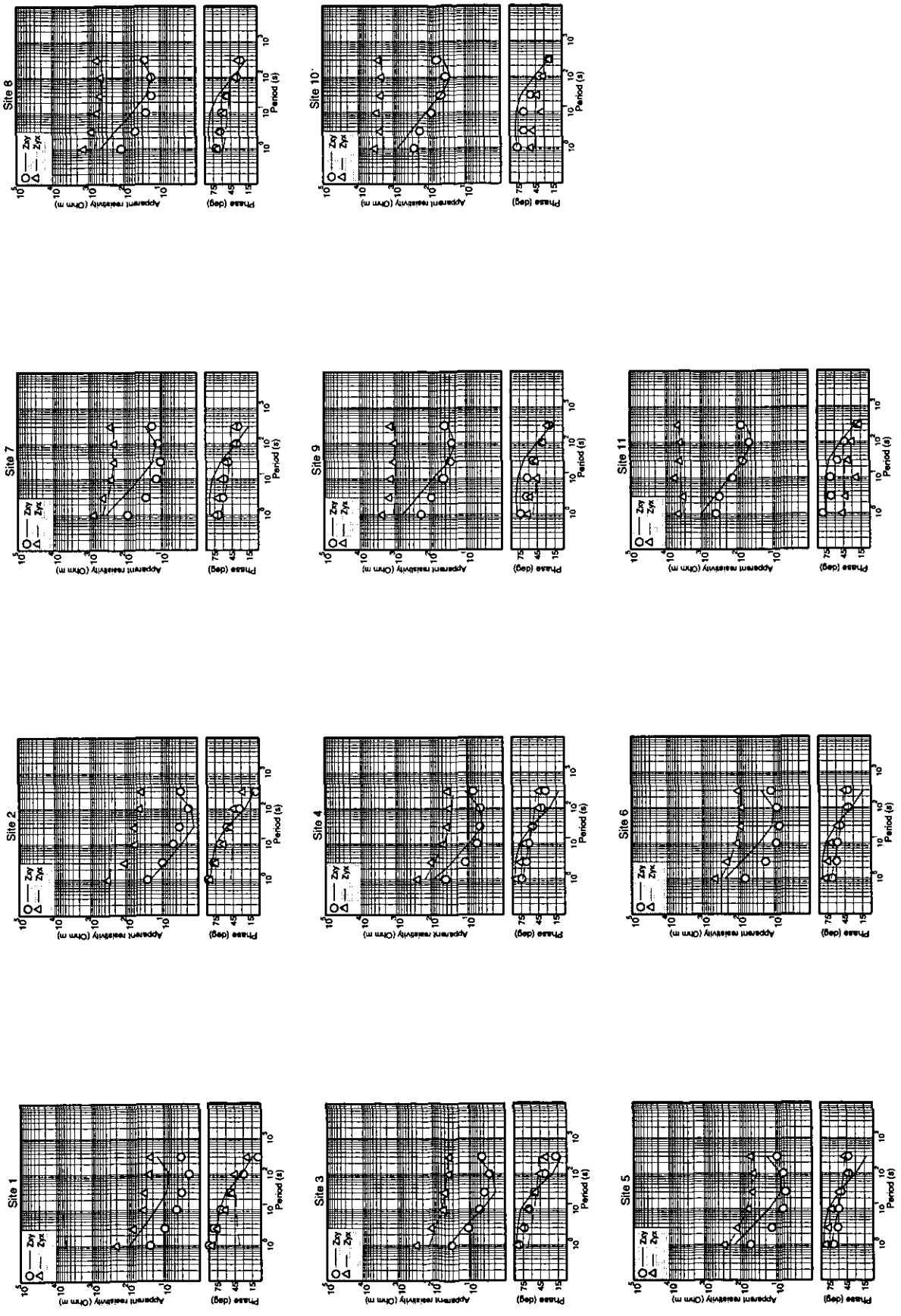

Figure 3.3 Measured (interpolated) MT data at 11 virtual sites for TM and TE modes (Zxy & Zyx) with 2D model response.

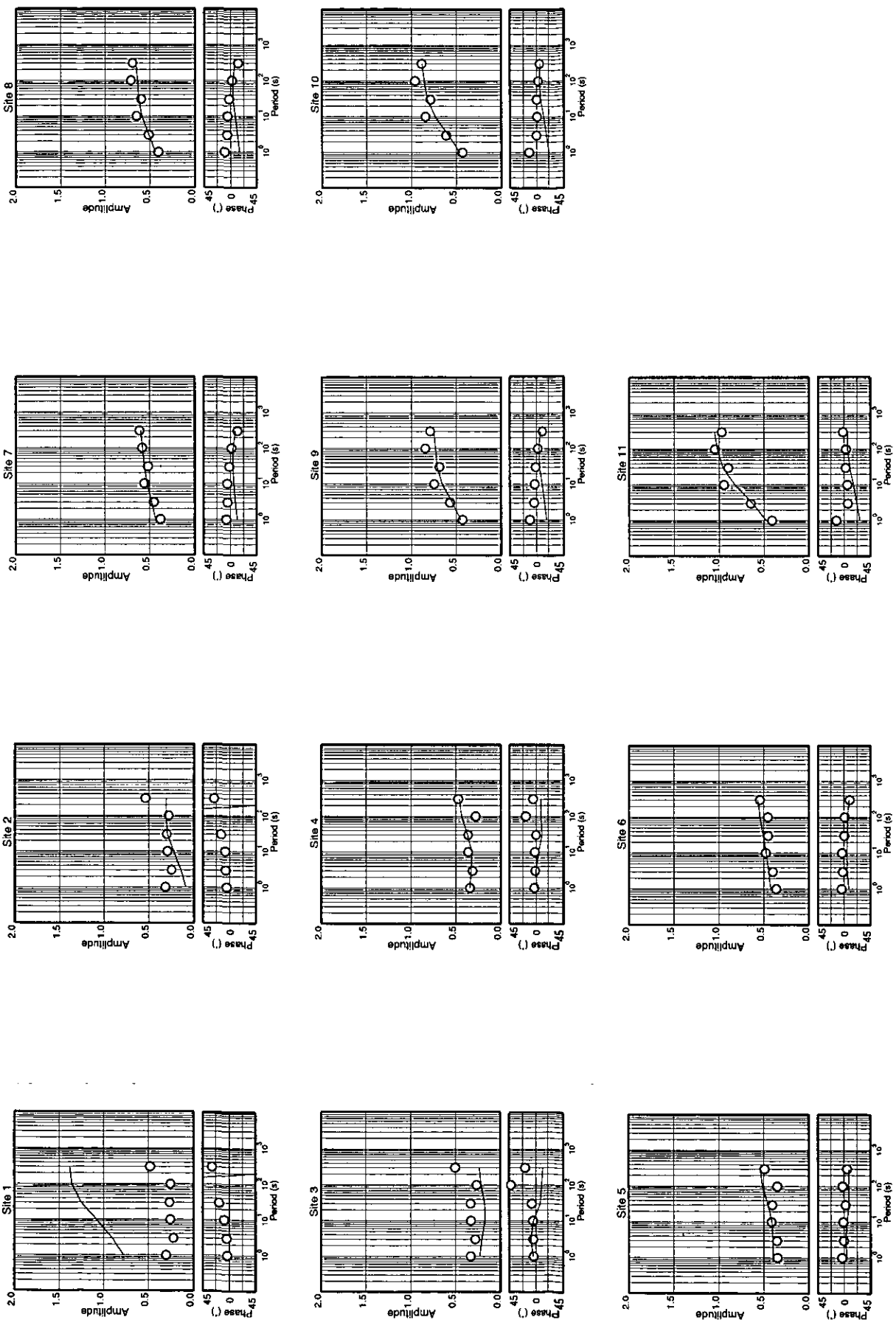

Figure 3.4 Measured (interpolated) amplitude and phase of GDS data at 11 virtual sites with 2D model response.

The previous results of the 2D modelling indicated that a single, thin, high conducting slab was embedded in the resistive matrix. We therefore limit our choice of 3D models to those which share these characteristics. The slab resistivity and thickness are given fixed values of 0.2 Ωm and 1 km. The parameters which are automatically adjusted by the programme are the decimal logarithms of

- the slab depth, $f_1(x,y)$,
- the resistivity of the rock matrix above the slab, $f_2(x,y)$,
- the resistivity of the rock matrix beneath the slab, $f_3(x,y)$.

These parameters are expressed as polynomials of the coordinates x and y with degrees set to 3, 2 and 2 respectively. No vertical resistivity variation is allowed within a given layer.

A dipping plane was proposed as initial model for f_1 and constant values for f_2 and f_3. Because the computing time is proportional to the number of period values at which the misfit is calculated, we restricted the values to 1 and 100 seconds. Isolines of the final 3D model are shown in Fig. 3.5 and 3D views in Fig. 3.9. Table 3.2 gives the polynomial coefficients of f_1, f_2 and f_3 with the origin of coordinates located in the rotated frame at X_0=46 km, Y_0=21 km.

	A	B_1	B_2	C_1	C_2	C_3	D_1	D_2	D_3	D_4
f_1	1.22918	-7.70580E-02	3.39274E-02	1.48388E-03	-1.45845E-03	-1.68562E-03	1.75891E-05	-2.00190E-05	3.48647E-05	-3.65097E-05
f_2	3.63125	5.60000E-03	3.20045E-03	0	-5.90070E-05	2.05746E-04	-	-	-	-
f_3	3.63068	-3.01378E-03	5.56242E-03	0	-3.72401E-04	0	-	-	-	-

Table 3.2: Polynomial coefficients of final 3D model. Decimal logarithm of each parameter f is a polynomial of the form $f=A+B_1y+B_2x+C_1y^2+C_2yx+C_3x^2+D_1y^3+D_2y^2x+D_3yx^2+D_4x^3$.

A comparison of model responses with interpolated measured data is shown in Fig. 3.6 for MT and Fig. 3.7 for GDS. The misfit of the model response is noticeably larger for 3D than for 2D modelling. Obviously, the cause is the oversimplification of the 3D model and the limited number of period values which were imposed by the computing time requirements. Moreover, static effects are likely to occur on MT data recorded on such rough topographic area. These effects are known to generate random displacements of the entire apparent resistivity curves and this cannot be accounted for in the modelling. However, the rather large number of sites used in the modelling somehow mitigates the static effects.

3.2 VLF modelling

The three profiles of Fig. 2.9 have been used to look for 1D models of the subsurface resistivity near borehole CH5. Because only three frequencies (183, 77.5 and 12.1 kHz) were available, the choice of models is restricted to 2-layer structures. Attempting to model with more layers would only lead to over-fitting and produce parameters which could be varied without noticeable effect on the misfit. The modelling scheme is based on a method developed for MT periods (Fischer and Le Quang, 1981).

Fig. 3.8 gives the resulting 1D models for the three profiles. Resistivity is always decreasing with depth. At the surface, values in excess of 100 Ωm are detected. The presence of this resistive material can be understood as a weathering layer which has been oxidised over time.

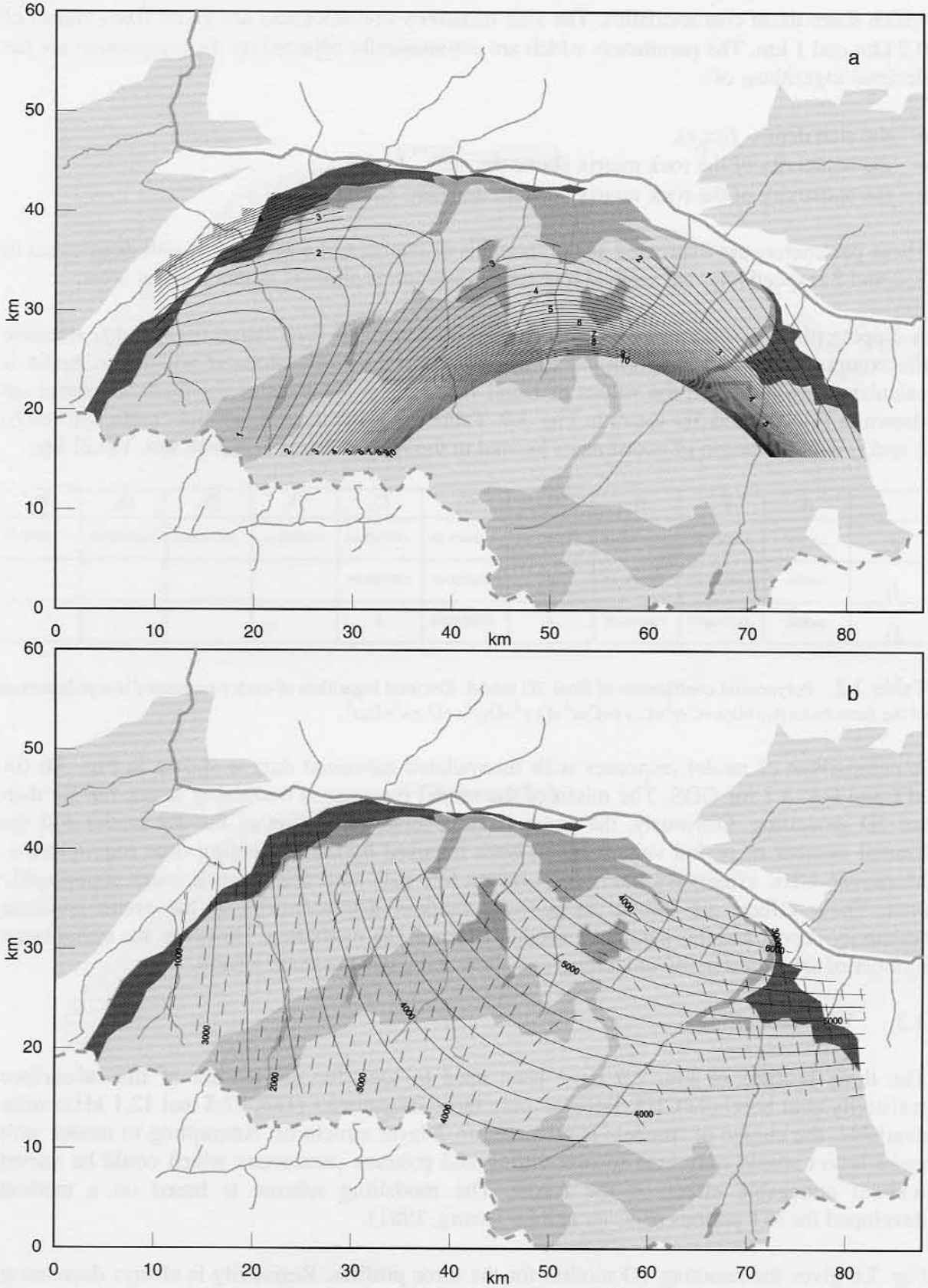

Figure 3.5 3D MT/GDS final model. (a) Isolines of the depth to the 0.2 Ωm body (km). (b) Isolines of the lateral resistivity distribution in the top layer (plain line) and third layer (broken line) in Ωm. Zone Houillère outcrop is represented in dark colour.

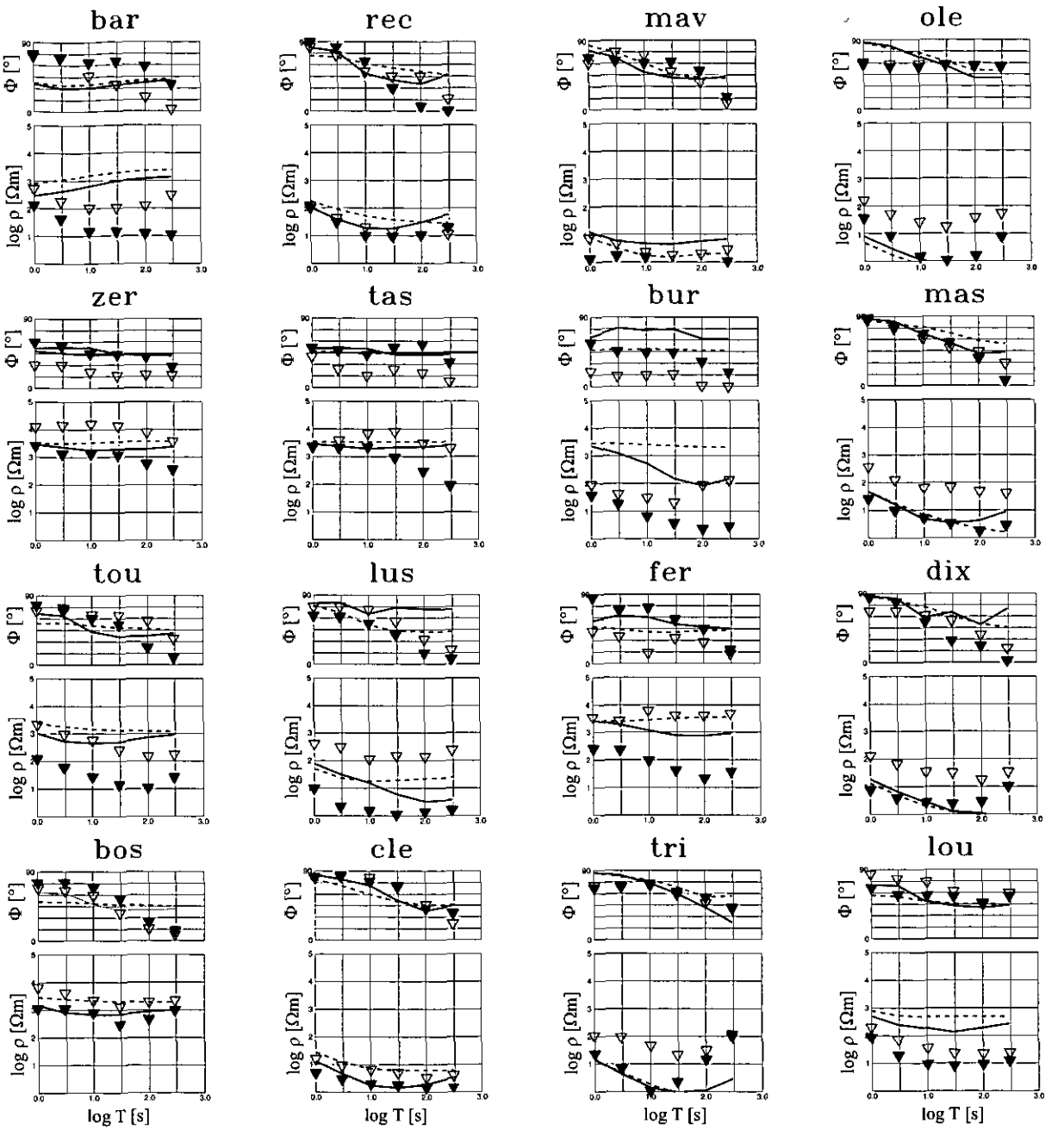

Figure 3.6 Measured (interpolated) apparent resistivity and phase data and 3D model response at 16 sites. Filled triangles and plain curve denote TM mode data and model response, whereas empty triangles and dashed curve correspond to TE mode.

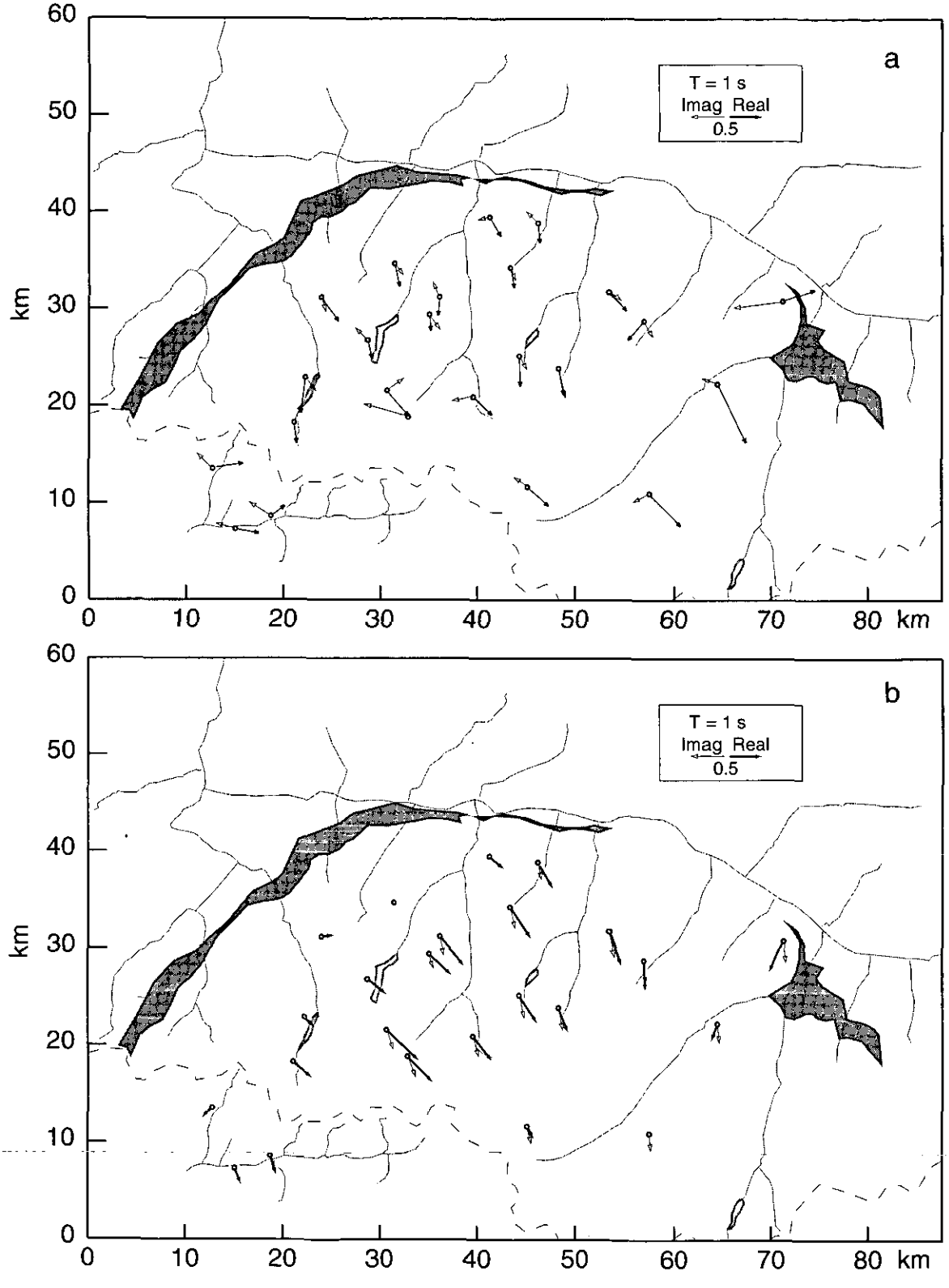

Figure 3.7 Measured (a) and calculated (3D model) (b) real and imaginary induction arrows at period of 1 second.

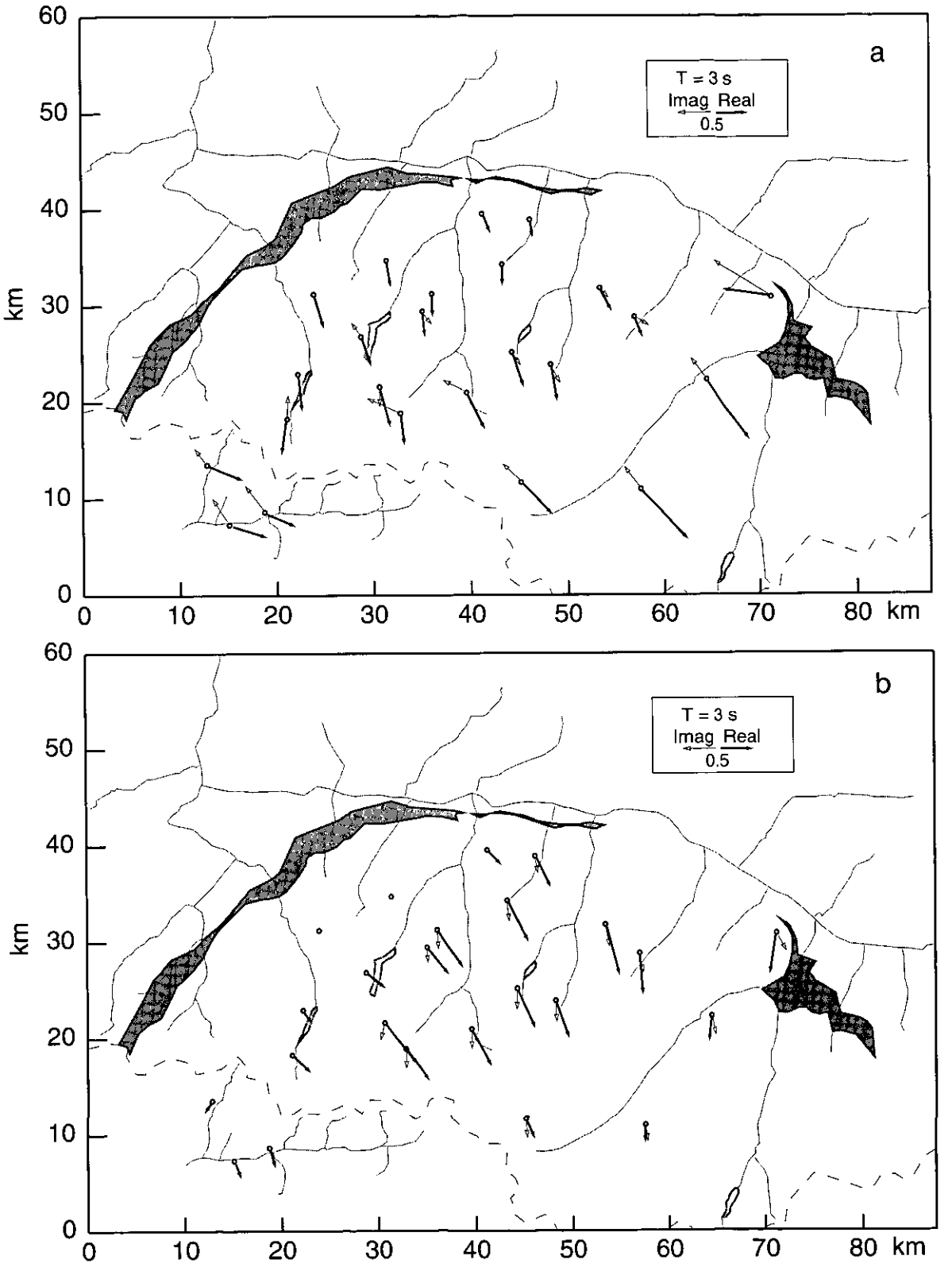

Figure 3.7(cont.) Measured (a) and calculated (3D model) (b) real and imaginary induction arrows at period of 3 sec.

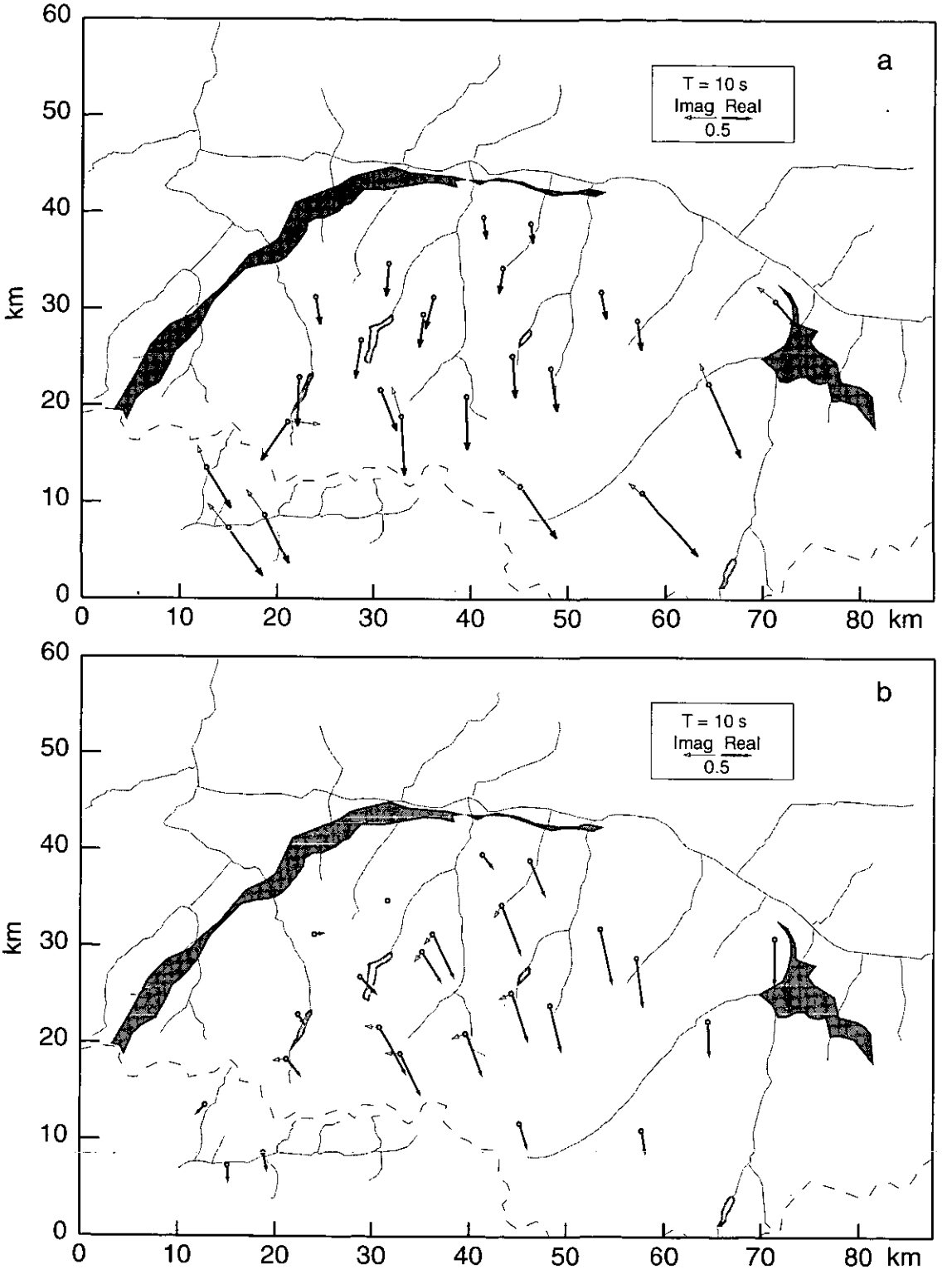

Figure 3.7(cont.) Measured (a) and calculated (3D model) (b) real and imaginary induction arrows at period of 10 sec.

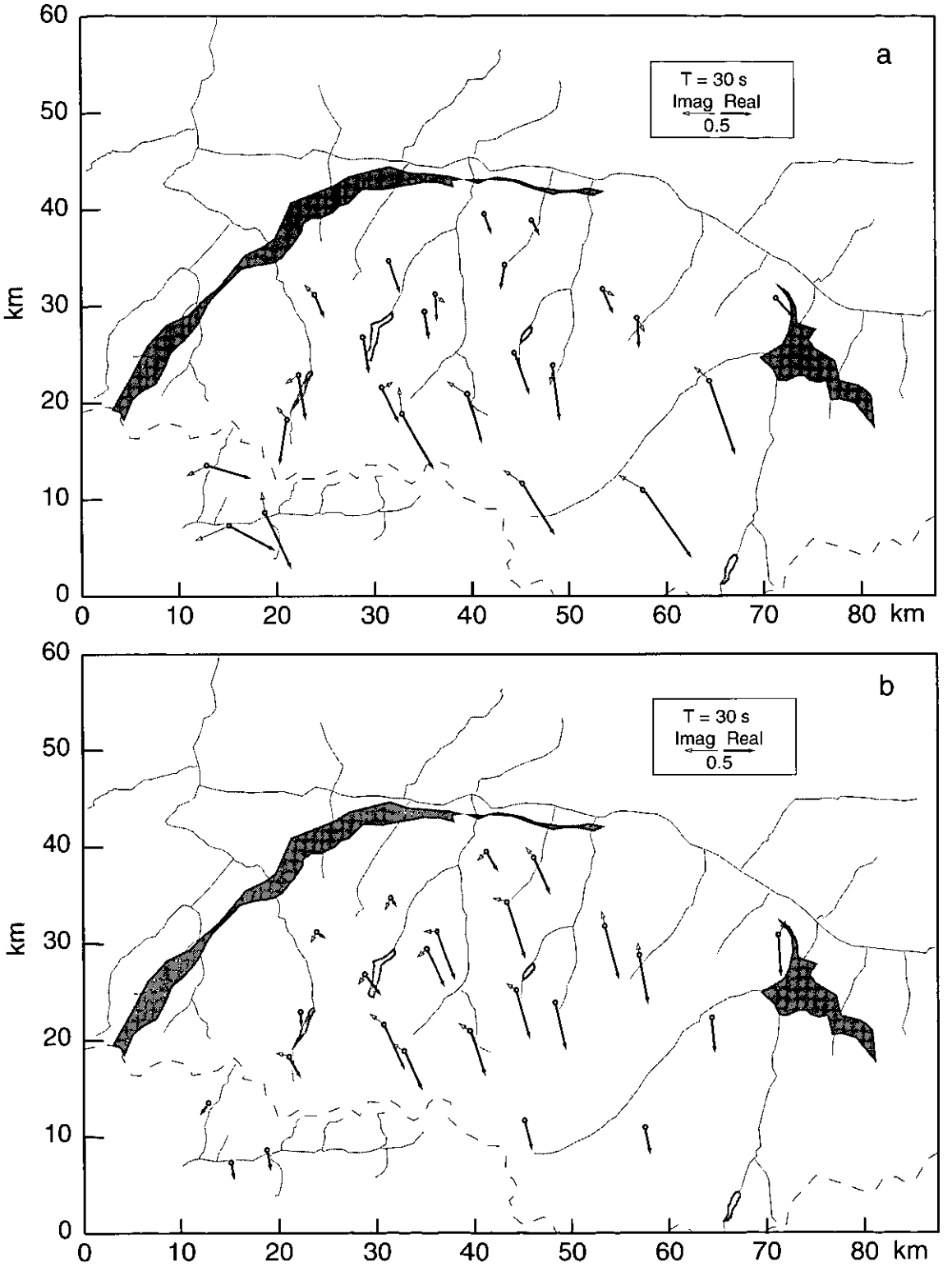

Figure 3.7(cont.) Measured (a) and calculated (3D model) (b) real and imaginary induction arrows at period of 30 sec.

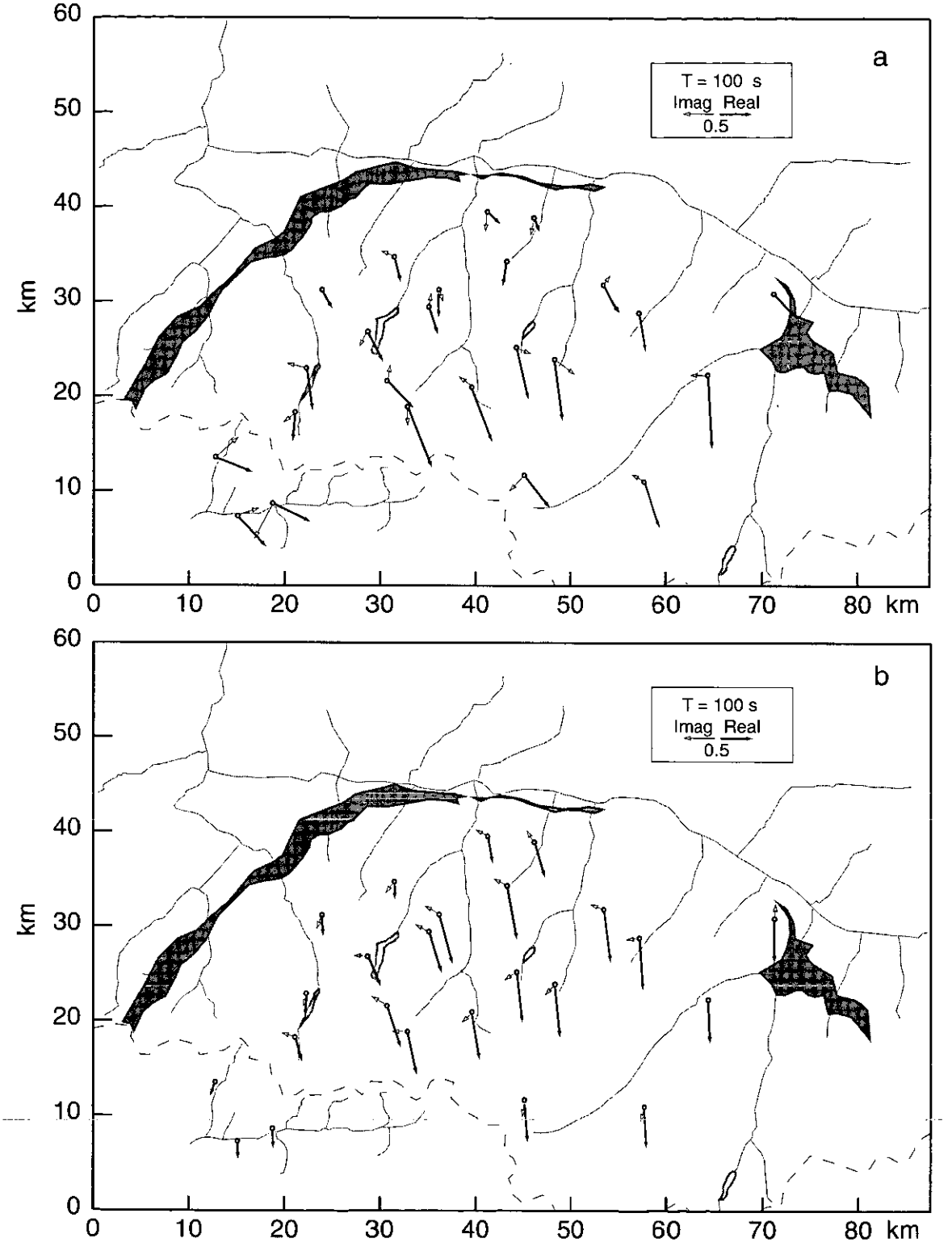

Figure 3.7(cont.) Measured (a) and calculated (3D model) (b) real and imaginary induction arrows at period of 100 sec.

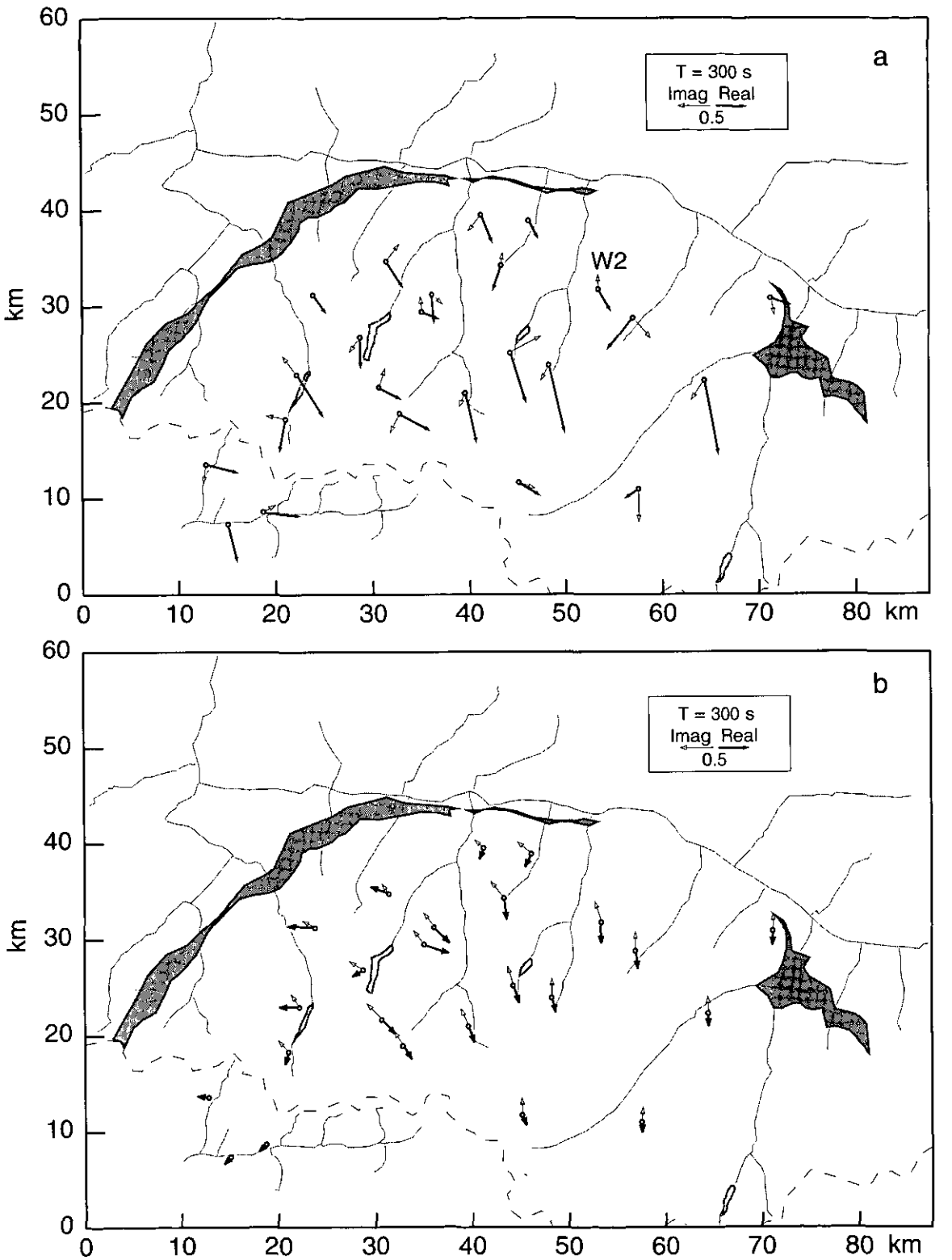

Figure 3.7(end) Measured (a) and calculated (3D model) (b) real and imaginary induction arrows at period of 300 sec.

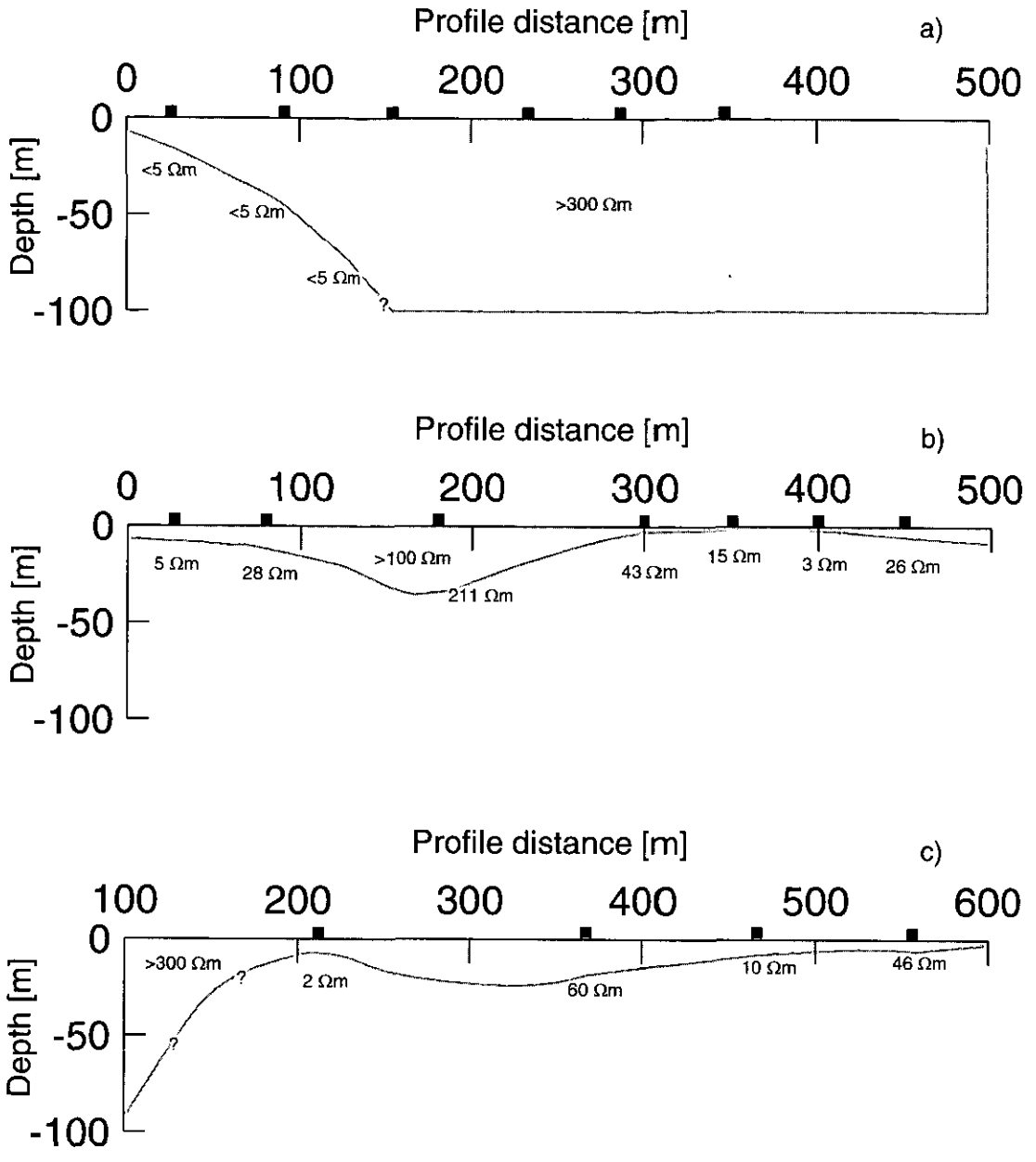

Figure 3.8 Resistivity model along VLF profile 1-3 (a-c). The filled squares represent the location of the VLF measurements. The low resistivity of the second layer indicates the presence of a very good conductor close to the surface. The profile origins are shown on Fig. 2.9 (opposite to arrow head).

Below this layer material of much higher conductivity is found, with resistivities of only a few Ωm. At the western end of profile 1, very low resistivity values were challenging for our VLF receiver, as the measured electric field almost vanished. Intermediate resistivity values (10 Ωm < ρ <100 Ωm) must be understood as averages of extremely low and high resistivities produced by a discontinuous subsurface distribution of black shale horizons. The detailed mapping of the area is not of particular interest here. Obviously, these VLF soundings shows that one can expect very high conductivities in the Zone Houillère, even at the surface.

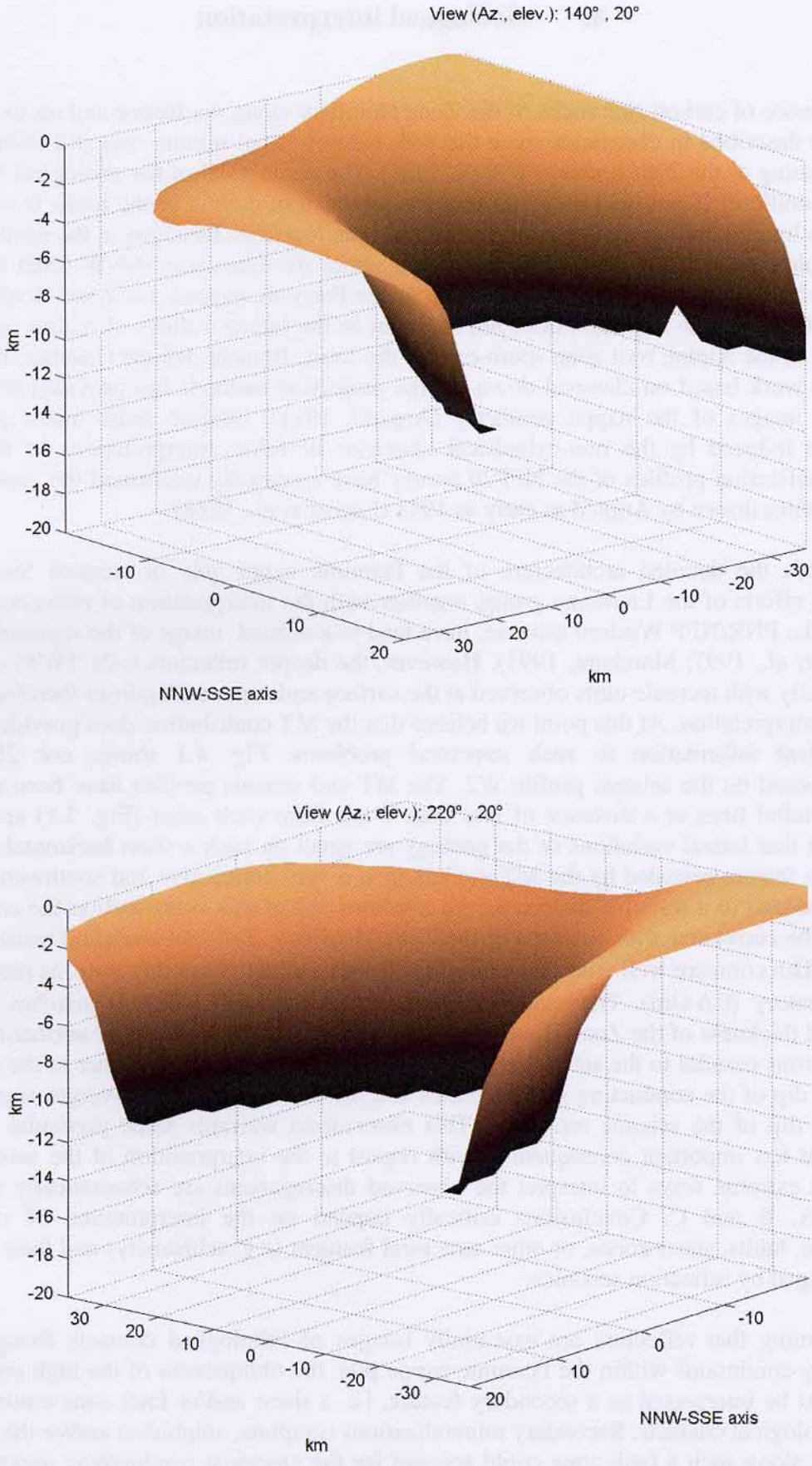

Figure 3.9 3D MT/GDS final model. The coloured form represents the high-conducting (0.2 Ωm) part of the model. The conductor thickness is fixed to 1000 m. The resistivity of the rock matrix above and below the conductor range between 2000 and 7000 Ωm.

4. Geological interpretation

The presence of carbon-rich rocks of the Zone Houillère along the Rhone and on its left bank has been described in chronicles since the 16th century. Coal mining was still flourishing at the beginning of the 20th century (Wehrli, 1925). The name itself of the geological formation "Zone Houillère" (Coal belt) indicates that the presence of carbon in the rocks is noticeable. While its longitudinal extension reaches 200 km (outcrop from Briançon in the south-west, to the Simplon pass in the east), little is known about its transverse (NNW-SSE) extent. In accord with the general large scale structure of the Penninic nappes, the Zone Houillère dips beneath the Penninic Alps and does not crop out in the lateral valleys of Valais nor does it reappear in the Alpine root zone south-east of the Dent. Blanche Klippe (Insubric backfold). Previous work based on classical down-plunge projection methods has provided remarkably accurate images of the nappe geometry (Argand, 1911). Despite some minor projection problems induced by the non-cylindrical character of folds, interpretations of the recent seismic reflection profiles of the NFP20 survey have essentially confirmed the general large scale profiles drawn by Argand as early as 1911 (Escher et al., 1988).

As regards the detailed architecture of the Penninic nappe pile in western Switzerland, mapping efforts of the Lausanne group, together with the interpretation of reflection seismic lines of the PNR/NFP Western traverse, have lead to a refined image of the regional geology (Escher et al., 1997; Marchant, 1993). However, the deeper reflectors (>2s TWT) cannot be tied directly with tectonic units observed at the surface and some ambiguities therefore remain in their interpretation. At this point we believe that the MT contribution does provide new and independent information to such structural problems. Fig. 4.1 shows our 2D model superimposed on the seismic profile W2. The MT and seismic profiles have been measured along parallel lines at a distance of less than 7 km from each other (Fig. 3.1) and we are confident that lateral variations of the geology are small on such a short horizontal distance. The main feature revealed by the MT modelling is a very conductive and southward dipping slab embedded in a resistive matrix. At the northern end of this cross-section the conducting slab can be correlated with outcrops of the Zone Houillère. The low modelled resistivities of only 0.2 Ωm compare well with those of selected rock samples from this zone, as measured in the laboratory (0.6 Ωm). The modelled thickness of this slab (~1 km) matches the total estimated thickness of the Zone Houillère (Escher et al., 1997). In its upper northern segment this slab runs parallel to the seismic reflectors. However, some 10 km further to the south the apparent dip of the conducting slab increases and the model conductor diverges significantly from the dip of the seismic reflectors. This observation warrants some particular attention because it has important consequences with regard to the interpretation of the seismic line. Different extreme ways to interpret the observed discrepancies are schematically shown in Fig. 4.2A, B and C. Conclusions critically depend on the interpretation of reflectors, conductor, faults, shear zones, or other structural features (e.g. schistosity) and their potential to be imaged by reflection seismics.

A) Assuming that reflectors are essentially images of lithological contacts thought to be regionally continuous within the Penninic nappe pile, the obliqueness of the high condutivity zone must be interpreted as a secondary feature, i.e. a shear and/or fault zone cutting across such lithological contacts. Secondary mineralizations (graphite, sulphides) and/or the presence of brines along such a fault zone could account for the electrical conductivity anomaly (Fig. 4.2A).

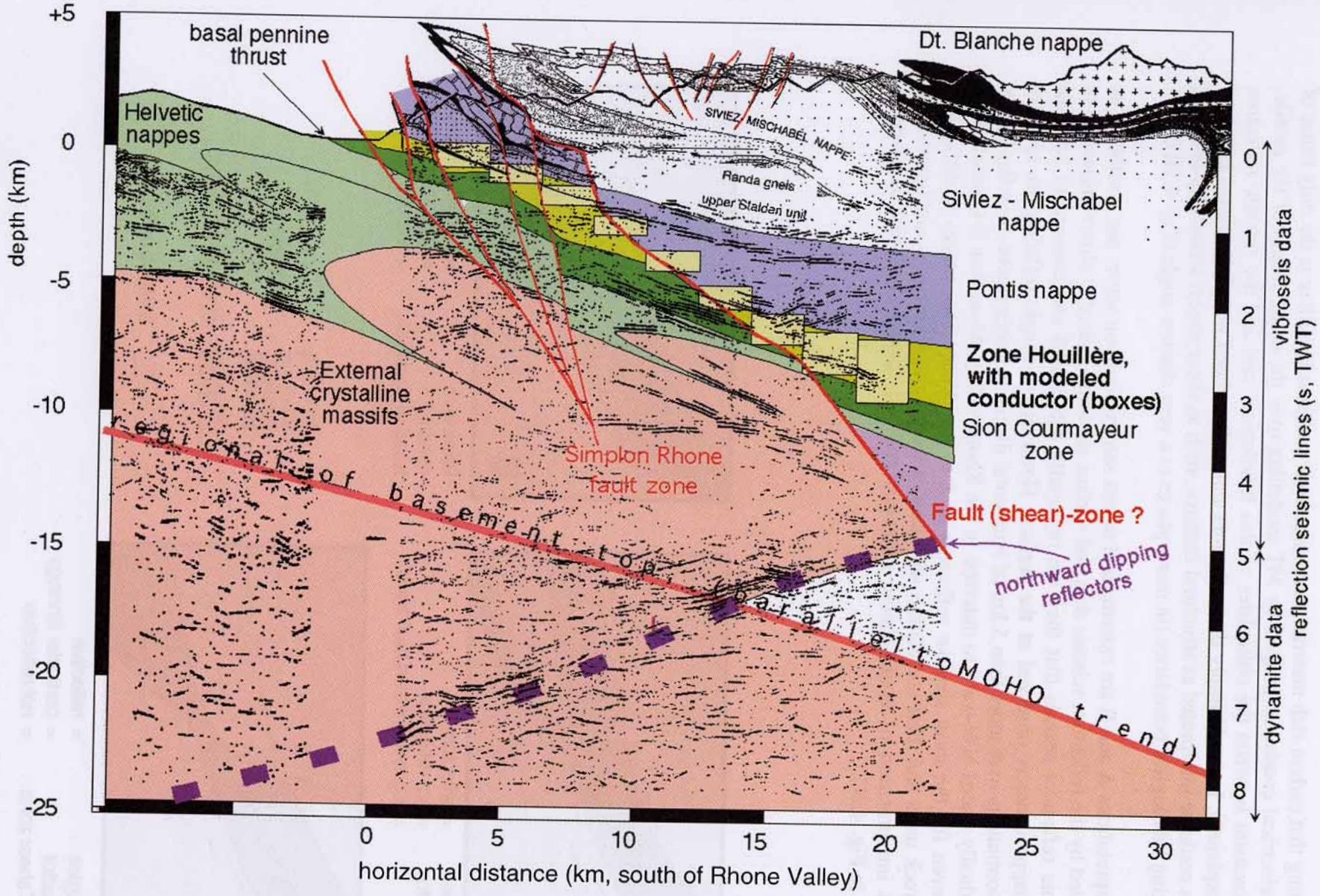

Figure 4.1 Interpreted geologic cross section in Central Valais. South of the Rhone valley, observed surface geology is taken from Escher et al. 1997 (Fig. 16-5, NFP 20 Atlas) and Escher 1988 (Fig.2). The modeled electric conductor is shown in yellow boxes and interpreted as southward continuation of the Zone Houillère. Reflection seismic data are according to NFP20 Atlas. An average velocity of 6 km/s has been used to establish the correlation between depth (scale in km to the left hand side) and TWT (scale in seconds on right hand side). Reflectors within the topmost 4 s are from vibroseis experiments whereas dynamite data have been used for the deeper parts. Note the obliquity between the electric conductor (Zone Houillère) and the general trend of seismic reflectors, south of the Rhone valley. For alternative geologic interpretations of the same seismic sections, see NFP 20 Atlas (Pfiffner et al. 1997).

B) Assuming that carbon-rich material stemming from the Zone Houillère is the only cause of the good electrical conductor imaged by MT modelling over the entire length of the profile, the disagreement betwenn the obliquities of this lithological unit and the seismic reflectors must be explained. It would imply that reflectors cannot be related with lithological contacts. Reflectors could be interpreted as structural features, such as shear zones, schistosity or faults, cross-cutting lithological boundaries (in many places at a very shallow angle (Fig. 4.2B).

Both interpretations A and B are extreme and do not satisfy common sense, nor is either A or B supported by the reflection seismic data and surface geology. Indeed, a closer inspection of the seismic reflectors reveals that they are regionally subparallel and concordant with the general nappe contacts observed at the surface. However, no single reflector, or reflector band, is continuous over more than 5 km of horizontal distance. Furthermore, no reflector can be individually traced NW-ward to outcrops in the Rhone valley. More than 5 kilometers are missing even for the most shallow reflectors at 2 to 4 s TWT. This makes it difficult to identify rock units and their correlation with known tectonic units remains ambiguous. Our preferred interpretation of both seismic reflectors and MT model conductor is therefore sketched in Fig. 4.2C :

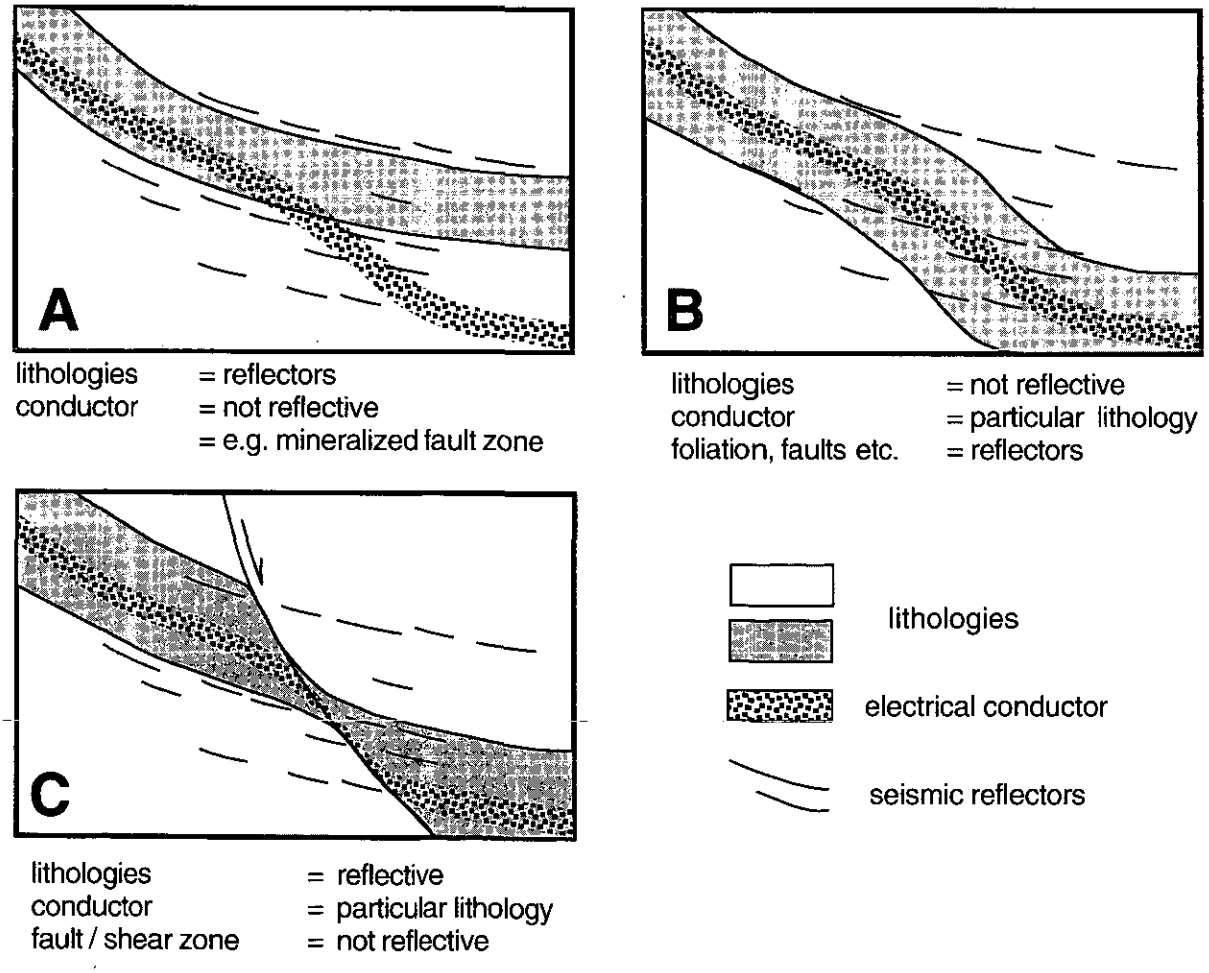

F igure 4.2 Three geological interpretations of the seismic reflector / conductor discrepancy.

C) Assuming that the electrical conductor is due to a single lithology (the Zone Houillère), the modelled depth of this unit across the profile allows to trace it down to 10 km depth, about 20 km to the south of its outcrop in the Rhone valley. The obvious shear between conductor and reflectors midway across this section is interpreted as due to a major shear zone (normal fault geometry) dragging down lithological contacts to the south. The shear zone itself and its associated faults do not show up as seismic reflectors. The conductor, on the other hand, still appears as continuous in the MT model, because slivers of carbon-rich rocks of the Zone Houillère (e.g. very low competency coals and anthracite) would have been smeared out, or scattered, along such a shear zone and/or fault plane.

This interpretation (Figs. 4.1 & 4.2C) is slightly different from previous ones (compare (Marchant, 1993) and (Escher et al., 1997). All interpretations include a Rhone-Simplon normal fault zone which cuts at a steep angle through the frontal Penninic units close to the Rhone valley to level out at depth of approximately 5 to 10 km where this fault zone is thought to run sub-parallel to the basal Penninic nappe contacts (and reflectors). Our MT model suggests that a significant normal fault- (or shear-) zone does offset the Zone Houillère at about 10 km south of the Rhone valley, i.e. below the Siviez-Mischabel nappe. The latter does not show any appreciable effect of this fault, which may have a stair case geometry. If this fault is correlated with the Simplon-Rhone fault zone, the latter would have a much shallower depth (and more southerly position) than previously thought in this part of the Penninic nappe pile. Our interpretation (Fig. 4.1) opens new questions about the nature of reflectors and volumes above and below the Zone Houillère.

It is also worth mentioning that the overall length of the modelled electric conductor is about 20 km. This means that the Zone Houillère ends at about 20 km south of the Rhone valley at a depth of roughly 10 km. The southern termination coincides with the approximate position of the topmost northward dipping reflectors seen on the seismic line. Note that the nature and actual location of these reflectors is still a matter of debate. Our Fig. 4.1 shows stacked, non-migrated data and migration would considerably change the position of these reflectors to a position further south. Whereas the Lausanne group (Escher et al., 1997; Marchant, 1993) interpret these reflectors as the inverted limb of a major backfold at the southern edge of the external crystalline massifs, other authors prefer a crustal scale retro-wedge interpretation (following the French ECORS interpretation, e.g. Mugnier et al., 1990). Whatever model is preferred, the MT modelling results do not support a downward continuation of a high conductivity zone, i.e. the Zone Houillère below northward dipping reflectors.

The results of the 3D modelling (Figs. 3.5 & 3.9) must be regarded as semi-quantitative only since many simplifications were required to ease the computing task (constant thickness and resistivity of the slab). The fit of the model response to the measured data is not as good as for the 2D model. However the model clearly shows that the shape of the conducting slab strongly departs from a cylindrical geometry and closely matches the uppermost crustal boundary (B), as determined with the seismic lines (Valasek and Müller, 1997). There is no doubt that the real shape of the conducting body is more complicated than can be described by our 3D model. In particular, transverse discontinuities of the conductivity, which are likely to exist along paths which cross numerous faults, cannot be accounted for by our simple representation using continuous polynomial functions. However, the general trend of the conducting body should not differ significantly from reality, since it displays the same curvature as the Alpine arc and shows a marked depression, matching the large scale geometry of tectonic units bordering features such as the external crystalline massif domes and the Rawil saddle to the NW and the Insubric backfold to the south-east.

APPENDIX 1

Table of MT impedance tensor in the measuring axes, corrected for instrumental response

Content:
title line:
abbreviation, coordinates, site name
1st line:
period(s), real part of Zxx, Zxy, Zyx, Zyy
2nd line:
imaginary part of Zxx, Zxy, Zyx, Zyy
3rd line:
standard errors on log10(ρxy),ϕxy, log10(ρyx),ϕyx (angles in rad)

ZIN 614890. 106780. Zinal

.552E+0	-.166E+3	.229E+3	-.887E+2	.629E+3
	-.862E+2	.134E+3	-.101E+3	.235E+3
	.439E-1	.129E-1	.133E+0	.413E-1
.690E+0	-.174E+3	.178E+3	-.788E+2	.530E+3
	-.715E+2	.140E+3	-.964E+2	.242E+3
	.531E-1	.158E-1	.145E+0	.455E-1
.867E+0	-.161E+3	.122E+3	-.545E+2	.436E+3
	-.714E+2	.127E+3	-.106E+3	.215E+3
	.713E-1	.214E-1	.157E+0	.496E-1
.108E+1	-.152E+3	.729E+2	-.342E+2	.351E+3
	-.681E+2	.121E+3	-.105E+3	.213E+3
	.932E-1	.284E-1	.175E+0	.559E-1
.138E+1	-.131E+3	.383E+2	-.592E+1	.247E+3
	-.700E+2	.115E+3	-.970E+2	.180E+3
	.981E-1	.299E-1	.181E+0	.579E-1
.179E+1	-.971E+2	.304E+2	.268E+2	.203E+3
	-.571E+2	.110E+3	-.797E+2	.165E+3
	.110E+0	.338E-1	.219E+0	.719E-1
.234E+1	-.689E+2	.325E+2	.301E+2	.167E+3
	-.548E+2	.881E+2	-.555E+2	.143E+3
	.111E+0	.340E-1	.233E+0	.765E-1
.304E+1	-.547E+2	.296E+2	.381E+2	.149E+3
	-.433E+2	.798E+2	-.375E+2	.133E+3
	.137E+0	.428E-1	.304E+0	.105E+0
.392E+1	-.316E+2	.416E+2	.360E+2	.130E+3
	-.423E+2	.579E+2	-.323E+2	.105E+3
	.142E+0	.444E-1	.287E+0	.977E-1
.506E+1	-.266E+2	.378E+2	.191E+2	.102E+3
	-.358E+2	.480E+2	-.326E+2	.855E+2
	.141E+0	.441E-1	.303E+0	.104E+0
.639E+1	-.206E+2	.398E+2	.123E+2	.886E+2
	-.282E+2	.433E+2	-.153E+2	.884E+2
	.143E+0	.448E-1	.474E+0	.181E+0
.810E+1	-.199E+2	.341E+2	.870E+1	.757E+2
	-.239E+2	.363E+2	-.171E+2	.717E+2
	.128E+0	.399E-1	.386E+0	.140E+0
.101E+2	-.173E+2	.329E+2	.476E+1	.606E+2
	-.209E+2	.316E+2	-.167E+2	.624E+2
	.154E+0	.485E-1	.450E+0	.170E+0
.121E+2	-.161E+2	.311E+2	.796E+1	.582E+2
	-.177E+2	.283E+2	-.180E+2	.513E+2
	.159E+0	.503E-1	.374E+0	.134E+0
.157E+2	-.140E+2	.277E+2	.562E+1	.462E+2
	-.189E+2	.180E+2	-.261E+2	.288E+2
	.174E+0	.552E-1	.265E+0	.893E-1
.203E+2	-.100E+2	.280E+2	.821E+1	.446E+2
	-.166E+2	.123E+2	-.179E+2	.288E+2
	.164E+0	.519E-1	.305E+0	.105E+0
.256E+2	-.109E+2	.235E+2	.849E+1	.399E+2
	-.147E+2	.959E+1	-.192E+2	.201E+2
	.213E+0	.695E-1	.278E+0	.941E-1
.324E+2	-.877E+1	.252E+2	.877E+1	.355E+2
	-.913E+1	.931E+1	-.965E+1	.249E+2
	.175E+0	.558E-1	.367E+0	.131E+0
.405E+2	-.148E+2	.151E+2	.180E+1	.221E+2
	-.107E+2	.360E+1	-.125E+2	.158E+2
	.299E+0	.103E+0	.397E+0	.145E+0
.486E+2	-.127E+2	.177E+2	.299E+1	.229E+2
	-.395E+1	.774E+1	-.489E+1	.186E+2
	.178E+0	.567E-1	.495E+0	.192E+0
.486E+2	-.114E+2	.177E+2	.462E+1	.239E+2
	-.403E+1	.721E+1	-.395E+1	.198E+2
	.179E+0	.571E-1	.477E+0	.183E+0
.627E+2	-.111E+2	.175E+2	.494E+1	.238E+2
	-.220E+1	.562E+1	-.254E+1	.164E+2
	.214E+0	.696E-1	.567E+0	.230E+0
.845E+2	-.986E+1	.163E+2	.464E+1	.217E+2
	-.359E+1	-.271E+1	-.337E+1	.940E+1
	.180E+0	.577E-1	.447E+0	.168E+0
.121E+3	-.107E+2	.117E+2	.246E+1	.157E+2
	-.244E+1	-.622E+1	-.137E+1	.539E+1
	.255E+0	.850E-1	.598E+0	.324E+0
.177E+3	-.155E+2	.625E+1	.165E+1	.143E+2
	.184E+1	-.873E+1	-.350E+0	.369E+1
	.463E+0	.176E+0	.599E+0	.743E+0

BOS 619960. 115370. Turtmanntal

.552E+0	-.734E+2	-.305E+2	-.995E+2	-.549E+2
	-.605E+2	.728E+2	-.182E+3	.862E+2
	.703E-1	.211E-1	.364E-1	.107E-1
.690E+0	-.703E+2	-.312E+2	-.837E+2	-.550E+2
	-.630E+2	.704E+2	-.163E+3	.893E+2
	.713E-1	.214E-1	.385E-1	.113E-1
.867E+0	-.619E+2	-.363E+2	-.796E+2	-.657E+2
	-.642E+2	.688E+2	-.148E+3	.965E+2
	.745E-1	.224E-1	.376E-1	.111E-1
.108E+1	-.495E+2	-.360E+2	-.713E+2	-.626E+2
	-.595E+2	.671E+2	-.133E+3	.780E+2
	.796E-1	.240E-1	.420E-1	.124E-1
.138E+1	-.363E+2	-.312E+2	-.594E+2	-.521E+2
	-.458E+2	.722E+2	-.113E+3	.580E+2
	.740E-1	.223E-1	.407E-1	.120E-1
.179E+1	-.253E+2	-.220E+2	-.529E+2	-.444E+2
	-.384E+2	.613E+2	-.978E+2	.352E+2
	.978E-1	.297E-1	.453E-1	.133E-1
.234E+1	-.151E+2	-.104E+2	-.406E+2	-.264E+2
	-.266E+2	.581E+2	-.779E+2	.256E+2
	.833E-1	.251E-1	.457E-1	.135E-1
.304E+1	-.994E+1	-.424E+1	-.344E+2	-.191E+2
	-.233E+2	.460E+2	-.646E+2	.179E+2
	.113E+0	.348E-1	.579E-1	.172E-1
.392E+1	-.779E+1	-.370E+1	-.291E+2	-.123E+2
	-.206E+2	.338E+2	-.542E+2	.854E+1
	.131E+0	.404E-1	.503E-1	.149E-1
.506E+1	.173E+1	.113E+2	-.233E+2	-.518E+1
	-.132E+2	.357E+2	-.432E+2	.831E+1
	.126E+0	.391E-1	.697E-1	.209E-1
.639E+1	.171E+1	.808E+1	-.213E+2	-.366E+1
	-.102E+2	.315E+2	-.358E+2	.527E+1
	.117E+0	.360E-1	.681E-1	.204E-1
.810E+1	.185E+1	.585E+1	-.198E+2	-.324E+1
	-.959E+1	.241E+2	-.289E+2	.396E+1
	.112E+0	.344E-1	.607E-1	.181E-1
.101E+2	.197E+1	.404E+1	-.184E+2	-.365E+1
	-.727E+1	.221E+2	-.249E+2	.618E+0
	.164E+0	.520E-1	.856E-1	.258E-1
.121E+2	.179E+1	.205E+1	-.174E+2	-.190E+1
	-.943E+1	.137E+2	-.210E+2	.128E+1
	.223E+0	.729E-1	.775E-1	.233E-1
.157E+2	.344E+1	.190E+1	-.150E+2	-.101E+1
	-.129E+2	.126E+1	-.179E+2	-.195E+1
	.599E+0	.329E+0	.551E-1	.164E-1
.203E+2	.459E+1	.318E+1	-.146E+2	-.203E-1
	-.719E+1	.756E+1	-.129E+2	.105E+0
	.266E+0	.897E-1	.573E-1	.171E-1
.256E+2	.439E+1	.245E+1	-.139E+2	.268E-1
	-.420E+1	.110E+2	-.951E+1	.150E+1
	.197E+0	.638E-1	.768E-1	.231E-1
.324E+2	.445E+1	.704E+0	-.132E+2	-.134E+0
	-.479E+1	.728E+1	-.667E+1	.176E+1
	.218E+0	.714E-1	.716E-1	.214E-1
.405E+2	.579E+1	.233E+1	-.132E+2	-.185E-1
	-.402E+1	.697E+1	-.488E+1	.107E+1
	.250E+0	.834E-1	.950E-1	.289E-1
.486E+2	.608E+1	.231E+1	-.136E+2	-.134E+1
	-.524E+1	.374E+1	-.440E+1	.785E+0
	.327E+0	.115E+0	.903E-1	.274E-1
.486E+2	.621E+1	.237E+1	-.136E+2	-.150E+1
	-.547E+1	.333E+1	-.394E+1	.233E+1
	.272E+0	.921E-1	.929E-1	.282E-1
.627E+2	.611E+1	.112E+1	-.138E+2	-.283E+1
	-.443E+1	.271E+1	-.141E+1	.262E+1
	.282E+0	.960E-1	.101E+0	.308E-1
.845E+2	.622E+1	.257E+1	-.128E+2	-.427E+1
	-.323E+1	.341E+1	-.170E+1	-.921E+0
	.256E+0	.855E-1	.154E+0	.486E-1
.121E+3	.561E+1	.164E+1	-.116E+2	-.308E+1
	-.364E+1	.354E+1	.222E+1	-.185E+1
	.356E+0	.127E+0	.182E+0	.582E-1
.177E+3	.582E+1	.769E+0	-.931E+1	-.396E+1
	-.238E+1	.452E+1	.649E+0	-.462E+1
	.535E+0	.213E+0	.308E+0	.107E+0

MOY 610790. 105890. Moiry

.552E+0	-.382E+2	.165E+2	-.648E+2	.238E+2
	-.107E+2	.228E+2	-.966E+1	.295E+2
	.644E-1	.192E-1	.427E-1	.126E-1
.690E+0	-.409E+2	.107E+2	-.671E+2	.106E+2
	-.912E+1	.167E+2	-.479E+1	.231E+2
	.934E-1	.284E-1	.439E-1	.129E-1
.867E+0	-.387E+2	.575E+1	-.653E+2	.980E+0
	-.831E+1	.133E+2	-.632E+0	.189E+2
	.130E+0	.404E-1	.471E-1	.140E-1
.108E+1	-.347E+2	.975E+0	-.601E+2	-.714E+1
	-.814E+1	.151E+2	-.201E+1	.224E+2
	.133E+0	.413E-1	.554E-1	.165E-1
.138E+1	-.254E+2	-.185E+0	-.466E+2	-.879E+1
	-.921E+1	.156E+2	-.673E+1	.219E+2
	.116E+0	.356E-1	.630E-1	.188E-1
.179E+1	-.177E+2	.467E+0	-.350E+2	-.697E+1
	-.867E+1	.165E+2	-.945E+1	.229E+2
	.112E+0	.345E-1	.840E-1	.253E-1
.234E+1	-.116E+2	.160E+1	-.233E+2	-.311E+1
	-.733E+1	.144E+2	-.900E+1	.196E+2
	.108E+0	.332E-1	.952E-1	.290E-1
.304E+1	-.685E+1	.410E+1	-.150E+2	.112E+1
	-.674E+1	.114E+2	-.852E+1	.158E+2
	.123E+0	.380E-1	.129E+0	.401E-1
.392E+1	-.325E+1	.529E+1	-.898E+1	.336E+1
	-.576E+1	.857E+1	-.860E+1	.108E+2
	.111E+0	.340E-1	.129E+0	.401E-1
.506E+1	-.294E+1	.469E+1	-.759E+1	.306E+1
	-.499E+1	.764E+1	-.802E+1	.920E+1
	.105E+0	.321E-1	.121E+0	.373E-1
.639E+1	-.329E+1	.329E+1	-.708E+1	.248E+1
	-.387E+1	.679E+1	-.641E+1	.781E+1
	.125E+0	.389E-1	.136E+0	.427E-1
.810E+1	-.279E+1	.341E+1	-.585E+1	.294E+1
	-.264E+1	.642E+1	-.489E+1	.717E+1
	.116E+0	.356E-1	.147E+0	.461E-1
.101E+2	-.256E+1	.288E+1	-.498E+1	.248E+1
	-.279E+1	.520E+1	-.526E+1	.505E+1
	.150E+0	.472E-1	.170E+0	.538E-1
.121E+2	-.172E+1	.317E+1	-.491E+1	.231E+1
	-.239E+1	.430E+1	-.472E+1	.398E+1
	.128E+0	.398E-1	.139E+0	.435E-1
.157E+2	-.125E+1	.281E+1	-.299E+1	.361E+1
	-.247E+1	.291E+1	-.387E+1	.253E+1
	.106E+0	.326E-1	.114E+0	.352E-1
.203E+2	-.128E+1	.148E+1	-.274E+1	.193E+1
	-.174E+1	.255E+1	-.274E+1	.282E+1
	.126E+0	.390E-1	.132E+0	.412E-1
.256E+2	-.956E+0	.143E+1	-.252E+1	.195E+1
	-.113E+1	.236E+1	-.209E+1	.232E+1
	.131E+0	.408E-1	.147E+0	.463E-1
.324E+2	-.102E+1	.126E+1	-.215E+1	.175E+1
	-.683E+0	.229E+1	-.106E+1	.272E+1
	.122E+0	.378E-1	.178E+0	.566E-1
.405E+2	-.108E+1	.962E+0	-.204E+1	.154E+1
	-.586E+0	.198E+1	-.980E+0	.227E+1
	.151E+0	.474E-1	.228E+0	.750E-1
.486E+2	-.854E+0	.100E+1	-.173E+1	.183E+1
	-.547E+0	.119E+1	-.710E+0	.130E+1
	.206E+0	.669E-1	.242E+0	.808E-1
.486E+2	-.950E+0	.800E+0	-.193E+1	.152E+1
	-.670E+0	.103E+1	-.899E+0	.109E+1
	.266E+0	.895E-1	.209E+0	.678E-1
.627E+2	-.919E+0	.554E+0	-.196E+1	.867E+0
	-.542E+0	.677E+0	-.101E+1	.391E+0
	.327E+0	.114E+0	.216E+0	.706E-1
.845E+2	-.108E+1	.313E+0	-.212E+1	.834E+0
	-.255E+0	.431E+0	-.581E+0	.247E+0
	.565E+0	.229E+0	.209E+0	.682E-1
.121E+3	-.115E+1	.455E+0	-.219E+1	.838E+0
	-.342E-1	.116E+0	-.144E+0	-.131E-2
	.597E+0	.346E+0	.275E+0	.930E-1
.177E+3	-.102E+1	.328E+0	-.191E+1	.127E+1
	.442E+0	.455E-2	.635E+0	-.648E+0
	.598E+0	.529E+0	.314E+0	.109E+0

CLE 589990. 109060. Cleuson

.552E+0	.237E+1	.307E+1	-.665E+1	-.418E+1
	.465E+1	.916E+1	-.724E+1	.154E+0
	.912E-1	.276E-1	.821E-1	.250E-1
.690E+0	.163E+1	.386E+1	-.511E+1	-.366E+1
	.359E+1	.912E+1	-.596E+1	-.889E+0
	.886E-1	.268E-1	.103E+0	.314E-1
.867E+0	.128E+1	.253E+1	-.384E+1	-.297E+1
	.344E+1	.850E+1	-.449E+1	-.367E+0
	.989E-1	.301E-1	.141E+0	.441E-1
.108E+1	.144E+1	.272E+1	-.348E+1	-.302E+1
	.263E+1	.783E+1	-.390E+1	-.103E+1
	.110E+0	.339E-1	.169E+0	.538E-1
.138E+1	.726E+0	.152E+1	-.211E+1	-.144E+1
	.167E+1	.739E+1	-.301E+1	-.790E+0
	.109E+0	.335E-1	.219E+0	.719E-1
.179E+1	-.744E+0	.770E+0	-.122E+1	-.115E+1
	.101E+1	.546E+1	-.276E+1	.270E+0
	.156E+0	.492E-1	.271E+0	.916E-1
.234E+1	-.112E+1	.875E+0	-.276E-1	-.125E+1
	.430E+0	.495E+1	-.234E+1	.164E+0
	.143E+0	.448E-1	.270E+0	.910E-1
.304E+1	-.156E+1	-.585E-1	.970E-1	-.139E+0
	-.266E+0	.375E+1	-.240E+1	.193E+0
	.207E+0	.674E-1	.278E+0	.944E-1
.392E+1	-.156E+1	-.348E+0	.245E+0	.781E-2
	-.499E+0	.211E+1	-.142E+1	.393E+0
	.343E+0	.121E+0	.422E+0	.157E+0
.506E+1	-.116E+1	.335E+0	.348E+0	-.801E-1
	-.389E+0	.221E+1	-.144E+1	.308E-1
	.316E+0	.110E+0	.384E+0	.139E+0
.639E+1	-.157E+1	-.479E-1	.139E+0	-.159E+0
	-.510E+0	.228E+1	-.126E+1	-.524E+0
	.321E+0	.112E+0	.435E+0	.163E+0
.810E+1	-.684E+0	.359E+0	-.547E-2	.700E-1
	-.689E-1	.214E+1	-.104E+1	-.212E+0
	.275E+0	.930E-1	.435E+0	.162E+0
.101E+2	-.404E+0	.249E+0	-.310E+0	.113E+0
	-.473E+0	.164E+1	-.527E+0	.102E+0
	.376E+0	.135E+0	.598E+0	.289E+0
.121E+2	-.939E+0	-.147E+0	.217E+0	.358E+0
	-.466E+0	.137E+1	-.401E+0	-.196E+0
	.399E+0	.146E+0	.598E+0	.368E+0
.157E+2	-.353E+0	.511E+0	-.216E-1	.128E+0
	-.785E+0	.811E+0	-.857E-1	.269E+0
	.576E+0	.236E+0	.597E+0	.191E+1
.203E+2	-.438E+0	.394E+0	-.149E-1	-.110E+0
	-.375E+0	.852E+0	-.160E+0	-.281E-1
	.515E+0	.202E+0	.598E+0	.873E+0
.256E+2	-.254E+0	.183E+0	.104E+0	.191E+0
	-.557E-2	.836E+0	-.355E+0	-.997E-1
	.586E+0	.242E+0	.598E+0	.407E+0
.324E+2	-.238E+0	.411E+0	-.565E-1	-.816E-1
	-.115E+0	.726E+0	-.166E+0	.237E-1
	.549E+0	.221E+0	.598E+0	.810E+0

.405E+2	.531E-1	.684E+0	-.214E+0	-.207E+0
	.288E+0	.969E+0	-.392E+0	-.284E+0
	.450E+0	.170E+0	.599E+0	.315E+0
.486E+2	-.131E+0	.446E+0	-.114E+0	-.154E+0
	-.246E+0	.229E+0	-.137E-1	.661E-1
	.597E+0	.372E+0	.599E+0	.125E+1
.486E+2	.956E-3	.691E+0	-.416E+0	-.553E+0
	-.260E+0	.375E+0	-.409E-1	-.626E-1
	.598E+0	.321E+0	.597E+0	.441E+0
.627E+2	.182E+0	.443E+0	-.520E+0	-.390E+0
	-.630E-1	.228E+0	.490E-1	.157E+0
	.598E+0	.466E+0	.597E+0	.338E+0
.845E+2	.399E-1	.234E+0	-.240E+0	-.227E-1
	-.116E+0	.152E+0	.431E-1	.123E+0
	.595E+0	.480E+0	.597E+0	.402E+0
.121E+3	.165E+0	.519E+0	-.131E+0	.666E-1
	.115E+0	.350E+0	-.342E+0	-.414E+0
	.598E+0	.354E+0	.597E+0	.400E+0
.177E+3	.142E+0	-.158E+0	.229E-1	.461E+0
	.106E+0	-.111E-1	-.577E-1	.806E-4
	.598E+0	.211E+1	.599E+0	.334E+1

TRI 594900. 107745. Combe de la Rosette

.116E+1	.349E+0	.788E+1	.134E+1	.700E+1
	.350E+0	.180E+2	.814E+1	.133E+2
	.492E-1	.146E-1	.106E+0	.325E-1
.146E+1	-.432E+0	.588E+1	.122E+0	.509E+1
	-.230E+0	.158E+2	.579E+1	.116E+2
	.559E-1	.167E-1	.139E+0	.434E-1
.183E+1	-.100E+1	.509E+1	-.249E+0	.463E+1
	-.931E+0	.140E+2	.378E+1	.100E+2
	.580E-1	.173E-1	.179E+0	.571E-1
.229E+1	-.118E+1	.478E+1	-.602E+0	.409E+1
	-.717E+0	.122E+2	.292E+1	.948E+1
	.646E-1	.193E-1	.205E+0	.664E-1
.291E+1	-.157E+1	.355E+1	-.602E+0	.370E+1
	-.117E+1	.103E+2	.209E+1	.786E+1
	.656E-1	.196E-1	.214E+0	.699E-1
.377E+1	-.145E+1	.292E+1	-.533E+0	.328E+1
	-.969E+0	.892E+1	.123E+1	.633E+1
	.709E-1	.213E-1	.301E+0	.104E+0
.492E+1	-.138E+1	.231E+1	-.639E+0	.262E+1
	-.149E+1	.672E+1	.662E+0	.541E+1
	.740E-1	.223E-1	.340E+0	.120E+0
.640E+1	-.131E+1	.169E+1	-.654E+0	.208E+1
	-.130E+1	.573E+1	.166E+0	.440E+1
	.972E-1	.296E-1	.470E+0	.179E+0
.826E+1	-.109E+1	.113E+1	-.519E+0	.144E+1
	-.145E+1	.465E+1	.131E+0	.389E+1
	.137E+0	.427E-1	.598E+0	.252E+0
.107E+2	-.956E+0	.679E+0	-.576E+0	.872E+0
	-.147E+1	.347E+1	-.385E+0	.280E+1
	.157E+0	.494E-1	.473E+0	.181E+0
.135E+2	-.807E+0	.598E+0	-.422E+0	.659E+0
	-.144E+1	.287E+1	-.527E+0	.237E+1
	.192E+0	.620E-1	.480E+0	.185E+0
.171E+2	-.602E+0	.441E+0	-.191E+0	.626E+0
	-.160E+1	.179E+1	-.511E+0	.187E+1
	.277E+0	.940E-1	.584E+0	.241E+0
.213E+2	.130E+0	.112E+1	.482E+0	.126E+1
	-.114E+1	.192E+1	-.458E+0	.161E+1
	.237E+0	.785E-1	.525E+0	.206E+0
.256E+2	.149E+0	.888E+0	.491E+0	.104E+1
	-.116E+1	.135E+1	-.628E+0	.120E+1
	.341E+0	.120E+0	.444E+0	.167E+0
.330E+2	.389E+0	.106E+1	.633E-1	.363E+0
	-.113E+1	.897E+0	-.403E+0	.927E+0
	.523E+0	.207E+0	.598E+0	.567E+0
.427E+2	.403E+0	.720E+0	.646E+0	.739E+0
	-.609E+0	.908E+0	-.558E-1	.102E+1
	.448E+0	.169E+0	.598E+0	.255E+0
.539E+2	.133E+1	.168E+1	-.146E+1	-.158E+1
	-.385E+0	.110E+1	.307E+0	.920E+0
	.597E+0	.407E+0	.598E+0	.483E+0
.683E+2	-.932E-1	.304E+0	-.359E+0	-.649E+0
	.560E+0	.176E+1	-.955E+0	-.568E+0
	.598E+0	.380E+0	.599E+0	.625E+0
.853E+2	.660E+0	.112E+1	-.926E+0	-.129E+1
	-.457E+0	.384E+0	.404E-1	.638E+0
	.597E+0	.534E+0	.596E+0	.679E+0
.102E+3	.159E+1	.199E+1	-.133E+1	-.148E+1
	-.336E+1	-.380E+1	.294E+1	.457E+1
	.597E+0	.326E+0	.598E+0	.404E+0
.102E+3	.978E+0	.906E+0	-.703E+0	-.431E+0
	-.117E+1	-.917E+0	.770E+0	.163E+1
	.598E+0	.106E+1	.596E+0	.131E+1
.132E+3	-.386E-1	-.116E+1	.675E-1	.109E+1
	-.211E+0	.123E+1	.373E+0	-.162E+0
	.598E+0	.753E+0	.598E+0	.336E+1
.178E+3	-.176E+1	-.156E+1	.162E+1	.147E+1
	.837E-1	-.228E+0	-.526E+0	.479E+0
	.598E+0	.752E+0	.598E+0	.650E+0
.256E+3	.185E+1	-.124E+0	-.170E+1	.140E+0
	.209E+0	.474E+0	-.338E+0	-.286E+0
	.599E+0	.156E+1	.596E+0	.485E+0
.372E+3	-.208E+1	-.239E+1	.207E+1	.244E+1
	.858E+0	-.955E+0	-.887E+0	.929E+0
	.590E+0	.243E+0	.597E+0	.291E+0

LOU 605397. 113295. Louché

.116E+1	-.143E+1	.866E+1	-.305E+1	-.313E+1
	-.535E+1	.184E+2	-.259E+2	-.113E+1
	.774E-1	.233E-1	.227E-1	.663E-2
.146E+1	-.163E+1	.666E+1	-.203E+1	-.166E+1
	-.484E+1	.146E+2	-.206E+2	-.123E+1
	.985E-1	.300E-1	.236E-1	.689E-2
.183E+1	-.200E+1	.549E+1	-.198E+1	-.156E+1
	-.557E+1	.109E+2	-.161E+2	-.472E+0
	.130E+0	.404E-1	.254E-1	.742E-2
.229E+1	-.103E+1	.496E+1	-.152E+1	-.124E+1
	-.516E+1	.885E+1	-.128E+2	-.432E+0
	.163E+0	.515E-1	.290E-1	.847E-2
.291E+1	-.164E+1	.398E+1	-.146E+1	-.768E+0
	-.512E+1	.584E+1	-.988E+1	.193E+0
	.225E+0	.739E-1	.299E-1	.873E-2
.377E+1	-.201E+1	.257E+1	-.127E+1	-.438E+0
	-.474E+1	.474E+1	-.785E+1	.154E+0
	.307E+0	.106E+0	.352E-1	.103E-1
.492E+1	-.131E+1	.242E+1	-.115E+1	-.236E+0
	-.440E+1	.304E+1	-.623E+1	-.186E-1
	.369E+0	.132E+0	.333E-1	.977E-2
.640E+1	-.110E+1	.201E+1	-.119E+1	-.244E+0
	-.371E+1	.296E+1	-.488E+1	-.135E+0
	.461E+0	.176E+0	.415E-1	.123E-1
.826E+1	-.122E+1	.203E+1	-.955E+0	.195E-1
	-.271E+1	.340E+1	-.379E+1	.136E-1
	.468E+0	.179E+0	.512E-1	.152E-1
.107E+2	.844E-1	.210E+1	-.107E+1	.127E+0
	-.397E+1	.573E+0	-.287E+1	.227E-1
	.597E+0	.332E+0	.592E-1	.176E-1
.135E+2	.495E+0	.548E+0	-.115E+1	.493E-1
	-.253E+1	.191E+1	-.228E+1	-.156E-1
	.598E+0	.409E+0	.687E-1	.205E-1
.171E+2	.672E+0	.248E+1	-.119E+1	.603E-1
	-.348E+1	.186E+0	-.177E+1	.870E-1
	.596E+0	.293E+0	.668E-1	.200E-1
.213E+2	.631E+0	.167E+1	-.119E+1	-.231E-2
	-.192E+1	.521E+0	-.142E+1	.205E+0
	.599E+0	.474E+0	.860E-1	.260E-1
.256E+2	.184E+0	.487E+0	-.118E+1	-.998E-2
	-.102E+1	.131E+1	-.126E+1	.124E+0
	.598E+0	.527E+0	.812E-1	.244E-1
.330E+2	.277E+0	-.219E+0	-.119E+1	.106E+0
	-.147E+1	.720E+0	-.100E+1	.909E-1
	.597E+0	.971E+0	.818E-1	.247E-1
.427E+2	.231E+0	-.498E+0	-.121E+1	-.848E-2
	-.134E+1	-.699E+0	-.900E+0	-.423E-1
	.597E+0	.797E+0	.869E-1	.263E-1
.539E+2	-.123E+1	-.676E+0	-.117E+1	.725E-1
	-.140E+1	.629E+0	-.751E+0	.188E-1
	.598E+0	.713E+0	.978E-1	.298E-1
.683E+2	.104E+1	.551E+0	-.114E+1	.532E-1
	-.571E+0	.698E+0	-.719E+0	-.827E-1
	.598E+0	.605E+0	.910E-1	.277E-1
.853E+2	.579E+0	-.562E+0	-.112E+1	.607E-1
	-.768E+0	-.607E+0	-.659E+0	-.223E-1
	.598E+0	.711E+0	.133E+0	.415E-1
.102E+3	-.657E-2	.939E+0	-.109E+1	.557E-1
	.185E+0	-.154E+0	-.641E+0	.625E-2
	.597E+0	.725E+0	.144E+0	.450E-1
.102E+3	-.277E+0	-.134E+0	-.115E+1	.491E-1
	.388E+0	-.159E+0	-.662E+0	-.645E-1
	.598E+0	.317E+1	.144E+0	.450E-1
.132E+3	.166E+1	-.378E+0	-.931E+0	.418E-1
	.256E+0	.496E+0	-.770E+0	.111E-1
	.598E+0	.123E+1	.167E+0	.531E-1
.178E+3	-.261E+0	.206E-1	-.571E+0	.810E-1
	-.244E+0	-.283E+0	-.811E+0	.509E-1
	.598E+0	.193E+1	.189E+0	.606E-1
.256E+3	-.448E+0	-.325E+0	-.288E+0	.622E-1
	-.275E+0	.513E+0	-.646E+0	-.878E-1
	.598E+0	.701E+0	.230E+0	.756E-1
.372E+3	.331E-1	.101E+0	-.900E-1	.930E-1
	.864E-1	.165E+0	-.285E+0	.749E-2
	.599E+0	.214E+1	.370E+0	.132E+0

ARO 600770. 96000. Montagne d'Arolla

.116E+1	.252E+1	.322E+0	.102E+1	.235E+1
	.293E+0	-.141E+1	.666E+1	.126E+1
	.593E+0	.284E+0	.262E+0	.881E-1
.146E+1	.171E+1	-.798E-2	.149E+1	.220E+1
	.367E+0	-.993E+0	.500E+1	.113E+1
	.587E+0	.359E+0	.322E+0	.112E+0
.183E+1	.225E+0	.357E-1	.147E+1	.139E+1
	.132E+1	.195E+0	.404E+1	.696E+0
	.602E+0	.163E+1	.390E+0	.141E+0
.229E+1	.113E+1	.360E+0	.683E+0	.156E+1
	-.327E+0	-.400E+0	.399E+1	.700E+0
	.602E+0	.535E+0	.408E+0	.150E+0
.291E+1	.505E+0	-.133E+0	.621E+0	.173E+1
	-.160E+0	-.308E+0	.326E+1	.867E+0
	.538E+0	.654E+0	.418E+0	.155E+0
.377E+1	.762E+0	.852E-1	-.253E-1	.837E+0
	-.256E+0	-.387E+0	.218E+1	.743E+0
	.602E+0	.474E+0	.544E+0	.218E+0
.492E+1	.255E-1	-.124E+0	.184E+0	.599E+0
	.197E-2	-.865E-1	.181E+1	.659E+0
	.602E+0	.708E+0	.430E+0	.161E+0
.640E+1	.254E+0	.156E-1	.264E+0	.692E+0
	.119E+0	-.198E+0	.995E+0	.117E+0
	.602E+0	.440E+0	.596E+0	.253E+0
.826E+1	.339E+0	.320E-1	.187E+0	.264E+0
	.266E-1	.382E-1	.908E+0	.325E+0
	.602E+0	.213E+1	.596E+0	.309E+0
.107E+2	.168E+0	-.446E-1	-.546E-1	-.128E+0
	-.116E+0	-.856E-1	.222E+0	.109E+0
	.602E+0	.104E+1	.602E+0	.112E+1
.135E+2	.450E-1	-.111E-1	.180E-1	.533E+0
	-.474E-2	-.307E-1	.779E+0	.348E+0
	.602E+0	.277E+1	.597E+0	.300E+0
.171E+2	.283E-1	.231E-1	-.558E-1	.114E+0
	.974E-2	-.423E-2	.617E+0	.567E+0
	.602E+0	.237E+1	.530E+0	.209E+0
.213E+2	.323E-1	.874E-1	-.178E+0	.217E+0
	.163E-1	.590E-2	.505E+0	.535E+0
	.602E+0	.580E+0	.599E+0	.259E+0
.256E+2	.691E-1	.667E-1	-.415E-1	.174E+0
	.604E-1	-.549E-2	.602E+0	.484E+0
	.602E+0	.682E+0	.597E+0	.248E+0
.330E+2	-.182E-1	.226E-1	.227E+0	.443E+0
	.142E+0	.195E-1	.429E+0	.556E+0
	.602E+0	.385E+1	.599E+0	.498E+0
.427E+2	.322E+0	-.379E-2	.189E+0	-.340E-1
	.846E-1	-.178E-1	.290E+0	-.690E-1
	.602E+0	.514E+1	.598E+0	.816E+0
.539E+2	-.844E-1	.204E-2	-.189E+0	-.379E-1
	-.201E+0	-.148E+0	.466E+0	.990E-1
	.584E+0	.805E+0	.597E+0	.526E+0
.683E+2	-.134E+0	.528E-1	-.120E+0	-.713E-1
	-.113E+0	.129E-1	.479E+0	.118E+0
	.602E+0	.149E+1	.598E+0	.470E+0
.853E+2	-.147E+0	.131E+0	.488E+0	-.154E+0
	-.301E+0	-.163E+0	.498E+0	.363E+0
	.596E+0	.433E+0	.598E+0	.387E+0
.102E+3	-.192E+0	.932E-1	.460E+0	-.710E-1
	.118E+0	-.150E+0	.788E-3	.297E+0
	.602E+0	.547E+0	.598E+0	.596E+0
.102E+3	-.321E+0	-.592E-1	-.593E-2	-.814E-1
	.202E+0	-.112E+0	.227E+0	.973E-1
	.602E+0	.150E+1	.598E+0	.135E+1
.132E+3	.663E-1	.726E-1	.416E+0	-.376E+0
	.248E+0	.839E-2	.772E+0	.309E-1
	.602E+0	.187E+1	.598E+0	.526E+0
.178E+3	-.296E-1	.112E+0	-.280E+0	-.139E+0
	.255E-1	-.427E-1	.224E-1	-.250E+0
	.602E+0	.106E+1	.597E+0	.113E+1
.256E+3	.182E+0	.641E-1	-.277E+0	-.375E+0
	-.187E+0	.102E+0	.823E+0	-.929E-1
	.596E+0	.742E+0	.598E+0	.397E+0
.372E+3	-.237E+0	-.298E-1	-.803E+0	.114E+0
	-.326E-1	-.875E-1	-.586E+0	-.401E+0
	.595E+0	.646E+0	.598E+0	.474E+0

OLE 590100. 100920. Louvie

.116E+1	.353E+1	.147E+1	.678E+1	.160E+2
	.190E+1	-.166E+2	.188E+2	.142E+2
	.401E+0	.147E+0	.160E+0	.504E-1
.146E+1	.755E+1	.665E+1	.488E+1	.132E+2
	.266E+1	-.122E+2	.150E+2	.130E+2
	.406E+0	.149E+0	.181E+0	.579E-1
.183E+1	.522E+1	.499E+1	.513E+1	.111E+2
	.107E+1	-.134E+2	.101E+2	.109E+2
	.336E+0	.118E+0	.220E+0	.720E-1
.229E+1	.404E+1	.262E+1	.204E+1	.831E+1
	.103E+1	-.112E+2	.825E+1	.882E+1
	.347E+0	.123E+0	.256E+0	.856E-1
.291E+1	.405E+1	.111E+1	.931E+0	.626E+1
	.852E+0	-.683E+1	.688E+1	.824E+1
	.400E+0	.146E+0	.267E+0	.899E-1
.377E+1	.190E+1	.926E+0	.207E+1	.580E+1
	.192E+1	-.481E+1	.476E+1	.569E+1
	.460E+0	.174E+0	.326E+0	.114E+0
.492E+1	.174E+1	.101E+1	.109E+1	.373E+1
	.195E+1	-.320E+1	.350E+1	.474E+1
	.395E+0	.144E+0	.305E+0	.105E+0
.640E+1	.203E+1	.778E+0	-.510E-1	.273E+1
	.228E+1	-.287E+1	.297E+1	.595E+1
	.384E+0	.139E+0	.341E+0	.120E+0
.826E+1	.205E+1	.123E+1	.394E+0	.217E+1
	.135E+1	-.256E+1	.244E+1	.455E+1
	.400E+0	.146E+0	.473E+0	.181E+0
.107E+2	.230E+1	.208E+1	.536E+0	.164E+1
	.157E+1	-.148E+1	.200E+1	.389E+1
	.447E+0	.168E+0	.510E+0	.200E+0
.135E+2	.206E+1	.289E+1	.165E+1	.180E+1
	.240E+1	.584E+0	.143E+1	.211E+1
	.427E+0	.159E+0	.524E+0	.207E+0
.171E+2	.295E+1	.314E+1	.121E+1	.120E+1
	.166E+1	.374E+0	.171E+1	.239E+1
	.316E+0	.110E+0	.367E+0	.132E+0
.213E+2	.206E+1	.249E+1	.109E+1	.903E+0
	.135E+1	.945E-1	.141E+1	.250E+1
	.454E+0	.172E+0	.498E+0	.194E+0
.256E+2	.191E+1	.246E+1	.790E+0	.658E+0
	.181E+1	.570E+0	.314E+0	.132E+1
	.357E+0	.127E+0	.597E+0	.403E+0
.330E+2	.177E+1	.211E+1	.122E+1	.161E+1
	.923E+0	.179E+1	.882E+0	.839E+0
	.402E+0	.147E+0	.598E+0	.357E+0
.427E+2	.311E+1	.357E+1	.132E+1	.144E+1
	.183E+1	.133E+1	.683E+0	.156E+1
	.324E+0	.113E+0	.598E+0	.393E+0
.539E+2	.189E+1	.300E+1	.156E+1	.150E+
	.272E+1	.225E+1	.301E+0	.174E+
	.360E+0	.128E+0	.598E+0	.376E+
.683E+2	.166E+1	.234E+1	.408E+0	.176E+1
	.276E+1	.253E+1	.783E+0	.122E+1
	.292E+0	.100E+0	.598E+0	.545E+0
.853E+2	.835E+0	.166E+1	.182E+0	.110E+1

.152E+1	.237E+1	.170E+1	.990E+0
.455E+0	.172E+0	.598E+0	.453E+0
.102E+3 .234E+1	.175E+1	.306E+0	.592E+0
.156E+1	.213E+1	.170E+1	.137E+1
.376E+0	.136E+0	.598E+0	.331E+0
.102E+3 .203E+1	.166E+1	.478E+0	.102E+1
.222E+1	.265E+1	.142E+1	.109E+1
.373E+0	.134E+0	.598E+0	.461E+0
.132E+3 .246E+1	.173E+1	-.626E+0	.831E+0
.223E+1	.253E+1	-.246E+0	.142E+1
.498E+0	.194E+0	.598E+0	.125E+1
.178E+3 -.649E+0	.113E+1	.558E+0	-.491E+0
.548E+0	.184E+1	.207E+1	.178E+1
.466E+0	.178E+0	.598E+0	.260E+0
.256E+3 -.580E+0	-.544E-1	.413E+0	-.394E+0
.126E+1	.161E+1	.137E+1	.115E+1
.557E+0	.225E+0	.598E+0	.411E+0
.372E+3 .454E+0	-.148E-1	-.423E+0	-.152E+0
.152E+0	.943E+0	.264E+0	.371E+0
.598E+0	.545E+0	.598E+0	.130E+1

TOU 615410. 116200. Tsa du Touno

.116E+1 .100E+1	.374E+2	-.524E+1	-.117E+2
-.129E+2	.819E+2	-.197E+2	-.231E+2
.219E-1	.637E-2	.357E-1	.105E-1
.146E+1 -.107E+1	.254E+2	-.413E+1	-.873E+1
-.993E+1	.700E+2	-.166E+2	-.198E+2
.212E-1	.620E-2	.335E-1	.986E-2
.183E+1 -.207E+0	.229E+2	-.345E+1	-.740E+1
-.691E+1	.613E+2	-.137E+2	-.175E+2
.250E-1	.733E-2	.367E-1	.108E-1
.229E+1 -.202E+0	.181E+2	-.277E+1	-.554E+1
-.505E+1	.517E+2	-.114E+2	-.149E+2
.259E-1	.759E-2	.363E-1	.106E-1
.291E+1 -.239E+0	.139E+2	-.241E+1	-.414E+1
-.468E+1	.394E+2	-.894E+1	-.111E+2
.199E-1	.576E-2	.309E-1	.908E-2
.377E+1 -.330E+0	.114E+2	-.228E+1	-.361E+1
-.391E+1	.325E+2	-.713E+1	-.908E+1
.242E-1	.707E-2	.389E-1	.114E-1
.492E+1 -.158E+0	.886E+1	-.214E+1	-.243E+1
-.358E+1	.264E+2	-.529E+1	-.747E+1
.237E-1	.689E-2	.474E-1	.141E-1
.640E+1 .351E+0	.766E+1	-.239E+1	-.216E+1
-.313E+1	.220E+2	-.383E+1	-.588E+1
.337E-1	.986E-2	.762E-1	.229E-1
.826E+1 .801E+0	.750E+1	-.222E+1	-.220E+1
-.296E+1	.180E+2	-.295E+1	-.503E+1
.475E-1	.141E-1	.946E-1	.288E-1
.107E+2 .116E+1	.585E+1	-.215E+1	-.137E+1
-.279E+1	.150E+2	-.228E+1	-.426E+1
.536E-1	.159E-1	.105E+0	.320E-1
.135E+2 .198E+1	.498E+1	-.219E+1	-.102E+1
-.204E+1	.118E+2	-.197E+1	-.361E+1
.581E-1	.173E-1	.977E-1	.298E-1
.171E+2 .195E+1	.367E+1	-.183E+1	-.449E+0
-.159E+1	.985E+1	-.169E+1	-.300E+1
.433E-1	.127E-1	.741E-1	.223E-1
.213E+2 .204E+1	.271E+1	-.169E+1	-.273E+0
-.118E+1	.815E+1	-.142E+1	-.249E+1
.516E-1	.153E-1	.841E-1	.254E-1
.256E+2 .208E+1	.234E+1	-.156E+1	-.378E+0
-.695E+0	.682E+1	-.134E+1	-.208E+1
.509E-1	.151E-1	.804E-1	.243E-1
.330E+2 .187E+1	.173E+1	-.138E+1	-.365E+0
-.187E+0	.537E+1	-.118E+1	-.159E+1
.527E-1	.156E-1	.953E-1	.291E-1
.427E+2 .198E+1	.178E+1	-.140E+1	-.292E+0
-.209E+0	.426E+1	-.826E+0	-.133E+1
.596E-1	.177E-1	.121E+0	.375E-1
.539E+2 .209E+1	.148E+1	-.147E+1	-.217E+0
-.237E+0	.378E+1	-.732E+0	-.127E+1
.867E-1	.263E-1	.137E+0	.426E-1
.683E+2 .209E+1	.141E+1	-.136E+1	-.962E-1
-.241E+0	.294E+1	-.481E+0	-.114E+1
.124E+0	.383E-1	.164E+0	.521E-1
.853E+2 .203E+1	.920E+0	-.139E+1	-.280E-1
-.200E+0	.228E+1	-.444E+0	-.821E+0
.184E+0	.588E-1	.214E+0	.697E-1
.102E+3 .164E+1	.951E+0	-.108E+1	.303E-1
-.115E+0	.234E+1	-.228E+0	-.960E+0
.156E+0	.492E-1	.271E+0	.915E-1
.102E+3 .153E+1	.824E+0	-.111E+1	.800E-1
-.255E+0	.214E+1	-.287E+0	-.991E+0
.196E+0	.632E-1	.277E+0	.938E-1
.132E+3 .175E+1	.102E+1	-.108E+1	.952E-1
-.948E-1	.157E+1	-.195E+0	-.606E+0
.259E+0	.867E-1	.307E+0	.106E+0
.178E+3 .178E+1	.948E+0	-.110E+1	.132E+0
-.106E-1	.145E+1	-.205E+0	-.721E+0
.243E+0	.807E-1	.352E+0	.125E+0
.256E+3 .172E+1	.107E+1	-.110E+1	-.124E+0
-.304E+0	.117E+1	-.118E+0	-.439E+0
.238E+0	.788E-1	.417E+0	.154E+0
.372E+3 .122E+1	.733E+0	-.123E+1	-.121E+0
-.827E+0	.622E+0	.363E+0	-.493E+0
.462E+0	.175E+0	.420E+0	.155E+0

LUS 600680. 105000. La Luesse

.116E+1 -.784E+1	.202E+2	.124E+2	-.423E+2
-.303E+1	.364E+2	-.839E+1	-.617E+2
.171E-1	.497E-2	.118E+0	.364E-1
.146E+1 -.667E+1	.155E+2	.116E+2	-.318E+2
-.153E+1	.320E+2	-.784E+1	-.548E+2
.170E-1	.497E-2	.103E+0	.315E-1
.183E+1 -.444E+1	.137E+2	.663E+1	-.291E+2
-.154E+1	.266E+2	-.681E+1	-.462E+2
.208E-1	.611E-2	.125E+0	.386E-1
.229E+1 -.280E+1	.120E+2	.443E+1	-.245E+2
.285E+0	.233E+2	-.899E+1	-.410E+2
.208E-1	.602E-2	.911E-1	.277E-1
.291E+1 -.261E+1	.889E+1	.399E+1	-.178E+2
.199E+0	.190E+2	-.714E+1	-.337E+2
.170E-1	.497E-2	.760E-1	.229E-1
.377E+1 -.270E+1	.677E+1	.428E+1	-.134E+2
.405E+0	.161E+2	-.553E+1	-.285E+2
.211E-1	.611E-2	.937E-1	.284E-1
.492E+1 -.313E+1	.503E+1	.495E+1	-.987E+1
-.474E+0	.136E+2	-.259E+1	-.243E+2
.211E-1	.611E-2	.106E+0	.325E-1
.640E+1 -.348E+1	.375E+1	.554E+1	-.734E+1
-.118E+1	.113E+2	-.221E+0	-.202E+2
.302E-1	.890E-2	.134E+0	.416E-1
.826E+1 -.325E+1	.313E+1	.488E+1	-.624E+1
-.135E+1	.947E+1	.649E+0	-.171E+2
.365E-1	.107E-1	.148E+0	.467E-1
.107E+2 -.178E+1	.301E+1	.203E+1	-.596E+1
-.137E+1	.746E+1	.105E+1	-.137E+2
.460E-1	.136E-1	.280E+0	.950E-1
.135E+2 -.669E+0	.306E+1	-.290E-1	-.590E+1
-.122E+1	.574E+1	.992E+0	-.106E+2
.543E-1	.161E-1	.516E+0	.202E+0
.171E+2 -.168E-1	.268E+1	-.104E+1	-.520E+1
-.427E+0	.505E+1	-.357E+0	-.949E+1
.411E-1	.121E-1	.320E+0	.111E+0
.213E+2 .266E+0	.195E+1	-.141E+1	-.365E+1
-.556E-1	.452E+1	-.900E+0	-.846E+1
.523E-1	.155E-1	.232E+0	.766E-1
.256E+2 .417E+0	.151E+1	-.161E+1	-.280E+1
.669E-1	.374E+1	-.100E+1	-.695E+1
.505E-1	.149E-1	.198E+0	.640E-1
.330E+2 .647E+0	.117E+1	-.178E+1	-.207E+1
.372E+0	.290E+1	-.141E+1	-.545E+1
.546E-1	.162E-1	.147E+0	.462E-1
.427E+2 .667E+0	.109E+1	-.195E+1	-.208E+1
.232E+0	.220E+1	-.109E+1	-.424E+1
.656E-1	.196E-1	.162E+0	.511E-1
.539E+2 .738E+0	.119E+1	-.199E+1	-.224E+1
.124E+0	.176E+1	-.803E+0	-.356E+1
.983E-1	.299E-1	.198E+0	.641E-1
.683E+2 .562E+0	.935E+0	-.178E+1	-.180E+1
.147E+0	.126E+1	-.650E+0	-.268E+1
.132E+0	.412E-1	.206E+0	.668E-1
.853E+2 .566E+0	.816E+0	-.190E+1	-.149E+1
-.988E-1	.104E+1	-.244E+0	-.207E+1
.177E+0	.564E-1	.263E+0	.884E-1
.102E+3 .245E+0	.764E+0	-.126E+1	-.150E+1
.645E-1	.909E+0	-.495E+0	-.196E+1
.198E+0	.640E-1	.362E+0	.129E+0
.102E+3 .280E+0	.706E+0	-.122E+1	-.133E+1
-.119E+0	.791E+0	-.109E+0	-.168E+1
.229E+0	.753E-1	.406E+0	.149E+0
.132E+3 .618E+0	.818E+0	-.180E+1	-.150E+1
.964E-1	.771E+0	-.495E+0	-.167E+1
.263E+0	.886E-1	.276E+0	.935E-1
.178E+3 .490E+0	.682E+0	-.158E+1	-.142E+1
.137E+0	.584E+0	-.405E+0	-.119E+1
.269E+0	.907E-1	.312E+0	.108E+0
.256E+3 .668E+0	.629E+0	-.168E+1	-.144E+1
-.239E-1	.536E+0	-.259E+0	-.110E+1
.303E+0	.105E+0	.333E+0	.117E+0
.372E+3 .452E+0	.600E+0	-.131E+1	-.963E+0
.710E-1	.342E+0	-.161E+0	-.695E+0
.428E+0	.159E+0	.432E+0	.161E+0

COL 604030. 94730. Les Collons

.116E+1 -.985E+1	.361E+2	-.125E+2	.480E+2
.372E+2	.823E+2	.553E+2	.120E+3
.807E-1	.244E-1	.257E+0	.861E-1
.146E+1 -.148E+1	.368E+2	-.326E+1	.495E+2
.114E+2	.602E+2	.186E+2	.857E+2
.101E+0	.307E-1	.598E+0	.275E+0
.183E+1 .711E+1	.393E+2	.953E+1	.530E+2
-.383E+1	.426E+2	-.216E+0	.630E+2
.120E+0	.371E-1	.598E+0	.622E+0
.229E+1 .537E+1	.341E+2	.763E+1	.472E+2
-.347E+1	.433E+2	-.424E+1	.632E+2
.112E+0	.346E-1	.598E+0	.656E+0
.291E+1 .473E+1	.241E+2	.748E+1	.304E+2
-.274E+1	.352E+2	-.697E+1	.505E+2
.106E+0	.327E-1	.597E+0	.375E+0
.377E+1 -.391E+0	.248E+2	-.772E+0	.330E+2
-.761E+1	.284E+2	-.119E+2	.413E+2
.128E+0	.396E-1	.598E+0	.380E+0
.492E+1 -.149E+1	.204E+2	-.303E+1	.272E+2
-.124E+1	.245E+2	-.629E+0	.368E+2
.152E+0	.477E-1	.598E+0	.146E+1
.640E+1 -.509E+1	.197E+2	-.663E+1	.280E+2
-.269E+1	.279E+2	-.694E+1	.397E+2
.183E+0	.586E-1	.598E+0	.517E+0
.826E+1 .343E+1	.193E+2	.189E+1	.261E+2
-.517E+1	.155E+2	-.643E+1	.237E+2
.257E+0	.865E-1	.597E+0	.753E+0
.107E+2 .758E+1	.202E+2	.110E+2	.281E+2
-.883E+1	.966E+1	-.106E+2	.158E+2
.265E+0	.895E-1	.598E+0	.293E+0
.135E+2 .338E+1	.177E+2	.564E+1	.264E+2
-.372E+1	.115E+2	-.364E+1	.184E+2
.268E+0	.904E-1	.599E+0	.591E+0
.171E+2 .661E+1	.135E+2	.941E+1	.195E+2
-.111E+2	.662E+1	-.163E+2	.108E+2
.355E+0	.126E+0	.483E+0	.186E+0
.213E+2 .475E+1	.133E+2	.613E+1	.191E+2
-.633E+1	.720E+1	-.564E+1	.115E+2
.371E+0	.134E+0	.598E+0	.411E+0
.256E+2 .261E+1	.107E+2	.451E+1	.145E+2
-.108E+1	.686E+1	-.165E+1	.118E+2
.329E+0	.115E+0	.598E+0	.621E+0
.330E+2 .540E+1	.122E+2	.839E+1	.195E+2
-.561E+1	.267E+1	-.538E+1	.654E+1
.318E+0	.110E+0	.583E+0	.239E+0
.427E+2 .153E+1	.869E+1	.151E+1	.115E+2
-.123E+1	.594E+1	-.252E+1	.760E+1
.395E+0	.144E+0	.597E+0	.802E+0
.539E+2 -.115E-1	.723E+1	.123E+1	.112E+2
-.288E+1	.306E+1	-.620E+1	.311E+1
.513E+0	.201E+0	.598E+0	.470E+0
.683E+2 .190E+1	.127E+2	.227E+1	.165E+2
.429E+0	.399E+1	-.482E+0	.712E+1
.324E+0	.113E+0	.598E+0	.125E+1
.853E+2 .259E+1	.943E+1	.216E+1	.124E+2
-.161E+1	.242E+1	-.210E+1	.356E+1
.418E+0	.154E+0	.599E+0	.101E+1
.102E+3 .503E+1	.782E+1	.832E+1	.128E+2
.643E-1	.418E+1	-.828E+0	.584E+1
.493E+0	.191E+0	.599E+0	.362E+0
.102E+3 .368E+1	.329E+1	.659E+1	.522E+1
-.128E+1	.281E+1	-.539E+0	.519E+1
.598E+0	.371E+0	.598E+0	.559E+0
.132E+3 .261E+0	.239E+1	.579E-2	.406E+1
.833E+0	.160E+1	.839E+0	.218E+1
.598E+0	.545E+0	.597E+0	.302E+1
.178E+3 .410E+1	.578E+1	.543E+1	.807E+1
.734E+0	.129E+1	.149E+1	.191E+1
.599E+0	.305E+0	.598E+0	.359E+0
.256E+3 .118E+1	.190E+1	.112E+1	.298E+1
-.156E+1	-.329E+0	-.267E+1	-.158E+1
.598E+0	.578E+0	.598E+0	.396E+0
.372E+3 .772E+0	.368E+1	.118E+1	.526E+1
-.187E+1	-.127E+1	-.345E+1	-.273E+1
.598E+0	.672E+0	.598E+0	.409E+0

FER 608790. 99880. Ferpècle

.116E+1 .446E+2	.793E+2	-.147E+2	-.164E+2
.167E+2	.767E+2	-.347E+2	-.110E+2
.284E-1	.829E-2	.373E-1	.110E-1
.146E+1 .431E+2	.721E+2	-.164E+2	-.161E+2
.614E+1	.639E+2	-.288E+2	-.101E+2
.320E-1	.943E-2	.444E-1	.131E-1
.183E+1 .370E+2	.609E+2	-.156E+2	-.143E+2
.405E+1	.570E+2	-.248E+2	-.854E+1
.350E-1	.103E-1	.513E-1	.152E-1
.229E+1 .294E+2	.504E+2	-.150E+2	-.121E+2
.487E+1	.516E+2	-.195E+2	-.704E+1
.376E-1	.111E-1	.560E-1	.167E-1
.291E+1 .270E+2	.461E+2	-.135E+2	-.100E+2
.733E+1	.450E+2	-.169E+2	-.576E+1
.336E-1	.986E-2	.493E-1	.146E-1
.377E+1 .240E+2	.394E+2	-.142E+2	-.937E+1
.345E+1	.369E+2	-.123E+2	-.313E+1
.439E-1	.130E-1	.606E-1	.181E-1
.492E+1 .332E+2	.425E+2	-.168E+2	-.101E+2
.253E+0	.250E+2	-.782E+1	-.725E-1
.521E-1	.154E-1	.602E-1	.179E-1
.640E+1 .392E+2	.463E+2	-.164E+2	-.990E+1
-.735E+0	.174E+2	-.595E+1	.647E+0
.616E-1	.183E-1	.666E-1	.199E-1
.826E+1 .417E+2	.471E+2	-.165E+2	-.106E+2
-.191E+1	.111E+2	-.402E+1	.174E+1
.655E-1	.195E-1	.728E-1	.218E-1
.107E+2 .370E+2	.433E+2	-.140E+2	-.913E+1
.920E+0	.123E+2	-.501E+1	-.572E+0
.690E-1	.207E-1	.729E-1	.219E-1
.135E+2 .328E+2	.404E+2	-.121E+2	-.753E+1
.281E+1	.137E+2	-.454E+1	-.133E+1
.722E-1	.216E-1	.764E-1	.230E-1
.171E+2 .251E+2	.316E+2	-.919E+1	-.539E+1
.212E+1	.141E+2	-.452E+1	-.292E+1
.634E-1	.189E-1	.644E-1	.192E-1
.213E+2 .170E+2	.215E+2	-.679E+1	-.274E+1
.442E+1	.165E+2	-.376E+1	-.302E+1
.710E-1	.213E-1	.762E-1	.229E-1
.256E+2 .145E+2	.187E+2	-.601E+1	-.243E+1
.523E+1	.165E+2	-.379E+1	-.353E+1
.556E-1	.165E-1	.671E-1	.201E-1
.330E+2 .120E+2	.149E+2	-.504E+1	-.217E+1
.503E+1	.143E+2	-.315E+1	-.308E+1
.587E-1	.174E-1	.823E-1	.249E-1
.427E+2 .133E+2	.153E+2	-.590E+1	-.347E+1
.400E+1	.124E+2	-.260E+1	-.299E+1
.745E-1	.224E-1	.104E+0	.318E-1
.539E+2 .108E+2	.141E+2	-.487E+1	-.359E+1
.228E+1	.916E+1	-.162E+1	-.179E+1
.997E-1	.304E-1	.155E+0	.488E-1
.683E+2 .978E+1	.120E+2	-.379E+1	-.235E+1
.201E+1	.823E+1	-.125E+1	-.173E+1
.930E-1	.283E-1	.163E+0	.515E-1
.853E+2 .990E+1	.105E+2	-.434E+1	-.194E+1
.162E+1	.729E+1	-.821E+0	-.175E+1

.135E+0	.420E-1	.196E+0	.632E-1
.102E+3 .741E+1	.816E+1	-.358E+1	-.130E+1
.160E+1	.476E+1	-.721E+0	-.142E+1
.242E+0	.802E-1	.235E+0	.777E-1
.102E+3 .720E+1	.824E+1	-.348E+1	-.163E+1
.973E+0	.475E+1	-.387E+0	-.153E+1
.228E+0	.750E-1	.240E+0	.794E-1
.132E+3 .848E+1	.985E+1	-.400E+1	-.150E+1
-.193E+1	.363E+1	.673E+0	-.121E+1
.280E+0	.950E-1	.250E+0	.832E-1
.178E+3 .702E+1	.936E+1	-.338E+1	-.171E+1
-.448E+0	.418E+1	.568E+0	-.182E+1
.261E+0	.878E-1	.334E+0	.117E+0
.256E+3 .476E+1	.878E+1	-.233E+1	-.157E+1
-.366E+1	.132E+1	.126E+1	-.987E+0
.292E+0	.100E+0	.486E+0	.187E+0
.372E+3 .279E+1	.760E+1	-.103E+1	-.126E+1
.550E-1	.120E+1	.272E+0	-.347E+0
.369E+0	.132E+0	.598E+0	.483E+0

DIX 596530. 99560. Dixence

.116E+1 .404E+1	.863E+1	-.246E+1	-.313E+1
.596E+1	.177E+2	-.829E+1	-.575E+1
.159E-1	.463E-2	.895E-1	.270E-1
.146E+1 .279E+1	.740E+1	-.742E+0	-.371E+1
.501E+1	.153E+2	-.636E+1	-.487E+1
.173E-1	.506E-2	.119E+0	.366E-1
.183E+1 .212E+1	.598E+1	-.579E+0	-.294E+1
.403E+1	.131E+2	-.557E+1	-.422E+1
.179E-1	.524E-2	.131E+0	.408E-1
.229E+1 .171E+1	.507E+1	-.109E+0	-.254E+1
.341E+1	.111E+2	-.488E+1	-.330E+1
.190E-1	.550E-2	.139E+0	.435E-1
.291E+1 .118E+1	.444E+1	-.683E+0	-.240E+1
.297E+1	.920E+1	-.436E+1	-.276E+1
.177E-1	.515E-2	.136E+0	.424E-1
.377E+1 .362E+0	.393E+1	-.101E+0	-.191E+1
.257E+1	.769E+1	-.334E+1	-.272E+1
.199E-1	.576E-2	.197E+0	.634E-1
.492E+1 -.152E+0	.329E+1	-.944E-1	-.142E+1
.168E+1	.629E+1	-.173E+1	-.213E+1
.191E-1	.550E-2	.316E+0	.110E+0
.640E+1 -.650E+0	.277E+1	-.176E+0	-.138E+1
.913E+0	.511E+1	-.140E+1	-.175E+1
.241E-1	.707E-2	.383E+0	.139E+0
.826E+1 -.455E+0	.233E+1	-.553E+0	-.111E+1
.742E-1	.409E+1	-.732E+0	-.142E+1
.308E-1	.899E-2	.561E+0	.227E+0
.107E+2 -.361E+0	.193E+1	-.896E+0	-.934E+0
-.162E+0	.328E+1	-.648E+0	-.110E+1
.358E-1	.105E-1	.444E+0	.167E+0
.135E+2 -.944E-1	.181E+1	-.102E+1	-.813E+0
-.120E+0	.269E+1	-.141E+0	-.890E+0
.403E-1	.119E-1	.443E+0	.167E+0
.171E+2 .303E+0	.153E+1	-.924E+0	-.662E+0
.369E+0	.231E+1	-.520E+0	-.904E+0
.441E-1	.131E-1	.298E+0	.102E+0
.213E+2 .608E+0	.147E+1	-.909E+0	-.491E+0
.835E+0	.189E+1	-.765E+0	-.757E+0
.606E-1	.181E-1	.232E+0	.765E-1
.256E+2 .465E+0	.114E+1	-.101E+1	-.459E+0
.111E+1	.168E+1	-.963E+0	-.609E+0
.656E-1	.195E-1	.137E+0	.428E-1
.330E+2 .505E+0	.108E+1	-.904E+0	-.294E+0
.112E+1	.136E+1	-.613E+0	-.505E+0
.866E-1	.262E-1	.188E+0	.604E-1
.427E+2 .433E+0	.945E+0	-.790E+0	-.318E+0
.636E+0	.976E+0	-.438E+0	-.333E+0
.107E+0	.329E-1	.224E+0	.735E-1
.539E+2 .507E+0	.834E+0	-.669E+0	-.241E+0
.604E+0	.839E+0	-.515E+0	-.363E+0
.148E+0	.465E-1	.167E+0	.531E-1
.683E+2 .462E+0	.578E+0	-.668E+0	-.268E+0
.309E+0	.518E+0	-.456E+0	-.232E+0
.191E+0	.616E-1	.163E+0	.518E-1
.853E+2 .545E+0	.557E+0	-.680E+0	-.261E+0
.291E+0	.475E+0	-.379E+0	-.206E+0
.229E+0	.756E-1	.228E+0	.750E-1
.102E+3 .189E+0	.594E+0	-.625E+0	-.293E+0
.165E+0	.373E+0	-.208E+0	-.143E+0
.237E+0	.785E-1	.316E+0	.110E+0
.102E+3 .326E+0	.632E+0	-.638E+0	-.270E+0
.192E-1	.440E+0	-.290E+0	-.162E+0
.241E+0	.799E-1	.289E+0	.988E-1
.132E+3 -.282E-1	.665E+0	-.581E+0	-.316E+0
-.681E-1	-.255E-2	-.578E-1	-.112E+0
.315E+0	.109E+0	.560E+0	.226E+0
.178E+3 .112E+0	.800E+0	-.732E+0	-.214E+0
-.106E+0	-.269E+0	.231E-1	-.168E+0
.328E+0	.115E+0	.488E+0	.189E+0
.256E+3 .395E+0	.799E+0	-.326E+0	-.181E+0
-.108E+0	-.225E+0	.316E+0	-.237E-1
.364E+0	.130E+0	.598E+0	.416E+0
.372E+3 -.121E+0	.533E+0	-.822E+0	-.304E+0
-.314E+0	-.219E+0	.629E+0	.105E+0
.598E+0	.283E+0	.496E+0	.193E+0

NOU 600710. 107100. La Nouva

.116E+1 .318E+2	.953E-2	.257E+2	-.120E+1
.618E+2	.313E+1	.479E+2	.129E+2
.337E+0	.119E+0	.204E-1	.593E-2
.146E+1 .286E+2	-.306E+1	.233E+2	-.404E+1
.517E+2	.736E+0	.413E+2	.865E+1

.296E+0	.102E+0	.243E-1	.707E-2
.183E+1 .225E+2	-.355E+1	.185E+2	-.407E+1
.442E+2	.942E+0	.350E+2	.838E+1
.228E+0	.750E-1	.273E-1	.803E-2
.229E+1 .187E+2	-.376E+1	.150E+2	-.364E+1
.383E+2	.166E+0	.304E+2	.638E+1
.203E+0	.658E-1	.320E-1	.934E-2
.291E+1 .164E+2	-.382E+1	.133E+2	-.309E+1
.332E+2	.160E+0	.266E+2	.544E+1
.171E+0	.545E-1	.329E-1	.960E-2
.377E+1 .121E+2	-.586E+1	.972E+1	-.446E+1
.289E+2	-.963E+0	.230E+2	.318E+1
.125E+0	.388E-1	.404E-1	.119E-1
.492E+1 .827E+1	-.612E+1	.652E+1	-.434E+1
.228E+2	-.227E+1	.179E+2	.914E+0
.105E+0	.323E-1	.475E-1	.141E-1
.640E+1 .574E+1	-.596E+1	.458E+1	-.396E+1
.177E+2	-.328E+1	.137E+2	-.660E+0
.112E+0	.342E-1	.648E-1	.194E-1
.826E+1 .557E+1	-.419E+1	.478E+1	-.248E+1
.136E+2	-.439E+1	.106E+2	-.195E+1
.131E+0	.406E-1	.834E-1	.252E-1
.107E+2 .399E+1	-.315E+1	.371E+1	-.147E+1
.101E+2	-.474E+1	.791E+1	-.251E+1
.125E+0	.387E-1	.950E-1	.289E-1
.135E+2 .388E+1	-.233E+1	.363E+1	-.627E+0
.833E+1	-.451E+1	.665E+1	-.250E+1
.147E+0	.460E-1	.105E+0	.323E-1
.171E+2 .337E+1	-.767E+0	.302E+1	.452E+0
.761E+1	-.311E+1	.613E+1	-.158E+1
.179E+0	.572E-1	.860E-1	.260E-1
.213E+2 .306E+1	.255E+0	.271E+1	.114E+1
.789E+1	-.132E+1	.637E+1	-.306E+0
.380E+0	.137E+0	.913E-1	.278E-1
.256E+2 .250E+1	.468E+0	.207E+1	.119E+1
.737E+1	.592E-2	.605E+1	.718E+0
.598E+0	.302E+0	.704E-1	.211E-1
.330E+2 .144E+1	.494E+0	.119E+1	.111E+1
.561E+1	-.399E+0	.454E+1	.287E+0
.597E+0	.246E+0	.983E-1	.299E-1
.427E+2 .194E+1	.825E+0	.163E+1	.140E+1
.412E+1	-.396E+0	.335E+1	.123E+0
.446E+0	.168E+0	.129E+0	.401E-1
.539E+2 .156E+1	.106E+1	.107E+1	.132E+1
.384E+1	.484E+0	.317E+1	.846E+0
.292E+0	.997E-1	.127E+0	.394E-1
.683E+2 .128E+1	.112E+1	.105E+1	.135E+1
.273E+1	.374E+0	.237E+1	.650E+0
.257E+0	.860E-1	.136E+0	.424E-1
.853E+2 .142E+1	.109E+1	.115E+1	.129E+1
.213E+1	.408E-1	.194E+1	.383E+0
.395E+0	.144E+0	.193E+0	.623E-1
.102E+3 .124E+1	.760E+0	.111E+1	.121E+1
.170E+1	-.181E+0	.153E+1	.871E-1
.512E+0	.201E+0	.193E+0	.622E-1
.102E+3 .128E+1	.744E+0	.119E+1	.119E+1
.172E+1	-.266E+0	.152E+1	-.163E-1
.461E+0	.175E+0	.180E+0	.577E-1
.132E+3 .134E+1	.586E+0	.140E+1	.126E+1
.538E+0	-.802E+0	.670E+0	-.737E+0
.598E+0	.309E+0	.373E+0	.134E+0
.178E+3 .172E+1	.152E+1	.148E+1	.195E+1
.701E+0	-.700E+0	.683E+0	-.702E+0
.458E+0	.174E+0	.399E+0	.146E+0
.256E+3 .842E+0	.295E+0	.575E+0	.684E+0
.409E+0	-.769E+0	.282E+0	-.909E+0
.598E+0	.352E+0	.598E+0	.433E+0
.372E+3 .893E+0	.698E+0	.740E+0	.103E+1
-.781E+0	-.145E+1	-.339E+0	-.110E+1
.598E+0	.252E+0	.598E+0	.371E+0

MAV 594090. 88310. Sud Mauvoisin

.116E+1 .166E-1	.155E+1	-.160E+1	-.340E+1
.746E+0	.236E+1	-.377E+1	-.188E+1
.225E+0	.737E-1	.476E-1	.138E-1
.146E+1 -.115E+0	.125E+1	-.111E+1	-.204E+1
.544E+0	.204E+1	-.373E+1	-.564E+0
.239E+0	.790E-1	.498E-1	.146E-1
.183E+1 -.440E+0	.942E+0	-.712E+0	-.709E+0
.399E+0	.120E+1	-.361E+1	-.184E+0
.342E+0	.120E+0	.528E-1	.154E-1
.229E+1 -.732E+0	.235E+0	-.484E+0	-.104E+0
.376E+0	.131E+1	-.321E+1	-.437E+0
.334E+0	.117E+0	.610E-1	.180E-1
.291E+1 -.639E+0	.877E+0	-.461E+0	-.433E+0
-.362E+0	.118E+1	-.331E+1	-.111E+1
.224E+0	.729E-1	.508E-1	.151E-1
.377E+1 -.762E+0	.841E+0	-.391E+0	-.419E+0
-.478E+0	.112E+1	-.290E+1	-.850E+0
.217E+0	.712E-1	.585E-1	.173E-1
.492E+1 -.791E+0	.602E+0	-.447E+0	-.415E+0
-.502E+0	.949E+0	-.241E+1	-.624E+0
.227E+0	.743E-1	.638E-1	.192E-1
.640E+1 -.584E+0	.609E+0	-.276E+0	-.118E+0
-.606E+0	.607E+0	-.190E+1	-.545E+0
.331E+0	.117E+0	.986E-1	.299E-1
.826E+1 -.714E+0	.321E+0	-.156E+0	-.952E-1
-.609E+0	.364E+0	-.145E+1	-.426E+0
.470E+0	.177E+0	.127E+0	.394E-1
.107E+2 -.481E+0	.498E+0	-.308E+0	-.594E+0
-.442E+0	.504E+0	-.125E+1	-.484E+0
.282E+0	.954E-1	.101E+0	.312E-1
.135E+2 -.312E+0	.781E+0	-.307E+0	-.549E+0

-.504E+0	.411E+0	-.114E+1	-.473E+0
.162E+0	.513E-1	.843E-1	.252E-1
.171E+2 -.209E+0	.678E+0	-.211E+0	-.428E+0
-.465E+0	.417E+0	-.887E+0	-.417E+0
.987E-1	.297E-1	.620E-1	.188E-1
.213E+2 -.105E+0	.532E+0	-.191E+0	-.378E+0
-.397E+0	.330E+0	-.692E+0	-.374E+0
.130E+0	.398E-1	.792E-1	.244E-1
.256E+2 -.666E-1	.372E+0	-.151E+0	-.390E+0
-.273E+0	.281E+0	-.582E+0	-.373E+0
.137E+0	.430E-1	.807E-1	.249E-1
.330E+2 -.133E-1	.275E+0	-.114E+0	-.374E+0
-.180E+0	.126E+0	-.437E+0	-.295E+0
.217E+0	.694E-1	.973E-1	.295E-1
.427E+2 .172E-1	.264E+0	-.857E-1	-.322E+0
-.154E+0	.139E+0	-.345E+0	-.242E+0
.185E+0	.585E-1	.134E+0	.414E-1
.539E+2 -.475E-1	.248E+0	-.120E+0	-.309E+0
-.117E+0	.210E+0	-.272E+0	-.252E+0
.197E+0	.641E-1	.166E+0	.529E-1
.683E+2 -.672E-1	.277E+0	-.112E+0	-.273E+0
-.113E+0	.201E+0	-.206E+0	-.200E+0
.163E+0	.520E-1	.187E+0	.608E-1
.853E+2 -.273E-1	.222E+0	-.894E-1	-.269E+0
-.963E-1	.182E+0	-.170E+0	-.182E+0
.222E+0	.736E-1	.270E+0	.920E-1
.102E+3 -.310E-1	.255E+0	-.129E+0	-.254E+0
-.569E-1	.111E+0	-.138E+0	-.136E+0
.247E+0	.814E-1	.265E+0	.877E-1
.102E+3 -.364E-1	.266E+0	-.107E+0	-.218E+0
-.585E-1	.994E-1	-.163E+0	-.134E+0
.242E+0	.810E-1	.266E+0	.905E-1
.132E+3 -.681E-1	.187E+0	-.133E+0	-.231E+0
-.981E-1	.775E-1	-.840E-1	-.983E-1
.363E+0	.130E+0	.383E+0	.136E+0
.178E+3 -.462E-1	.232E+0	-.123E+0	-.247E+0
-.448E-1	.461E-1	-.540E-1	-.680E-1
.231E+0	.760E-1	.352E+0	.122E+0
.256E+3 -.291E-1	.189E+0	-.937E-1	-.262E+0
-.579E-1	.778E-2	-.262E-1	-.251E-1
.288E+0	.979E-1	.444E+0	.165E+0
.372E+3 -.488E-1	.246E+0	-.101E+0	-.266E+0
-.241E-1	-.160E-1	-.314E-1	-.400E-1
.259E+0	.869E-1	.597E+0	.244E+0

SAL 574720. 92500. Saleina

.116E+1 -.502E+2	.338E+2	.462E+2	-.307E+2
-.370E+1	.429E+2	.277E+1	-.394E+2
.311E-1	.908E-2	.109E-1	.314E-2
.146E+1 -.465E+2	.314E+2	.427E+2	-.291E+2
-.690E+1	.402E+2	.592E+1	-.368E+2
.253E-1	.742E-2	.989E-2	.288E-2
.183E+1 -.425E+2	.267E+2	.391E+2	-.247E+2
-.994E+1	.353E+2	.878E+1	-.322E+2
.285E-1	.838E-2	.105E-1	.305E-2
.229E+1 -.378E+2	.240E+2	.347E+2	-.221E+2
-.114E+2	.308E+2	.102E+2	-.284E+2
.407E-1	.120E-1	.128E-1	.375E-2
.291E+1 -.341E+2	.217E+2	.314E+2	-.197E+2
-.110E+2	.288E+2	.979E+1	-.267E+2
.435E-1	.128E-1	.137E-1	.401E-2
.377E+1 -.314E+2	.184E+2	.288E+2	-.167E+2
-.103E+2	.259E+2	.923E+1	-.235E+2
.556E-1	.166E-1	.172E-1	.497E-2
.492E+1 -.295E+2	.185E+2	.274E+2	-.160E+2
-.701E+1	.259E+2	.616E+1	-.235E+2
.518E-1	.154E-1	.186E-1	.541E-2
.640E+1 -.285E+2	.147E+2	.264E+2	-.130E+2
-.473E+1	.248E+2	.405E+1	-.226E+2
.694E-1	.208E-1	.239E-1	.698E-2
.826E+1 -.283E+2	.151E+2	.263E+2	-.138E+2
-.332E+1	.250E+2	.285E+1	-.227E+2
.800E-1	.241E-1	.281E-1	.820E-2
.107E+2 -.294E+2	.108E+2	.272E+2	-.978E+1
-.188E+1	.224E+2	.158E+1	-.207E+2
.835E-1	.252E-1	.285E-1	.829E-2
.135E+2 -.273E+2	.994E+1	.254E+2	-.900E+1
-.469E+0	.170E+2	.480E+0	-.156E+2
.885E-1	.268E-1	.318E-1	.934E-2
.171E+2 -.244E+2	.110E+2	.228E+2	-.101E+2
-.164E+1	.112E+2	.144E+1	-.102E+2
.869E-1	.264E-1	.326E-1	.951E-2
.213E+2 -.220E+2	.974E+1	.206E+2	-.896E+1
-.223E+1	.869E+1	.199E+1	-.802E+1
.117E+0	.360E-1	.436E-1	.128E-1
.256E+2 -.206E+2	.798E+1	.192E+2	-.738E+1
-.198E+1	.830E+1	.188E+1	-.767E+1
.132E+0	.412E-1	.461E-1	.136E-1
.330E+2 -.183E+2	.673E+1	.170E+2	-.629E+1
-.302E+1	.572E+1	.286E+1	-.527E+1
.170E+0	.539E-1	.542E-1	.161E-1
.427E+2 -.171E+2	.774E+1	.159E+2	-.708E+1
-.236E+1	.535E+1	.226E+1	-.487E+1
.173E+0	.551E-1	.585E-1	.174E-1
.539E+2 -.161E+2	.549E+1	.151E+2	-.510E+1
-.239E+1	.214E+1	.222E+1	-.191E+1
.294E+0	.101E+0	.680E-1	.203E-1
.683E+2 -.168E+2	.395E+1	.157E+2	-.364E+1
-.120E+1	.148E+1	.112E+1	-.126E+1
.411E+0	.151E+0	.754E-1	.227E-1
.853E+2 -.154E+2	.514E+1	.143E+2	-.484E+1
-.498E+0	-.135E+0	.399E+0	.215E+0
.453E+0	.171E+0	.104E+0	.317E-1

.102E+3	-.148E+2	.421E+1	.138E+2	-.392E+1
	-.382E+0	.537E+0	.325E+0	-.475E+0
	.596E+0	.247E+0	.119E+0	.368E-1
.102E+3	-.155E+2	.625E+1	.145E+2	-.596E+1
	-.797E+0	-.942E+0	.749E+0	.768E+0
	.439E+0	.165E+0	.126E+0	.389E-1
.132E+3	-.164E+2	.529E+1	.152E+2	-.475E+1
	.301E+1	.101E+1	-.273E+1	-.863E+0
	.570E+0	.232E+0	.131E+0	.407E-1
.178E+3	-.140E+2	.596E+1	.131E+2	-.559E+1
	.273E+1	-.429E+0	-.262E+1	.473E+0
	.523E+0	.206E+0	.139E+0	.435E-1
.256E+3	-.141E+2	.657E+1	.132E+2	-.617E+1
	.273E+1	.367E-2	-.262E+1	.554E-1
	.507E+0	.198E+0	.131E+0	.407E-1
.372E+3	-.107E+2	.471E+1	.989E+1	-.434E+1
	.338E+1	.696E+0	-.319E+1	-.601E+0
	.598E+0	.302E+0	.219E+0	.717E-1

ZER 618260. 94630. Zermatt

.116E+1	-.315E+2	.143E+3	-.118E+3	.110E+3
	-.177E+1	.100E+3	-.929E+2	.156E+2
	.195E-1	.567E-2	.249E-1	.724E-2
.146E+1	-.322E+2	.129E+3	-.100E+3	.105E+3
	-.740E+1	.905E+2	-.907E+2	.186E+2
	.205E-1	.593E-2	.278E-1	.812E-2
.183E+1	-.313E+2	.112E+3	-.976E+2	.859E+2
	-.387E+1	.868E+2	-.699E+2	.256E+2
	.240E-1	.698E-2	.384E-1	.113E-1
.229E+1	-.261E+2	.105E+3	-.767E+2	.871E+2
	-.833E+1	.751E+2	-.660E+2	.255E+2
	.244E-1	.707E-2	.449E-1	.133E-1
.291E+1	-.244E+2	.950E+2	-.645E+2	.795E+2
	-.871E+1	.694E+2	-.558E+2	.291E+2
	.212E-1	.620E-2	.433E-1	.127E-1
.377E+1	-.241E+2	.915E+2	-.627E+2	.769E+2
	-.210E+1	.646E+2	-.370E+2	.306E+2
	.228E-1	.663E-2	.593E-1	.176E-1
.492E+1	-.256E+2	.888E+2	-.666E+2	.739E+2
	.165E+1	.587E+2	-.219E+2	.311E+2
	.245E-1	.716E-2	.695E-1	.209E-1
.640E+1	-.259E+2	.815E+2	-.635E+2	.682E+2
	-.130E+1	.492E+2	-.198E+2	.238E+2
	.362E-1	.106E-1	.996E-1	.304E-1
.826E+1	-.200E+2	.752E+2	-.534E+2	.655E+2
	-.509E+1	.372E+2	-.178E+2	.154E+2
	.449E-1	.133E-1	.121E+0	.373E-1
.107E+2	-.736E+1	.625E+2	-.323E+2	.562E+2
	-.220E+2	.187E+2	-.400E+2	-.871E+1
	.580E-1	.173E-1	.104E+0	.317E-1
.135E+2	-.765E+0	.530E+2	-.227E+2	.474E+2
	-.236E+2	.129E+2	-.407E+2	-.121E+2
	.602E-1	.179E-1	.919E-1	.279E-1
.171E+2	-.689E+1	.430E+2	-.296E+2	.396E+2
	-.153E+2	.121E+2	-.288E+2	-.105E+2
	.633E-1	.189E-1	.920E-1	.279E-1
.213E+2	-.110E+2	.350E+2	-.343E+2	.332E+2
	-.124E+2	.125E+2	-.243E+2	-.806E+1
	.758E-1	.228E-1	.105E+0	.321E-1
.256E+2	-.992E+1	.333E+2	-.319E+2	.332E+2
	-.898E+1	.132E+2	-.175E+2	-.499E+1
	.764E-1	.229E-1	.123E+0	.381E-1
.330E+2	-.106E+2	.291E+2	-.297E+2	.315E+2
	-.201E+1	.141E+2	-.769E+1	-.327E+0
	.961E-1	.292E-1	.170E+0	.542E-1
.427E+2	-.601E+1	.188E+2	-.213E+2	.193E+2
	.723E+0	.108E+2	-.426E+1	.609E+0
	.119E+0	*.368E-1*	*.233E+0*	*.769E-1*
.539E+2	-.613E+0	.162E+2	-.121E+2	.161E+2
	.664E+0	.903E+1	-.538E+1	-.363E+0
	.133E+0	.413E-1	.322E+0	.112E+0
.683E+2	.204E+1	.114E+2	-.680E+1	.923E+1
	.149E+1	.813E+1	-.330E+1	.201E+1
	.178E+0	.571E-1	.471E+0	.180E+0
.853E+2	-.254E+1	.121E+2	-.123E+2	.136E+2
	.719E+0	.444E+1	-.222E+1	-.235E+1
	.253E+0	.846E-1	.421E+0	.156E+0
.102E+3	-.364E+0	.137E+2	-.850E+1	.166E+2
	.621E+0	.197E+1	-.224E+1	-.444E+1
	.213E+0	.696E-1	.544E+0	.218E+0
.102E+3	.131E+0	.147E+2	-.775E+1	.175E+2
	.103E+1	.737E+0	-.708E+0	-.673E+1
	.231E+0	.763E-1	.598E+0	.289E+0
.132E+3	.935E+0	.101E+2	-.692E+1	.111E+2
	.151E+0	.558E+1	-.317E+1	.413E+1
	.268E+0	.903E-1	.598E+0	.310E+0
.178E+3	.161E+1	.980E+1	-.538E+1	.106E+2
	.101E+1	.396E+1	-.147E+1	.208E+1
	.277E+0	.940E-1	.598E+0	.374E+0
.256E+3	.246E+1	.688E+1	-.243E+1	.625E+1
	.301E+1	.232E+1	.279E+1	.160E+1
	.425E+0	.158E+0	.598E+0	.501E+0
.372E+3	.282E-1	.720E+1	-.542E+1	.606E+1
	.188E+0	*.108E-1*	*-.285E+0*	*-.182E+1*
	.467E+0	.178E+0	.598E+0	.450E+0

TAS 629340. 100210. Täschalp

.116E+1	-.172E+1	.660E+2	-.826E+2	-.210E+2
	-.224E+2	.813E+2	-.627E+2	-.190E+2
	.245E-1	.716E-2	.524E-1	.155E-1
.146E+1	-.204E+1	.592E+2	-.831E+2	-.403E+1
	-.195E+2	.743E+2	-.538E+2	-.199E+2
	.255E-1	.742E-2	.554E-1	.165E-1
.183E+1	-.264E+1	.524E+2	-.802E+2	.420E+1
	-.207E+2	.647E+2	-.484E+2	-.172E+2
	.300E-1	.881E-2	.681E-1	.204E-1
.229E+1	-.193E+1	.480E+2	-.687E+2	.190E+2
	-.149E+2	.566E+2	-.389E+2	-.116E+2
	.300E-1	.881E-2	.734E-1	.221E-1
.291E+1	-.355E+1	.418E+2	-.666E+2	.293E+2
	-.128E+2	.525E+2	-.302E+2	-.110E+2
	.262E-1	.768E-2	.642E-1	.192E-1
.377E+1	-.347E+1	.373E+2	-.722E+2	.364E+2
	-.793E+1	.463E+2	-.157E+2	-.627E+1
	.290E-1	.847E-2	.736E-1	.221E-1
.492E+1	-.419E+1	.355E+2	-.826E+2	.398E+2
	-.545E+1	.417E+2	-.811E+1	.947E+0
	.297E-1	.873E-2	.717E-1	.215E-1
.640E+1	-.903E+0	.330E+2	-.843E+2	.425E+2
	-.546E+1	.365E+2	-.499E-1	.143E+0
	.406E-1	.120E-1	.922E-1	.280E-1
.826E+1	.347E+1	.307E+2	-.734E+2	.427E+2
	-.549E+1	.283E+2	-.137E+2	-.891E+1
	.496E-1	.148E-1	.108E+0	.333E-1
.107E+2	.608E+1	.234E+2	-.426E+2	.406E+2
	-.760E+1	.214E+2	-.262E+2	-.278E+2
	.580E-1	.173E-1	.117E+0	.359E-1
.135E+2	.769E+1	.194E+2	-.334E+2	.350E+2
	-.692E+1	.164E+2	-.350E+2	-.352E+2
	.631E-1	.189E-1	.998E-1	.305E-1
.171E+2	.564E+1	.147E+2	-.372E+2	.266E+2
	-.450E+1	.143E+2	-.266E+2	-.321E+2
	.619E-1	.185E-1	.951E-1	.290E-1
.213E+2	.376E+1	.105E+2	-.423E+2	.228E+2
	-.327E+1	.122E+2	-.235E+2	-.239E+2
	.771E-1	.232E-1	.103E+0	.315E-1
.256E+2	.313E+1	.884E+1	-.388E+2	.213E+2
	-.219E+1	.105E+2	-.186E+2	-.181E+2
	.814E-1	.246E-1	.123E+0	.380E-1
.330E+2	.287E+1	.688E+1	-.346E+2	.219E+2
	-.693E+0	.102E+2	-.117E+2	-.152E+2
	.946E-1	.288E-1	.163E+0	.517E-1
.427E+2	.307E+1	.403E+1	-.272E+2	.926E+1
	-.368E-1	.723E+1	-.567E+1	-.108E+2
	.103E+0	.314E-1	.203E+0	.659E-1
.539E+2	.273E+1	.358E+1	-.133E+2	.522E+1
	.106E+1	.609E+1	-.740E+1	-.978E+1
	.111E+0	.340E-1	.318E+0	.111E+0
.683E+2	.265E+1	.254E+1	-.113E+2	-.177E+1
	.105E+1	.437E+1	-.520E+1	-.683E+1
	.136E+0	.423E-1	.344E+0	.121E+0
.853E+2	.213E+1	.236E+1	-.144E+2	.654E+1
	.294E+0	.344E+1	-.224E+1	-.837E+1
	.242E+0	.802E-1	.419E+0	.155E+0
.102E+3	.188E+1	.240E+1	-.111E+2	.100E+2
	.443E+0	.329E+1	-.371E+1	-.880E+1
	.199E+0	.644E-1	.480E+0	.184E+0
.102E+3	*.223E+1*	*.273E+1*	*-.969E+1*	*.103E+2*
	.325E+0	.351E+1	-.217E+1	-.115E+2
	.181E+0	.579E-1	.598E+0	.247E+0
.132E+3	.254E+1	.134E+1	-.124E+2	.289E+1
	.492E+0	.246E+1	-.391E+1	.992E+0
	.252E+0	.839E-1	.457E+0	.173E+0
.178E+3	.230E+1	.159E+1	-.976E+1	.187E+1
	.447E+0	.197E+1	-.168E+0	-.106E+1
	.253E+0	.847E-1	.564E+0	.229E+0
.256E+3	.175E+1	.111E+1	-.572E+1	-.202E+0
	.217E+0	.696E+0	.153E+1	-.101E+0
	.461E+0	.175E+0	.598E+0	.298E+0
.372E+3	.180E+1	.904E+0	-.540E+1	-.929E+0
	.467E+0	*.566E+0*	*-.341E+0*	*.755E+0*
	.523E+0	.206E+0	.598E+0	.355E+0

BUR 631290. 124280. Bürchen

.116E+1	.558E+1	.139E+2	-.106E+2	-.154E+2
	-.152E+1	.103E+2	-.636E+1	-.914E+0
	.303E-1	.890E-2	.404E-1	.119E-1
.146E+1	.391E+1	.124E+2	-.843E+1	-.141E+2
	-.186E+1	.853E+1	-.503E+1	-.357E+0
	.344E-1	.100E-1	.467E-1	.138E-1
.183E+1	.198E+1	.977E+1	-.565E+1	-.111E+2
	-.185E+1	.584E+1	-.418E+1	.115E+1
	.481E-1	.142E-1	.719E-1	.215E-1
.229E+1	.175E+1	.919E+1	-.543E+1	-.102E+2
	-.171E+1	.456E+1	-.327E+1	.918E+0
	.602E-1	.180E-1	.696E-1	.209E-1
.291E+1	.118E+1	.703E+1	-.462E+1	-.862E+1
	-.161E+1	.297E+1	-.255E+1	.721E+0
	.908E-1	.276E-1	.720E-1	.215E-1
.377E+1	.112E+1	.636E+1	-.388E+1	-.690E+1
	-.125E+1	.330E+1	-.193E+1	.757E-1
	.866E-1	.263E-1	.758E-1	.228E-1
.492E+1	.665E+0	.453E+1	-.343E+1	-.502E+1
	-.113E+1	.269E+1	-.145E+1	-.236E+0
	.929E-1	.282E-1	.714E-1	.214E-1
.640E+1	.491E+0	.309E+1	-.312E+1	-.358E+1
	-.104E+1	.213E+1	-.113E+1	-.788E+0
	.146E+0	.456E-1	.844E-1	.255E-1
.826E+1	.786E+0	.405E+1	-.329E+1	-.388E+1
	-.912E+0	.131E+1	-.520E+0	.427E+0
	.138E+0	.429E-1	.794E-1	.239E-1
.107E+2	.390E+0	.219E+1	-.290E+1	-.244E+1
	-.859E+0	.112E+1	-.551E+0	-.695E+0
	.215E+0	.702E-1	.773E-1	.232E-1
.135E+2	.178E+0	.868E+0	-.240E+1	-.943E+0
	-.691E+0	.132E+1	-.826E+0	-.231E+1
	.196E+0	.634E-1	.661E-1	.198E-1
.171E+2	.180E+0	.660E+0	-.220E+1	-.202E+0
	-.489E+0	.126E+1	-.790E+0	-.228E+1
	.103E+0	.315E-1	.434E-1	.128E-1
.213E+2	.212E+0	.554E+0	-.214E+1	-.193E+0
	-.433E+0	.122E+1	-.618E+0	-.202E+1
	.868E-1	.263E-1	.514E-1	.153E-1
.256E+2	.214E+0	.355E+0	-.183E+1	.641E+0
	-.327E+0	.110E+1	-.527E+0	-.173E+1
	.864E-1	.260E-1	.560E-1	.168E-1
.330E+2	.252E+0	.257E+0	-.195E+1	.757E+0
	-.273E+0	.898E+0	-.212E+0	-.927E+0
	.118E+0	.363E-1	.600E-1	.179E-1
.427E+2	.250E+0	.191E+0	-.208E+1	.872E-1
	-.239E+0	.788E+0	-.373E-2	-.108E+1
	.157E+0	.495E-1	.721E-1	.216E-1
.539E+2	.278E+0	.186E+0	-.207E+1	-.172E-1
	-.269E+0	.616E+0	.159E+0	-.101E+1
	.172E+0	.546E-1	.920E-1	.279E-1
.683E+2	.314E+0	.221E+0	-.193E+1	.251E+0
	-.240E+0	.556E+0	.155E+0	-.859E+0
	.191E+0	.614E-1	.975E-1	.297E-1
.853E+2	.357E+0	.211E+0	-.227E+1	-.151E+0
	-.298E+0	.374E+0	.386E+0	-.595E+0
	.311E+0	.107E+0	.116E+0	.356E-1
.102E+3	.401E+0	.322E+0	-.229E+1	-.337E+0
	-.282E+0	.344E+0	.487E+0	-.427E+0
	.361E+0	.129E+0	.128E+0	.396E-1
.102E+3	.421E+0	.330E+0	-.244E+1	-.463E+0
	-.299E+0	.304E+0	.507E+0	-.491E+0
	.373E+0	.134E+0	.117E+0	.360E-1
.132E+3	.235E+0	.807E-1	-.190E+1	.124E+0
	-.236E+0	.298E+0	.480E+0	-.783E+0
	.515E+0	.203E+0	.186E+0	.596E-1
.178E+3	.271E+0	.322E-1	-.172E+1	.172E+0
	-.253E+0	.218E+0	.740E+0	-.878E-1
	.597E+0	.331E+0	.217E+0	.710E-1
.256E+3	.319E+0	.333E+0	-.179E+1	-.313E+0
	-.250E+0	.276E+0	.946E+0	-.474E+0
	.373E+0	.134E+0	.222E+0	.728E-1
.372E+3	.822E-1	.199E+0	-.912E+0	-.256E+0
	-.707E-1	*.997E-1*	*.347E+0*	*-.646E-1*
	.599E+0	.376E+0	.445E+0	.167E+0

NAN 640810. 117990. Nanztal

.116E+1	-.281E+2	-.311E+1	-.401E+2	-.181E+2
	-.478E+1	.252E+1	-.704E+1	-.840E+1
	.950E-1	.290E-1	.850E-2	.244E-2
.146E+1	-.272E+2	-.152E+1	-.391E+2	-.150E+2
	-.404E+1	.225E+1	-.563E+1	-.741E+1
	.148E+0	.460E-1	.878E-2	.253E-2
.183E+1	-.266E+2	-.693E+0	-.388E+2	-.128E+2
	-.320E+1	.162E+1	-.411E+1	-.704E+1
	.233E+0	.771E-1	.903E-2	.262E-2
.229E+1	*-.262E+2*	*.271E+0*	*-.388E+2*	*-.112E+2*
	-.236E+1	.117E+1	-.263E+1	-.626E+1
	.361E+0	.128E+0	.972E-2	.279E-2
.291E+1	-.264E+2	-.603E-1	-.394E+2	-.106E+2
	-.129E+1	.131E+1	-.114E+1	-.484E+1
	.323E+0	.111E+0	.828E-2	.236E-2
.377E+1	-.264E+2	-.376E-1	-.399E+2	-.101E+2
	-.732E+0	.447E+0	.366E-1	-.416E+1
	.602E+0	.383E+0	.907E-2	.262E-2
.492E+1	-.268E+2	-.109E+1	-.407E+2	-.110E+2
	-.479E-1	.119E+0	.802E+0	-.352E+1
	.454E+0	.171E+0	.845E-2	.244E-2
.640E+1	-.270E+2	-.125E+1	-.410E+2	-.108E+2
	.481E+0	*-.149E+0*	*.139E+1*	*-.326E+1*
	.547E+0	.219E+0	.116E-1	.340E-2
.826E+1	-.295E+2	-.782E+1	-.443E+2	-.183E+2
	.198E+1	.377E+1	.323E+1	.229E+1
	.109E+0	.334E-1	.109E-1	.314E-2
.107E+2	-.290E+2	-.684E+1	-.436E+2	-.163E+2
	.202E+1	.248E+1	.325E+1	.141E+1
	.163E+0	.516E-1	.139E-1	.401E-2
.135E+2	-.284E+2	-.458E+1	-.421E+2	-.112E+2
	.211E+1	.135E+1	.342E+1	.876E-1
	.335E+0	.118E+0	.212E-1	.620E-2
.171E+2	-.264E+2	-.217E-1	-.392E+2	-.375E+1
	.906E+0	-.487E+1	.170E+1	-.828E+1
	.370E+0	.133E+0	*.271E-1*	*.794E-2*
.213E+2	-.246E+2	.534E+1	-.361E+2	.608E+1
	-.287E+0	-.108E+2	.246E-1	-.164E+2
	.205E+0	.665E-1	.370E-1	.109E-1
.256E+2	-.231E+2	.815E+1	-.337E+2	.106E+2
	.157E+1	-.526E+1	.250E+1	-.853E+1
	.214E+0	.700E-1	.376E-1	.111E-1
.330E+2	-.223E+2	.722E+1	-.325E+2	.989E+1
	.375E+1	.306E+1	.554E+1	.360E+1
	.291E+0	.997E-1	.511E-1	.152E-1
.427E+2	-.211E+2	.187E+1	-.309E+2	.225E+1
	.224E+1	-.363E+1	.334E+1	-.588E+1
	.517E+0	.203E+0	.685E-1	.205E-1
.539E+2	-.224E+2	.139E+0	-.327E+2	-.160E+0
	.221E+1	-.854E+1	.322E+1	-.128E+2
	.256E+0	.856E-1	.782E-1	.236E-1
.683E+2	-.213E+2	.101E+1	-.312E+2	.121E+1
	.428E+1	-.622E+1	.616E+1	-.943E+1
	.286E+0	.974E-1	.820E-1	.248E-1
.853E+2	-.205E+2	.487E+0	-.299E+2	.470E+0
	.445E+1	-.242E+1	.643E+1	-.384E+1
	.598E+0	.367E+0	.119E+0	.367E-1
.102E+3	-.213E+2	.979E+0	-.312E+2	.979E+0

.698E+1	.419E+0	.101E+2	.337E+0
.598E+0	.105E+1	.127E+0	.393E-1
.102E+3	-.188E+2	.389E+1	-.274E+2	.526E+1
.727E+1	-.269E+1	.104E+2	-.417E+1
.598E+0	.249E+0	.148E+0	.464E-1
.132E+3	-.196E+2	-.172E+1	-.286E+2	-.294E+1
.776E+1	-.340E+1	.113E+2	-.511E+1
.598E+0	.411E+0	.161E+0	.509E-1
.178E+3	-.156E+2	-.602E+1	-.227E+2	-.903E+1
.880E+1	.151E+1	.127E+2	.195E+1
.598E+0	.258E+0	.197E+0	.637E-1
.256E+3	-.101E+2	-.264E+1	-.148E+2	-.390E+1
.854E+1	-.349E+1	.124E+2	-.518E+1
.598E+0	.328E+0	.290E+0	.993E-1
.372E+3	-.645E+1	-.331E-1	-.924E+1	-.210E+0
.944E+1	.313E+1	.136E+2	.431E+1
.598E+0	.663E+0	.414E+0	.153E+0

NES 642520. 122780. Nesseltal

.116E+1	-.687E+2	.148E+3	-.316E+2	.344E+2
-.242E+2	.496E+2	-.108E+2	.147E+2
.197E-1	.576E-2	.349E-1	.102E-1
.146E+1	-.612E+2	.141E+3	-.289E+2	.331E+2
-.246E+2	.438E+2	-.976E+1	.119E+2
.209E-1	.611E-2	.317E-1	.925E-2
.183E+1	-.535E+2	.129E+3	-.273E+2	.307E+2
-.224E+2	.400E+2	-.852E+1	.980E+1
.230E-1	.672E-2	.313E-1	.916E-2
.229E+1	-.488E+2	.123E+3	-.262E+2	.296E+2
-.189E+2	.351E+2	-.626E+1	.743E+1
.258E-1	.751E-2	.274E-1	.803E-2
.291E+1	-.471E+2	.113E+3	-.266E+2	.273E+2
-.150E+2	.290E+2	-.450E+1	.547E+1
.266E-1	.777E-2	.216E-1	.628E-2
.377E+1	-.456E+2	.105E+3	-.266E+2	.258E+2
-.114E+2	.226E+2	-.281E+1	.383E+1
.336E-1	.986E-2	.224E-1	.654E-2
.492E+1	-.462E+2	.937E+2	-.277E+2	.231E+2
-.899E+1	.129E+2	-.172E+1	.133E+1
.398E-1	.117E-1	.204E-1	.593E-2
.640E+1	-.515E+2	.748E+2	-.289E+2	.194E+2
-.738E+1	.697E+1	-.995E+0	-.583E+0
.720E-1	.216E-1	.255E-1	.742E-2
.826E+1	-.534E+2	.672E+2	-.301E+2	.159E+2
-.309E+1	.673E+1	.659E+0	.835E+0
.100E+0	.305E-1	.289E-1	.847E-2
.107E+2	-.562E+2	.554E+2	-.305E+2	.143E+2
-.200E+1	.342E+1	.495E+0	-.192E+1
.137E+0	.425E-1	.317E-1	.925E-2
.135E+2	-.583E+2	.456E+2	-.307E+2	.138E+2
-.252E+1	-.475E+1	.377E+0	-.384E+1
.176E+0	.561E-1	.352E-1	.103E-1
.171E+2	-.571E+2	.378E+2	-.297E+2	.135E+2
-.475E+1	-.137E+2	-.715E+0	-.861E+1
.197E+0	.637E-1	.432E-1	.127E-1
.213E+2	-.566E+2	.356E+2	-.293E+2	.143E+2
-.550E+1	-.243E+2	-.184E+1	-.144E+2
.196E+0	.633E-1	.511E-1	.152E-1
.256E+2	-.549E+2	.367E+2	-.284E+2	.159E+2
.311E+0	-.638E+1	.116E+1	-.584E+1
.189E+0	.606E-1	.489E-1	.145E-1
.330E+2	-.561E+2	.270E+2	-.278E+2	.132E+2
.689E+1	.630E+1	.434E+1	.207E+1
.243E+0	.808E-1	.581E-1	.173E-1
.427E+2	-.494E+2	.156E+2	-.251E+2	.713E+1
.413E+1	-.293E+1	.250E+1	-.341E+1
.395E+0	.144E+0	.834E-1	.252E-1
.539E+2	-.519E+2	.848E+1	-.261E+2	.341E+1
.324E+1	-.176E+2	.235E+1	-.983E+1
.313E+0	.109E+0	.976E-1	.298E-1
.683E+2	-.473E+2	.871E+1	-.247E+2	.353E+1
.618E+1	-.116E+2	.379E+1	-.658E+1
.342E+0	.120E+0	.106E+0	.324E-1
.853E+2	-.460E+2	.822E+1	-.244E+2	.282E+1
.810E+1	-.435E+1	.506E+1	-.343E+1
.598E+0	.292E+0	.144E+0	.449E-1
.102E+3	-.450E+2	.158E+2	-.234E+2	.685E+1
.115E+2	-.342E+1	.653E+1	-.247E+1
.482E+0	.185E+0	.154E+0	.484E-1
.102E+3	-.441E+2	.200E+2	-.223E+2	.920E+1
.163E+2	-.693E+1	.878E+1	-.459E+1
.402E+0	.147E+0	.167E+0	.529E-1
.132E+3	-.457E+2	.535E+1	-.232E+2	.203E+1
.153E+2	-.159E+2	.929E+1	-.766E+1
.598E+0	.251E+0	.206E+0	.668E-1
.178E+3	-.291E+2	.561E+0	-.159E+2	-.462E+0
.164E+2	.624E+1	.977E+1	.289E+1
.598E+0	.623E+0	.247E+0	.822E-1
.256E+3	-.202E+2	.162E+0	-.106E+2	-.781E+0
.194E+2	-.574E+1	.112E+2	-.330E+1
.598E+0	.583E+0	.298E+0	.102E+0
.372E+3	-.139E+2	.239E+1	-.768E+1	.337E+0
.130E+2	.551E+1	.736E+1	.314E+1
.598E+0	.730E+0	.523E+0	.206E+0

MAS 601000. 116800. Mase

.116E+1	-.289E+0	.958E+1	.172E+1	-.290E+1
.101E+2	.328E+2	-.123E+2	-.951E+1
.383E-1	.113E-1	.679E-1	.203E-1
.146E+1	-.532E+0	.755E+1	.138E+1	-.253E+1
.695E+1	.258E+2	-.104E+2	-.874E+1
.381E-1	.112E-1	.625E-1	.187E-1
.183E+1	-.789E+0	.480E+1	.110E+1	-.830E+0

.532E+1	.210E+2	-.823E+1	-.694E+1
.418E-1	.123E-1	.656E-1	.195E-1
.229E+1	-.482E+0	.455E+1	.317E+0	-.136E+1
.390E+1	.176E+2	-.637E+1	-.539E+1
.436E-1	.128E-1	.743E-1	.223E-1
.291E+1	.101E+0	.425E+1	-.454E+0	-.122E+1
.323E+1	.142E+2	-.516E+1	-.457E+1
.408E-1	.120E-1	.659E-1	.197E-1
.377E+1	.354E+0	.416E+1	-.352E+0	-.925E+0
.255E+1	.114E+2	-.450E+1	-.429E+1
.503E-1	.149E-1	.733E-1	.221E-1
.492E+1	.479E+0	.353E+1	-.593E+0	-.673E+0
.116E+1	.840E+1	-.302E+1	-.297E+1
.595E-1	.177E-1	.100E+0	.306E-1
.640E+1	.766E+0	.380E+1	-.839E+0	-.117E+1
.805E+0	.665E+1	-.231E+1	-.231E+1
.836E-1	.253E-1	.144E+0	.448E-1
.826E+1	.794E+0	.290E+1	-.912E+0	-.788E+0
.487E+0	.532E+1	-.159E+1	-.151E+1
.113E+0	.347E-1	.203E+0	.656E-1
.107E+2	.106E+1	.271E+1	-.825E+0	-.573E+0
.348E+0	.466E+1	-.127E+1	-.151E+1
.109E+0	.334E-1	.212E+0	.692E-1
.135E+2	.139E+1	.304E+1	-.116E+1	-.932E+0
.118E+0	.353E+1	-.988E+0	-.120E+1
.133E+0	.413E-1	.214E+0	.698E-1
.171E+2	.139E+1	.228E+1	-.121E+1	-.919E+0
.569E-1	.299E+1	-.848E+0	-.113E+1
.138E+0	.432E-1	.184E+0	.593E-1
.213E+2	.141E+1	.205E+1	-.110E+1	-.782E+0
.301E+0	.286E+1	-.812E+0	-.111E+1
.166E+0	.527E-1	.219E+0	.717E-1
.256E+2	.122E+1	.145E+1	-.105E+1	-.643E+0
.351E+0	.247E+1	-.764E+0	-.810E+0
.164E+0	.520E-1	.176E+0	.562E-1
.330E+2	.138E+1	.148E+1	-.115E+1	-.578E+0
.283E+0	.202E+1	-.668E+0	-.891E+0
.161E+0	.508E-1	.160E+0	.506E-1
.427E+2	.103E+1	.945E+0	-.823E+0	-.306E+0
.351E+0	.179E+1	-.559E+0	-.748E+0
.156E+0	.493E-1	.174E+0	.555E-1
.539E+2	.107E+1	.705E+0	-.943E+0	-.181E+0
.387E+0	.153E+1	-.322E+0	-.571E+0
.160E+0	.503E-1	.174E+0	.554E-1
.683E+2	.934E+0	.760E+0	-.842E+0	-.327E+0
.266E+0	.118E+1	-.293E+0	-.453E+0
.154E+0	.486E-1	.174E+0	.554E-1
.853E+2	.807E+0	.824E+0	-.685E+0	-.228E+0
.177E+0	.116E+1	-.275E+0	-.446E+0
.162E+0	.512E-1	.224E+0	.734E-1
.102E+3	.676E+0	.605E+0	-.723E+0	-.209E+0
.161E+0	.913E+0	-.263E+0	-.511E+0
.225E+0	.740E-1	.197E+0	.635E-1
.102E+3	.669E+0	.713E+0	-.681E+0	-.297E+0
.161E+0	.916E+0	-.251E+0	-.538E+0
.204E+0	.662E-1	.211E+0	.687E-1
.132E+3	.804E+0	.576E+0	-.742E+0	-.205E+0
.927E-1	.753E+0	-.111E+0	-.449E+0
.226E+0	.741E-1	.207E+0	.675E-1
.178E+3	.780E+0	.594E+0	-.660E+0	-.323E+0
.370E-1	.529E+0	-.794E-2	-.377E+0
.294E+0	.101E+0	.294E+0	.101E+0
.256E+3	.724E+0	.491E+0	-.584E+0	-.359E+0
-.130E+0	.568E+0	.174E+0	-.167E+0
.598E+0	.260E+0	.513E+0	.201E+0
.372E+3	.478E+0	-.179E+0	-.471E+0	.160E+0
.269E-1	.245E+0	.516E-1	-.382E+0
.598E+0	.269E+1	.598E+0	.348E+0

REC 605575. 118725. Réchy

.116E+1	.324E+0	.325E+1	.164E+1	-.183E+1
-.368E+1	.229E+2	-.183E+2	-.337E+0
.299E-1	.873E-2	.586E-1	.174E-1
.146E+1	-.785E-1	.276E+1	.900E+0	-.172E+1
-.282E+1	.178E+2	-.140E+2	.399E+0
.292E-1	.855E-2	.562E-1	.167E-1
.183E+1	.174E+0	.313E+1	.775E+0	-.901E+0
-.216E+1	.138E+2	-.104E+2	.546E+0
.322E-1	.943E-2	.741E-1	.223E-1
.229E+1	-.105E+0	.284E+1	-.383E+0	-.124E+1
-.191E+1	.108E+2	-.853E+1	-.152E+0
.353E-1	.104E-1	.602E-1	.179E-1
.291E+1	-.188E-1	.263E+1	-.815E+0	-.843E+0
-.149E+1	.873E+1	-.678E+1	-.928E-1
.333E-1	.977E-2	.518E-1	.154E-1
.377E+1	.515E-3	.250E+1	-.894E+0	-.645E+0
-.121E+1	.684E+1	-.530E+1	-.135E+0
.410E-1	.120E-1	.590E-1	.175E-1
.492E+1	.809E-2	.216E+1	-.972E+0	-.537E+0
-.101E+1	.555E+1	-.378E+1	-.336E-1
.460E-1	.136E-1	.705E-1	.211E-1
.640E+1	.178E-1	.185E+1	-.891E+0	-.207E+0
-.852E+0	.436E+1	-.295E+1	-.190E+0
.690E-1	.207E-1	.102E+0	.311E-1
.826E+1	.183E+0	.212E+1	-.799E+0	.114E+0
-.703E+0	.335E+1	-.227E+1	-.113E+0
.832E-1	.251E-1	.122E+0	.377E-1
.107E+2	.406E+0	.204E+1	-.857E+0	.137E+0
-.616E+0	.269E+1	-.149E+1	-.957E-1
.952E-1	.289E-1	.147E+0	.464E-1
.135E+2	.386E+0	.187E+1	-.958E+0	-.366E-1
-.530E+0	.215E+1	-.116E+1	-.190E+0
.117E+0	.360E-1	.166E+0	.527E-1

.171E+2	.421E+0	.169E+1	-.101E+1	.145E+0
-.328E+0	.200E+1	-.930E+0	-.731E-1
.109E+0	.333E-1	.152E+0	.479E-1
.213E+2	.431E+0	.155E+1	-.974E+0	.152E+0
-.305E+0	.147E+1	-.746E+0	-.180E+0
.142E+0	.442E-1	.188E+0	.605E-1
.256E+2	.314E+0	.120E+1	-.987E+0	.252E+0
-.271E+0	.138E+1	-.588E+0	-.506E-1
.127E+0	.394E-1	.158E+0	.498E-1
.330E+2	.345E+0	.107E+1	-.938E+0	.432E+0
-.229E+0	.106E+1	-.507E+0	-.217E+0
.144E+0	.449E-1	.150E+0	.471E-1
.427E+2	.285E+0	.799E+0	-.964E+0	.308E+0
-.180E+0	.904E+0	-.356E+0	-.165E+0
.154E+0	.484E-1	.149E+0	.467E-1
.539E+2	.317E+0	.633E+0	-.108E+1	.236E+0
-.461E-1	.756E+0	-.379E+0	-.316E+0
.165E+0	.525E-1	.133E+0	.413E-1
.683E+2	.236E+0	.482E+0	-.869E+0	.147E+0
-.550E-1	.525E+0	-.273E+0	-.265E+0
.179E+0	.571E-1	.145E+0	.452E-1
.853E+2	.239E+0	.473E+0	-.832E+0	.227E+0
-.392E-1	.484E+0	-.143E+0	-.373E+0
.200E+0	.649E-1	.168E+0	.533E-1
.102E+3	.189E+0	.454E+0	-.805E+0	.174E+0
.918E-2	.340E+0	-.101E+0	-.389E+0
.230E+0	.758E-1	.165E+0	.522E-1
.102E+3	.183E+0	.411E+0	-.780E+0	.157E+0
-.643E-2	.313E+0	-.102E+0	-.425E+0
.266E+0	.895E-1	.167E+0	.531E-1
.132E+3	.238E+0	.429E+0	-.710E+0	.156E+0
-.789E-1	.393E+0	-.543E-1	-.485E+0
.253E+0	.846E-1	.213E+0	.695E-1
.178E+3	.221E+0	.465E+0	-.677E+0	.133E-1
-.581E-1	.304E+0	-.858E-2	-.361E+0
.290E+0	.992E-1	.252E+0	.839E-1
.256E+3	.232E+0	.384E+0	-.670E+0	.296E-1
-.348E-1	.124E+0	.919E-1	-.116E-1
.598E+0	.250E+0	.389E+0	.141E+0
.372E+3	.210E+0	.333E+0	-.402E+0	-.100E-1
-.495E-1	.120E-1	-.688E-1	-.540E+0
.598E+0	.569E+0	.598E+0	.263E+0

THO 594380. 75820. Thoules

.112E+1	-.310E+1	.480E+1	-.582E+1	.707E+1
-.412E+1	-.181E+1	-.916E+1	.812E+0
.176E-1	.532E-2	.121E-1	.358E-2
.140E+1	-.242E+1	.454E+1	-.452E+1	.652E+1
-.374E+1	-.817E+0	-.816E+1	.159E+1
.202E-1	.602E-2	.145E-1	.419E-2
.175E+1	-.188E+1	.422E+1	-.353E+1	.587E+1
-.338E+1	-.646E-1	-.707E+1	.218E+1
.233E-1	.689E-2	.192E-1	.558E-2
.219E+1	-.141E+1	.392E+1	-.276E+1	.532E+1
-.269E+1	.541E+0	-.584E+1	.248E+1
.249E-1	.716E-2	.280E-1	.829E-2
.279E+1	-.115E+1	.343E+1	-.226E+1	.460E+1
-.218E+1	.841E+0	-.471E+1	.259E+1
.233E-1	.698E-2	.385E-1	.114E-1
.361E+1	-.515E+0	.295E+1	-.115E+1	.390E+1
-.190E+1	.985E+0	-.397E+1	.241E+1
.282E-1	.820E-2	.625E-1	.186E-1
.473E+1	.487E+0	.258E+1	.630E-1	.332E+1
-.157E+1	.869E+0	-.317E+1	.204E+1
.292E-1	.855E-2	.795E-1	.240E-1
.614E+1	.889E+0	.223E+1	.578E+0	.285E+1
-.155E+1	.714E+0	-.282E+1	.163E+1
.416E-1	.123E-1	.107E+0	.328E-1
.793E+1	.747E+0	.189E+1	.370E+0	.239E+1
-.142E+1	.548E+0	-.253E+1	.126E+1
.509E-1	.150E-1	.122E+0	.378E-1
.102E+2	.383E+0	.139E+1	.232E+0	.177E+1
-.116E+1	.432E+0	-.208E+1	.972E+0
.677E-1	.203E-1	.117E+0	.360E-1
.129E+2	.966E-1	.112E+1	-.545E-1	.143E+1
-.669E+0	.438E+0	-.144E+1	.850E+0
.781E-1	.236E-1	.975E-1	.299E-1
.164E+2	.192E+0	.582E+0	.118E+0	.789E+0
-.448E+0	.331E+0	-.986E+0	.687E+0
.950E-1	.289E-1	.522E-1	.152E-1
.205E+2	.219E+0	.403E+0	.153E+0	.557E+0
-.332E+0	.280E+0	-.779E+0	.550E+0
.138E+0	.435E-1	.649E-1	.199E-1
.246E+2	.199E+0	.390E+0	.140E+0	.521E+0
-.235E+0	.278E+0	-.616E+0	.507E+0
.141E+0	.434E-1	.844E-1	.259E-1
.317E+2	.151E+0	.382E+0	.783E-1	.514E+0
-.170E+0	.242E+0	-.454E+0	.423E+0
.169E+0	.540E-1	.131E+0	.415E-1
.410E+2	.174E+0	.373E+0	.140E+0	.456E+0
-.130E+0	.205E+0	-.360E+0	.325E+0
.175E+0	.556E-1	.168E+0	.530E-1
.517E+2	.200E+0	.285E+0	.152E+0	.419E+0
-.107E+0	.127E+0	-.284E+0	.230E+0
.226E+0	.754E-1	.221E+0	.713E-1
.655E+2	.137E+0	.181E+0	.797E-1	.267E+0
-.601E-1	.976E-1	-.198E+0	.193E+0
.269E+0	.886E-1	.303E+0	.105E+0
.819E+2	.109E+0	.148E+0	.752E-1	.227E+0
-.314E-1	.879E-1	-.153E+0	.147E+0
.322E+0	.114E+0	.476E+0	.182E+0
.983E+2	.119E+0	.173E+0	.100E+0	.255E+0
-.252E-1	.778E-1	-.117E+0	.156E+0

```
          .332E+0   .118E+0   .593E+0   .252E+0
.983E+2   .129E+0   .172E+0   .984E-1   .261E+0
         -.997E-2   .856E-1  -.134E+0   .137E+0
          .336E+0   .118E+0   .586E+0   .241E+0
.127E+3   .294E-1   .123E+0  -.438E-1   .212E+0
         -.529E-1   .600E-1  -.138E+0   .991E-1
          .574E+0   .230E+0   .602E+0   .300E+0
.171E+3   .908E-1   .171E+0   .381E-1   .255E+0
         -.762E-1   .374E-1  -.147E+0   .389E-1
          .444E+0   .167E+0   .596E+0   .261E+0
.246E+3   .427E-1   .103E+0   .486E-2   .204E+0
          .147E-1  -.281E-1  -.247E-1  -.792E-1
          .594E+0   .282E+0   .602E+0   .147E+1
.358E+3   .124E+0   .110E+0   .105E+0   .195E+0
         -.807E-1  -.257E-1  -.953E-1  -.313E-1
          .597E+0   .304E+0   .599E+0   .278E+0

BAR  589280.   80050.   Barlia
.112E+1  -.310E+1   .156E+2  -.108E+2   .693E+1
         -.176E+2   .390E+2  -.265E+2   .202E+2
          .109E-1   .314E-2   .141E-1   .410E-2
.140E+1   .139E+0   .114E+2  -.742E+1   .429E+1
         -.147E+2   .329E+2  -.226E+2   .174E+2
          .124E-1   .358E-2   .153E-1   .448E-2
.175E+1   .111E+1   .878E+1  -.575E+1   .235E+1
         -.111E+2   .264E+2  -.184E+2   .140E+2
          .148E-1   .428E-2   .195E-1   .567E-2
.219E+1   .254E+1   .747E+1  -.437E+1   .177E+1
         -.845E+1   .216E+2  -.152E+2   .119E+2
          .177E-1   .515E-2   .287E-1   .838E-2
.279E+1   .374E+1   .609E+1  -.293E+1   .922E+0
         -.543E+1   .165E+2  -.113E+2   .914E+1
          .189E-1   .550E-2   .404E-1   .119E-1
.361E+1   .553E+1   .586E+1  -.136E+1   .863E+0
         -.372E+1   .127E+2  -.836E+1   .689E+1
          .228E-1   .663E-2   .649E-1   .194E-1
.473E+1   .677E+1   .605E+1  -.695E+0   .106E+1
         -.263E+1   .913E+1  -.572E+1   .496E+1
          .237E-1   .689E-2   .883E-1   .267E-1
.614E+1   .665E+1   .614E+1  -.778E+0   .114E+1
         -.205E+1   .710E+1  -.434E+1   .358E+1
          .320E-1   .934E-2   .123E+0   .382E-1
.793E+1   .547E+1   .591E+1  -.615E+0   .139E+1
         -.126E+1   .531E+1  -.289E+1   .269E+1
          .349E-1   .102E-1   .173E+0   .552E-1
.102E+2   .349E+1   .539E+1  -.981E+0   .152E+1
         -.100E+1   .435E+1  -.267E+1   .196E+1
          .378E-1   .111E-1   .148E+0   .463E-1
.129E+2   .211E+1   .482E+1  -.971E+0   .143E+1
         -.672E+0   .368E+1  -.274E+1   .137E+1
          .419E-1   .124E-1   .835E-1   .252E-1
.164E+2   .137E+1   .398E+1  -.940E+0   .117E+1
         -.441E+0   .343E+1  -.237E+1   .116E+1
          .340E-1   .995E-2   .347E-1   .101E-1
.205E+2   .153E+1   .353E+1  -.781E+0   .953E+0
         -.516E+0   .301E+1  -.210E+1   .979E+0
          .409E-1   .120E-1   .386E-1   .113E-1
.246E+2   .162E+1   .353E+1  -.604E+0   .101E+1
         -.252E+0   .266E+1  -.182E+1   .800E+0
          .401E-1   .118E-1   .448E-1   .132E-1
.317E+2   .137E+1   .339E+1  -.577E+0   .116E+1
         -.201E-2   .217E+1  -.139E+1   .610E+0
          .540E-1   .161E-1   .651E-1   .195E-1
.410E+2   .162E+1   .347E+1  -.325E+0   .119E+1
          .141E+0   .163E+1  -.114E+1   .393E+0
          .610E-1   .181E-1   .943E-1   .287E-1
.517E+2   .151E+1   .301E+1  -.314E+0   .114E+1
         -.781E-2   .134E+1  -.951E+0   .287E+0
          .732E-1   .219E-1   .151E+0   .476E-1
.655E+2   .122E+1   .256E+1  -.314E+0   .921E+0
         -.810E-1   .122E+1  -.830E+0   .227E+0
          .708E-1   .212E-1   .152E+0   .477E-1
.819E+2   .127E+1   .248E+1  -.144E+0   .972E+0
         -.616E-1   .994E+0  -.824E+0   .176E+0
          .902E-1   .273E-1   .251E+0   .843E-1
.983E+2   .119E+1   .242E+1  -.321E+0   .879E+0
          .257E-1   .719E+0  -.394E+0   .245E-1
          .113E+0   .347E-1   .439E+0   .165E+0
.983E+2   .922E+0   .243E+1  -.354E+0   .910E+0
          .939E-2   .781E+0  -.454E+0   .863E-1
          .111E+0   .340E-1   .436E+0   .163E+0
.127E+3   .365E+0   .250E+1  -.589E+0   .971E+0
         -.242E+0   .352E+0  -.455E+0  -.525E-1
          .134E+0   .418E-1   .350E+0   .124E+0
.171E+3   .909E+0   .242E+1  -.411E+0   .928E+0
         -.497E+0  -.795E-1  -.370E+0  -.179E+0
          .158E+0   .499E-1   .490E+0   .190E+0
.246E+3   .889E+0   .206E+1  -.424E+0   .719E+0
          .505E-1  -.309E+0  -.776E-1  -.368E+0
          .184E+0   .589E-1   .564E+0   .229E+0
.358E+3   .136E+1   .225E+1  -.165E+0   .962E+0
         -.338E+0  -.408E-1  -.308E+0  -.109E+0
          .222E+0   .727E-1   .598E+0   .277E+0
```

Table of induction coefficients in the measuring axes

Content:
title line:
abbreviation, coordinates
1st line:
period(s), real part of A,B
2nd line:
imaginary part of A,B

ZIN 614890. 106780.

.274E+0	-.110E+0	-.772E+0
	-.616E-1	.777E-1
.365E+0	-.307E-1	-.748E+0
	-.122E+0	.186E+0
.487E+0	.158E+0	-.308E+0
	-.142E+0	.434E+0
.649E+0	-.177E-1	.803E-1
	-.307E+0	.474E+0
.866E+0	-.239E+0	.234E+0
	-.321E+0	.328E+0
.115E+1	-.312E+0	.265E+0
	-.279E+0	.262E+0
.154E+1	-.345E+0	.302E+0
	-.219E+0	.231E+0
.219E+1	-.401E+0	.360E+0
	-.157E+0	.222E+0
.274E+1	-.415E+0	.355E+0
	-.158E+0	.215E+0
.365E+1	-.443E+0	.375E+0
	-.139E+0	.191E+0
.487E+1	-.419E+0	.430E+0
	-.144E+0	.176E+0
.520E+1	-.400E+0	.491E+0
	-.158E+0	.187E+0
.866E+1	-.494E+0	.440E+0
	-.169E+0	.882E-1
.924E+1	-.519E+0	.412E+0
	-.168E+0	.154E+0
.116E+2	-.550E+0	.412E+0
	-.191E+0	.965E-1
.164E+2	-.569E+0	.459E+0
	-.230E+0	.146E+0
.205E+2	-.581E+0	.519E+0
	-.217E+0	.105E+0
.292E+2	-.686E+0	.527E+0
	-.220E+0	.529E-1
.390E+2	-.805E+0	.446E+0
	-.207E+0	.193E+0
.520E+2	-.906E+0	.492E+0
	-.256E+0	.580E-1
.693E+2	-.884E+0	.573E+0
	-.971E-1	.215E+0
.924E+2	-.830E+0	.604E+0
	-.219E-1	.341E+0
.123E+3	-.824E+0	.710E+0
	-.594E-1	.221E+0
.164E+3	-.888E+0	.724E+0
	-.107E+0	.359E+0
.219E+3	-.777E+0	.780E+0
	.108E+0	.438E+0
.292E+3	-.858E+0	.782E+0
	-.153E+0	.429E-1

BOS 619960. 115370.

.284E+0	-.242E+0	-.266E+0
	-.861E-2	.130E-2
.379E+0	-.225E+0	-.245E+0
	-.504E-1	.161E-1
.505E+0	-.363E+0	-.152E-1
	-.292E-1	-.667E-1
.674E+0	-.325E+0	-.260E-1
	-.566E-1	.170E+0
.898E+0	-.396E+0	-.102E+0
	-.975E-1	.151E+0
.120E+1	-.345E+0	.269E-1
	-.772E-1	.189E+0
.160E+1	-.347E+0	.101E+0
	-.379E-1	.177E+0
.213E+1	-.354E+0	.161E+0
	-.590E-1	.938E-1
.227E+1	-.218E+0	.171E+0
	-.417E-1	-.110E-1
.379E+1	-.317E+0	.191E+0
	-.141E-1	.169E+0
.404E+1	-.280E+0	.152E+0
	-.316E-1	.295E-1
.539E+1	-.299E+0	.143E+0
	-.480E-1	.417E-1
.674E+1	-.327E+0	.220E+0
	-.377E-1	.112E+0
.898E+1	-.319E+0	.283E+0
	-.589E-1	.711E-1
.128E+2	-.378E+0	.126E+0
	-.494E-1	.548E-1
.160E+2	-.373E+0	.267E+0
	-.755E-1	.855E-1
.227E+2	-.384E+0	.236E+0
	-.432E-1	.113E+0
.303E+2	-.386E+0	.249E+0
	-.813E-1	.896E-1
.379E+2	-.403E+0	.335E+0
	-.758E-1	.111E+0
.539E+2	-.443E+0	.275E+0
	-.660E-1	.102E+0
.719E+2	-.466E+0	.290E+0
	-.125E+0	.600E-1
.958E+2	-.426E+0	.350E+0
	-.472E-2	.660E-2
.128E+3	-.428E+0	.329E+0
	.736E-2	.141E+0
.170E+3	-.549E+0	.401E-1
	-.245E-1	.357E+0
.227E+3	-.512E+0	.205E+0
	-.888E-1	.137E+0

LOE 632190. 142770.

.284E+0	.943E-1	-.138E+1
	.263E+0	-.603E-1
.379E+0	-.454E+0	-.152E+1
	.356E+0	.855E-1
.505E+0	-.726E+0	.148E+1
	.129E+0	.821E+0
.674E+0	-.324E+0	-.144E+1
	.274E+0	.252E+0
.898E+0	-.993E+0	.882E+0
	-.126E+0	.170E+1
.120E+1	-.134E+1	-.137E+1
	-.611E+0	.814E+0
.160E+1	-.906E+0	.146E+1
	-.478E+0	.129E+1
.213E+1	-.503E+0	.110E+1
	-.763E+0	.730E+0
.284E+1	-.811E+0	.124E+1
	-.491E+0	.879E+0
.303E+1	-.959E+0	.196E+1
	-.888E+0	.655E+0
.505E+1	-.142E+1	.274E+1
	-.597E+0	.229E+1
.539E+1	.100E+1	.270E+1
	-.857E+0	.423E+0
.674E+1	-.712E+0	.319E+1
	-.173E+1	.187E+1
.898E+1	.155E+1	.313E+1
	-.188E+1	.152E+1
.128E+2	-.109E+1	.153E+1
	-.192E+1	.240E+1
.170E+2	.176E+1	.299E+1
	-.157E+1	-.883E+0
.227E+2	.197E+1	-.159E+1
	-.171E+1	-.117E+1
.284E+2	.240E+1	.279E+1
	.614E+0	.147E+1
.379E+2	.183E+1	.214E+1
	-.237E+1	-.153E+1
.539E+2	.197E+1	.152E+1
	-.197E+1	-.269E+0
.674E+2	.913E+0	.101E+1
	-.188E+1	.149E+1
.958E+2	.870E+0	.123E+1
	-.245E+1	.610E+0
.128E+3	-.210E+1	-.294E-2
	.399E+0	.179E+1
.170E+3	-.145E+1	.246E+1
	-.255E+1	.147E+1
.227E+3	.335E+1	-.191E+1
	.266E+1	-.129E+1

MOY 610790. 105890.

.284E+0	-.535E+0	.167E+0
	.260E-3	-.562E-2
.379E+0	-.428E+0	.150E+0
	.688E-2	.347E-1
.505E+0	-.388E+0	.141E+0
	-.351E-1	.576E-1
.674E+0	-.351E+0	.179E+0
	-.726E-1	.798E-1
.898E+0	-.377E+0	.218E+0
	-.708E-1	.103E+0
.120E+1	-.364E+0	.284E+0
	-.662E-1	.956E-1
.160E+1	-.382E+0	.323E+0
	-.618E-1	.102E+0
.213E+1	-.399E+0	.337E+0
	-.683E-1	.894E-1
.284E+1	-.383E+0	.376E+0
	-.526E-1	.121E+0
.379E+1	-.390E+0	.383E+0
	-.547E-1	.118E+0
.505E+1	-.403E+0	.398E+0
	-.475E-1	.112E+0
.539E+1	-.451E+0	.417E+0
	-.544E-1	.101E+0
.674E+1	-.450E+0	.392E+0
	-.841E-1	.739E-1
.958E+1	-.525E+0	.396E+0
	-.941E-1	.829E-1
.120E+2	-.517E+0	.383E+0
	-.821E-1	.513E-1
.160E+2	-.515E+0	.385E+0
	-.523E-1	.803E-1
.213E+2	-.477E+0	.446E+0
	-.453E-1	.932E-1
.284E+2	-.426E+0	.498E+0
	-.473E-1	.750E-1
.404E+2	-.492E+0	.678E+0
	-.137E+0	.777E-1
.539E+2	-.519E+0	.641E+0
	-.252E+0	.368E-1
.719E+2	-.624E+0	.609E+0
	-.793E-1	.109E+0
.958E+2	-.633E+0	.579E+0
	.434E-1	.127E+0
.128E+3	-.633E+0	.546E+0
	.642E-1	.199E+0
.170E+3	-.641E+0	.620E+0
	.342E+0	.315E+0
.227E+3	-.585E+0	.564E+0
	.140E+0	.174E+0

MAU 592800. 92910.

.284E+0	-.590E+0	-.110E+0
	.323E-2	-.931E-2
.379E+0	-.607E+0	-.952E-1
	.175E-1	-.325E-1
.505E+0	-.618E+0	-.101E+0
	.285E-1	.819E-1
.674E+0	-.562E+0	.728E-1
	-.723E-2	.147E+0
.898E+0	-.523E+0	.179E+0
	-.419E-1	.141E+0
.120E+1	-.521E+0	.290E+0
	-.869E-1	.714E-1
.160E+1	-.449E+0	.354E+0
	-.343E-1	.125E+0
.213E+1	-.450E+0	.393E+0
	-.857E-1	.122E+0
.284E+1	-.489E+0	.417E+0
	-.844E-1	.935E-1
.303E+1	-.416E+0	.312E+0
	-.318E-1	.560E-1
.505E+1	-.517E+0	.387E+0
	-.979E-1	.323E-1
.539E+1	-.443E+0	.324E+0
	-.252E-1	.453E-1
.719E+1	-.452E+0	.320E+0
	-.559E-1	.374E-1
.898E+1	-.621E+0	.351E+0
	-.102E+0	-.292E-1
.128E+2	-.636E+0	.308E+0
	-.831E-1	-.607E-1
.160E+2	-.650E+0	.413E+0
	-.119E+0	-.438E-1
.228E+2	-.558E+0	.398E+0
	-.113E+0	-.852E-1
.284E+2	-.550E+0	.442E+0
	-.106E+0	-.863E-1
.379E+2	-.539E+0	.489E+0
	-.168E+0	-.909E-1
.540E+2	-.561E+0	.435E+0
	-.378E-1	-.132E+0
.719E+2	-.464E+0	.484E+0
	-.118E+0	-.877E-1
.959E+2	-.529E+0	.407E+0
	-.945E-1	-.213E+0
.128E+3	-.495E+0	.440E+0
	.611E-1	.393E-3
.171E+3	-.413E+0	.503E+0
	.143E+0	-.336E-1
.228E+3	-.445E+0	.626E+0
	.795E-1	-.130E+0

CLE 589990. 109060.

.274E+0	-.437E+0	-.177E+0
	-.299E-1	.345E-2
.365E+0	-.378E+0	-.123E+0
	-.664E-1	.119E+0
.487E+0	-.375E+0	.110E+0
	-.632E-1	.949E-1
.649E+0	-.313E+0	.126E+0
	-.997E-1	.602E-1
.866E+0	-.356E+0	.200E+0
	-.241E-1	.711E-1
.115E+1	-.399E+0	.165E+0
	-.760E-1	.503E-1
.154E+1	-.395E+0	.191E+0
	-.326E-1	.674E-2
.219E+1	-.291E+0	.914E-1
	.308E-1	-.284E-1
.274E+1	-.367E+0	.183E+0
	.188E-1	-.649E-1
.365E+1	-.352E+0	.166E+0
	.161E-1	-.127E+0
.487E+1	-.377E+0	.147E+0
	.306E-1	-.116E+0
.649E+1	-.424E+0	.164E+0
	.185E+0	-.140E+0
.866E+1	-.387E+0	.163E-1
	.249E-1	-.182E+0
.924E+1	-.464E+0	-.155E+0
	.538E-2	-.232E+0
.116E+2	-.379E+0	-.728E-1
	.584E-1	-.156E+0
.164E+2	-.521E+0	-.274E+0
	-.131E+0	-.262E+0
.219E+2	-.495E+0	-.304E+0
	.571E-1	-.239E+0
.274E+2	-.354E+0	-.584E-1
	.518E-1	-.230E+0
.390E+2	-.209E+0	-.167E+0
	-.102E+0	-.338E+0
.520E+2	-.771E-1	-.331E-1
	-.129E+0	-.278E+0
.693E+2	.128E+0	.369E+0
	.670E+0	.153E+0
.924E+2	-.523E+0	-.448E+0
	.363E+0	.434E+0
.123E+3	-.382E+0	-.256E+0
	-.537E+0	-.576E+0
.164E+3	-.175E+0	-.487E+0
	-.310E+1	-.259E+1
.219E+3	.132E+0	.157E+0
	.315E+0	.280E+0
.292E+3	.496E+0	.493E+0
	.770E+0	.984E+0

TRI 594900. 107745.

.577E+0	-.287E+0	.194E+0
	-.161E-1	.683E-1
.770E+0	-.262E+0	.217E+0
	-.323E-1	.779E-1
.103E+1	-.260E+0	.238E+0
	-.295E-1	.701E-1
.137E+1	-.226E+0	.279E+0
	-.297E-1	.392E-1
.183E+1	-.275E+0	.264E+0
	-.303E-1	.520E-1
.243E+1	-.275E+0	.253E+0
	-.915E-2	.327E-1
.325E+1	-.297E+0	.224E+0
	.131E-2	.150E-2
.433E+1	-.298E+0	.237E+0
	-.114E-1	-.427E-1
.616E+1	-.298E+0	.193E+0
	-.270E-1	-.105E+0
.821E+1	-.304E+0	.217E+0
	.887E-2	-.912E-1
.109E+2	-.368E+0	.197E+0
	.298E-1	-.742E-1
.137E+2	-.374E+0	.236E+0
	.356E-1	-.926E-1
.195E+2	-.389E+0	.539E-1
	-.967E-1	-.204E+0
.244E+2	-.321E+0	.286E+0
	.603E-1	-.989E-1
.325E+2	-.331E+0	.278E+0
	.755E-1	-.609E-1
.346E+2	-.333E+0	.157E+0
	.452E-1	-.125E+0
.577E+2	-.323E+0	.285E+0
	.109E+0	-.302E-1
.616E+2	-.224E+0	.308E+0
	.149E-1	-.176E+0
.821E+2	-.225E+0	.342E+0
	.200E-1	-.137E+0
.110E+3	-.231E+0	.197E+0
	-.127E-1	-.125E+0
.146E+3	-.236E+0	.317E+0
	.156E+0	-.121E-1
.195E+3	-.226E+0	.297E+0
	.291E-1	-.751E-2
.260E+3	-.207E+0	.394E+0
	.226E+0	.380E-1

LOU 605397. 113295.

.577E+0	-.232E+0	.160E+0
	-.276E-1	.575E-1
.770E+0	-.218E+0	.220E+0
	-.692E-1	.764E-1
.103E+1	-.228E+0	.188E+0
	-.315E-1	.520E-1
.137E+1	-.206E+0	.174E+0
	-.156E-1	.495E-1
.183E+1	-.198E+0	.180E+0
	.406E-2	.219E-1
.243E+1	-.225E+0	.140E+0
	.164E-1	.256E-1
.325E+1	-.246E+0	.132E+0
	-.657E-3	.272E-1
.433E+1	-.251E+0	.121E+0
	-.136E-2	.366E-1
.577E+1	-.256E+0	.113E+0
	.149E-2	-.213E-2
.821E+1	-.284E+0	.103E+0
	-.529E-2	-.431E-1
.103E+2	-.301E+0	.114E+0
	-.148E-2	.992E-2
.146E+2	-.292E+0	.860E-1
	-.213E-3	-.243E-1
.183E+2	-.317E+0	.119E+0
	.174E-1	-.505E-2
.244E+2	-.317E+0	.910E-1
	.951E-2	-.520E-1
.325E+2	-.315E+0	.993E-1
	.212E-1	-.414E-1
.346E+2	-.317E+0	.747E-1
	.313E-1	.226E-1
.577E+2	-.298E+0	.944E-1
	.305E-1	-.179E-1
.616E+2	-.307E+0	.805E-1
	.185E-1	-.194E-1
.821E+2	-.291E+0	.114E+0
	.599E-2	-.108E-1
.110E+3	-.272E+0	.105E+0
	.387E-1	-.153E-1
.146E+3	-.317E+0	.113E+0
	-.849E-2	.168E-1
.195E+3	-.307E+0	.780E-1
	-.219E-1	-.102E+0
.260E+3	-.363E+0	.898E-1
	.547E-1	-.320E-1

ARO 600770. 96000.

.577E+0	.396E+0	.707E+0
	-.427E-1	.396E-1
.770E+0	.314E+0	.800E+0
	-.161E-1	.110E+0
.103E+1	-.203E+0	.510E+0
	.187E+0	.101E+0
.137E+1	-.206E+0	.400E+0
	-.304E+0	.126E+0
.183E+1	-.314E+0	.405E+0
	-.177E+0	.120E+0
.243E+1	-.379E+0	.432E+0
	-.119E+0	.113E+0
.325E+1	-.468E+0	.459E+0
	-.143E+0	.914E-1
.462E+1	-.466E+0	.393E+0
	-.133E+0	.531E-1
.577E+1	-.536E+0	.413E+0
	-.598E-1	.882E-1
.770E+1	-.530E+0	.457E+0
	-.806E-1	.699E-1
.109E+2	-.392E+0	.497E+0
	-.946E-1	.991E-2
.146E+2	-.330E+0	.523E+0
	.416E-1	.126E+0
.183E+2	-.481E+0	.550E+0
	-.974E-1	-.263E-1
.244E+2	-.433E+0	.519E+0
	-.646E-2	.466E-1
.260E+2	-.343E+0	.532E+0
	.299E-1	.458E-1
.346E+2	-.424E+0	.523E+0
	.697E-1	.877E-1
.462E+2	-.382E+0	.540E+0
	.123E+0	.104E+0
.616E+2	-.266E+0	.550E+0
	.201E+0	.105E+0
.821E+2	-.245E+0	.527E+0
	.142E+0	.162E-2
.110E+3	-.988E-1	.540E+0
	.170E+0	-.338E-1
.146E+3	-.181E+0	.432E+0
	.134E+0	-.304E-3
.195E+3	.188E-1	.411E+0
	.202E+0	-.950E-1
.260E+3	-.126E-1	.411E+0
	.182E+0	-.481E-1

OLE 590100. 100920.

.577E+0	-.343E+0	.338E+0
	-.441E-1	.840E-1
.770E+0	-.213E+0	.567E+0
	-.200E-1	.150E+0
.103E+1	-.205E+0	.428E+0
	-.108E+0	.744E-1
.137E+1	-.276E+0	.397E+0
	-.585E-1	.966E-1
.183E+1	-.293E+0	.410E+0
	-.229E-1	.158E-1
.243E+1	-.333E+0	.329E+0
	-.226E-1	.283E-2
.325E+1	-.308E+0	.311E+0
	-.217E-1	-.585E-1
.433E+1	-.330E+0	.277E+0
	.530E-2	-.751E-1
.616E+1	-.283E+0	.290E+0
	.194E-1	-.908E-1
.770E+1	-.298E+0	.259E+0
	.264E-1	-.926E-1
.109E+2	-.240E+0	.229E+0
	.209E-1	-.103E+0
.146E+2	-.229E+0	.256E+0
	.398E-1	-.901E-1
.195E+2	-.219E+0	.228E+0
	.403E-1	-.793E-1
.244E+2	-.227E+0	.259E+0
	.424E-1	-.825E-1
.325E+2	-.232E+0	.241E+0
	.359E-1	-.702E-1
.346E+2	-.226E+0	.222E+0
	.431E-1	-.539E-1

.577E+2 -.200E+0 .237E+0
.113E-1 -.370E-1
.616E+2 -.135E+0 .250E+0
.269E-1 .176E-1
.821E+2 -.129E+0 .190E+0
.231E-1 -.370E-1
.110E+3 -.118E+0 .243E+0
.329E-2 -.360E-2
.146E+3 -.122E+0 .292E+0
-.858E-3 -.492E-1
.195E+3 -.941E-1 .279E+0
.628E-1 -.344E-1
.260E+3 -.107E+0 .268E+0
.472E-1 -.339E-1

TOU 615410. 116200.
.577E+0 -.123E+0 .293E+0
.777E-3 .708E-1
.770E+0 -.119E+0 .328E+0
-.356E-2 .110E+0
.103E+1 -.116E+0 .317E+0
-.774E-2 .103E+0
.137E+1 -.118E+0 .320E+0
-.167E-1 .891E-1
.183E+1 -.133E+0 .331E+0
-.143E-1 .736E-1
.243E+1 -.153E+0 .304E+0
-.116E-1 .572E-1
.325E+1 -.176E+0 .264E+0
-.248E-1 .534E-1
.433E+1 -.190E+0 .250E+0
-.230E-1 .612E-1
.462E+1 -.174E+0 .265E+0
-.269E-1 .460E-1
.577E+1 -.210E+0 .249E+0
-.293E-1 .574E-1
.616E+1 -.186E+0 .303E+0
-.142E-1 .699E-1
.770E+1 -.217E+0 .252E+0
-.307E-1 .555E-1
.821E+1 -.218E+0 .253E+0
-.449E-1 .498E-1
.103E+2 -.240E+0 .247E+0
-.467E-1 .573E-1
.109E+2 -.231E+0 .262E+0
-.257E-1 .899E-1
.137E+2 -.255E+0 .240E+0
-.327E-1 .706E-1
.146E+2 -.262E+0 .253E+0
-.168E-1 .999E-1
.183E+2 -.261E+0 .252E+0
-.947E-2 .108E+0
.195E+2 -.255E+0 .277E+0
-.165E-1 .130E+0
.244E+2 -.238E+0 .297E+0
-.829E-2 .105E+0
.260E+2 -.225E+0 .334E+0
-.595E-2 .114E+0
.325E+2 -.233E+0 .324E+0
.299E-2 .962E-1
.346E+2 -.207E+0 .333E+0
.138E-1 .101E+0
.433E+2 -.237E+0 .339E+0
.828E-2 .911E-1
.462E+2 -.260E+0 .287E+0
.122E-1 .846E-1
.577E+2 -.239E+0 .342E+0
.955E-2 .824E-1
.616E+2 -.240E+0 .386E+0
.108E-1 .887E-1
.770E+2 -.231E+0 .357E+0
.224E-1 .517E-1
.821E+2 -.239E+0 .420E+0
.992E-1 .322E-1
.110E+3 -.245E+0 .349E+0
.228E-1 .329E-1
.137E+3 -.229E+0 .370E+0
.307E-1 .352E-1
.146E+3 -.195E+0 .323E+0
.120E+0 -.208E-1
.195E+3 -.144E+0 .376E+0
.109E+0 -.922E-1
.260E+3 -.131E+0 .331E+0
.119E+0 -.693E-1
.346E+3 -.179E+0 .312E+0
.102E+0 -.786E-1
.462E+3 -.115E-2 .277E+0
.126E+0 -.125E+0
.616E+3 -.105E+0 .187E+0
-.175E-1 -.262E-1

LUS 600680. 105000.
.577E+0 -.115E+0 .383E+0
-.124E+0 .167E+0
.770E+0 -.110E+0 .100E+0
-.656E-1 .234E+0
.103E+1 -.166E+0 .145E+0
-.839E-1 .203E+0
.137E+1 -.212E+0 .171E+0
-.812E-1 .184E+0
.183E+1 -.233E+0 .212E+0
-.642E-1 .154E+0
.243E+1 -.257E+0 .220E+0

-.572E-1 .128E+0
.325E+1 -.271E+0 .215E+0
-.515E-1 .103E+0
.433E+1 -.299E+0 .216E+0
-.434E-1 .778E-1
.462E+1 -.323E+0 .174E+0
-.231E-1 .540E-1
.577E+1 -.352E+0 .219E+0
-.585E-1 .338E-1
.616E+1 -.359E+0 .181E+0
-.360E-1 .335E-1
.770E+1 -.382E+0 .206E+0
-.543E-1 .633E-2
.821E+1 -.401E+0 .180E+0
-.600E-1 -.489E-2
.103E+2 -.387E+0 .191E+0
-.586E-1 .291E-2
.109E+2 -.384E+0 .198E+0
-.280E-1 .131E-1
.137E+2 -.383E+0 .202E+0
-.538E-2 .962E-2
.146E+2 -.372E+0 .215E+0
-.104E-1 .224E-1
.183E+2 -.339E+0 .229E+0
.209E-1 .374E-1
.195E+2 -.305E+0 .237E+0
.214E-1 .273E-1
.244E+2 -.295E+0 .261E+0
.176E-1 .287E-1
.260E+2 -.287E+0 .246E+0
.273E-1 .289E-2
.325E+2 -.274E+0 .267E+0
.353E-1 .155E-1
.346E+2 -.271E+0 .249E+0
.406E-1 .175E-1
.433E+2 -.265E+0 .267E+0
.422E-1 .492E-2
.462E+2 -.261E+0 .268E+0
.550E-1 .174E-1
.577E+2 -.253E+0 .264E+0
.474E-1 .637E-2
.616E+2 -.245E+0 .241E+0
.621E-1 .792E-2
.770E+2 -.231E+0 .270E+0
.478E-1 .236E-2
.821E+2 -.233E+0 .242E+0
.108E+0 -.421E-1
.110E+3 -.290E+0 .311E+0
.331E-1 .188E-1
.137E+3 -.216E+0 .261E+0
.803E-1 .872E-3
.146E+3 -.175E+0 .342E+0
.959E-1 -.108E-1
.195E+3 -.750E-1 .262E+0
.154E+0 -.208E-1
.260E+3 -.597E-1 .254E+0
.164E+0 -.182E-1
.346E+3 .155E+0 .245E+0
.581E-1 -.104E+0
.462E+3 -.105E+0 .260E+0
.110E+0 -.116E+0
.616E+3 -.851E-1 .327E+0
.156E+0 -.579E-1

COL 604030. 94730.
.577E+0 .218E+0 -.593E+0
.139E+0 -.216E+0
.770E+0 .456E-1 -.250E+0
-.122E+0 -.715E+0
.103E+1 -.241E-1 -.350E-1
-.158E+0 -.693E+0
.137E+1 -.144E+0 .242E-1
-.148E+0 -.743E+0
.183E+1 -.265E+0 .138E+0
-.236E+0 -.689E+0
.243E+1 -.308E+0 .194E+0
-.151E+0 -.605E+0
.325E+1 -.403E+0 .307E+0
-.260E-1 -.501E+0
.433E+1 -.549E+0 .373E+0
.988E-1 -.426E+0
.577E+1 -.725E+0 .415E+0
.279E+0 -.239E+0
.821E+1 -.781E+0 .488E+0
.193E+0 -.236E+0
.109E+2 -.833E+0 .490E+0
.329E+0 -.289E+0
.137E+2 -.913E+0 .486E+0
.233E+0 -.154E+0
.183E+2 -.805E+0 .552E+0
.297E+0 -.213E+0
.244E+2 -.712E+0 .701E+0
.249E+0 -.180E+0
.325E+2 -.615E+0 .874E+0
.170E+0 -.169E+0
.346E+2 -.720E+0 .759E+0
.393E-1 -.635E-1
.462E+2 -.756E+0 .784E+0
-.227E-1 -.255E-1
.616E+2 -.712E+0 .758E+0
.140E+0 .706E-1
.821E+2 -.644E+0 .917E+0
.176E+0 .142E+0

.110E+3 -.669E+0 .761E+0
-.224E+0 .737E-1
.137E+3 -.487E+0 .644E+0
.179E+0 -.491E-2
.195E+3 .115E+0 .550E+0
-.252E+0 -.869E-1
.260E+3 -.199E+0 .499E+0
-.367E+0 .209E+0
.346E+3 .292E+0 .627E+0
-.771E-1 -.157E+0
.462E+3 .137E+0 .662E+0
.804E-1 .278E+0
.616E+3 -.955E-1 .482E+0
.986E-1 -.698E+0

FER 608790. 99880.
.577E+0 -.136E+0 .259E+0
-.819E-2 -.739E-1
.770E+0 -.121E+0 .343E+0
-.661E-1 -.142E+0
.103E+1 -.108E+0 .397E+0
-.165E+0 -.184E+0
.137E+1 -.168E+0 .437E+0
-.191E+0 -.230E+0
.183E+1 -.249E+0 .463E+0
-.162E+0 -.265E+0
.243E+1 -.290E+0 .493E+0
-.224E-1 -.266E+0
.325E+1 -.361E+0 .505E+0
.259E-1 -.239E+0
.462E+1 -.549E+0 .466E+0
.902E-1 -.116E+0
.577E+1 -.588E+0 .484E+0
.174E+0 -.800E-1
.821E+1 -.648E+0 .486E+0
.145E+0 -.121E+0
.109E+2 -.728E+0 .456E+0
.126E+0 -.134E+0
.137E+2 -.726E+0 .491E+0
.145E+0 -.923E-1
.195E+2 -.672E+0 .582E+0
.859E-1 -.137E+0
.244E+2 -.594E+0 .598E+0
.187E-1 -.226E+0
.325E+2 -.587E+0 .581E+0
.424E-2 -.214E+0
.346E+2 -.607E+0 .573E+0
.402E-1 -.203E+0
.577E+2 -.538E+0 .551E+0
.147E-2 -.138E+0
.616E+2 -.544E+0 .617E+0
.750E-1 -.825E-1
.821E+2 -.521E+0 .683E+0
-.464E-1 -.147E+0
.110E+3 -.634E+0 .763E+0
.920E-1 -.145E+0
.146E+3 -.579E+0 .726E+0
.136E+0 -.146E+0
.195E+3 -.628E+0 .761E+0
-.128E+0 -.320E-1
.260E+3 -.647E+0 .594E+0
.310E-2 -.123E+0
.346E+3 -.591E+0 .568E+0
-.275E+0 .148E+0
.462E+3 -.634E+0 .493E+0
-.246E+0 .574E-1
.616E+3 -.159E+0 .503E+0
-.501E+0 .338E+0

DIX 596530. 99560.
.577E+0 -.129E+0 .854E-1
.517E-1 -.105E+0
.770E+0 -.129E+0 .117E+0
.526E-1 -.162E+0
.103E+1 -.163E+0 .160E+0
.556E-1 -.160E+0
.137E+1 -.221E+0 .225E+0
.414E-1 -.167E+0
.183E+1 -.255E+0 .265E+0
.435E-1 -.161E+0
.243E+1 -.279E+0 .300E+0
.392E-1 -.144E+0
.325E+1 -.305E+0 .321E+0
.730E-1 -.978E-1
.462E+1 -.429E+0 .287E+0
.870E-1 -.218E-1
.616E+1 -.518E+0 .254E+0
.106E+0 .252E-1
.770E+1 -.536E+0 .236E+0
.126E+0 .469E-1
.103E+2 -.566E+0 .213E+0
.129E+0 .752E-1
.137E+2 -.591E+0 .208E+0
.140E+0 .112E+0
.195E+2 -.495E+0 .285E+0
.497E-1 .771E-1
.244E+2 -.453E+0 .312E+0
.456E-1 .694E-1
.325E+2 -.405E+0 .339E+0
.382E-1 .804E-1
.346E+2 -.377E+0 .333E+0
.810E-1 .101E+0
.577E+2 -.331E+0 .362E+0

.617E-2 .845E-1
.616E+2 -.368E+0 .352E+0
-.297E-1 .109E+0
.770E+2 -.293E+0 .397E+0
-.353E-1 .552E-1
.110E+3 -.296E+0 .374E+0
-.161E+0 -.235E-2
.137E+3 -.313E+0 .378E+0
-.428E-1 .288E-1
.195E+3 -.331E+0 .261E+0
.215E-1 .950E-2
.260E+3 -.412E+0 .241E+0
-.174E+0 -.375E-1
.346E+3 -.325E+0 .217E+0
-.854E-1 .863E-2
.462E+3 -.272E+0 .376E+0
-.960E-1 -.329E-1
.616E+3 -.754E-1 .433E+0
-.368E+0 .828E-1

NOU 600710. 107100.
.577E+0 -.215E+0 .433E-1
.583E-1 -.614E-1
.770E+0 -.206E+0 .892E-1
.939E-1 -.101E+0
.103E+1 -.231E+0 .108E+0
.824E-1 -.978E-1
.137E+1 -.263E+0 .158E+0
.434E-1 -.971E-1
.183E+1 -.276E+0 .173E+0
.390E-1 -.896E-1
.243E+1 -.277E+0 .185E+0
.295E-1 -.716E-1
.325E+1 -.295E+0 .189E+0
.386E-1 -.402E-1
.462E+1 -.349E+0 .154E+0
.312E-1 .137E-2
.577E+1 -.366E+0 .146E+0
.420E-1 .282E-1
.770E+1 -.404E+0 .124E+0
.440E-1 .453E-1
.103E+2 -.416E+0 .114E+0
.390E-1 .697E-1
.137E+2 -.427E+0 .109E+0
.458E-1 .908E-1
.195E+2 -.376E+0 .132E+0
.125E-1 .621E-1
.244E+2 -.351E+0 .177E+0
-.910E-2 .479E-1
.260E+2 -.322E+0 .178E+0
-.158E-1 .731E-1
.346E+2 -.316E+0 .208E+0
.807E-2 .647E-1
.462E+2 -.319E+0 .205E+0
-.701E-2 .100E+0
.616E+2 -.284E+0 .206E+0
-.511E-1 .558E-1
.770E+2 -.269E+0 .218E+0
-.467E-1 .385E-1
.110E+3 -.269E+0 .166E+0
-.432E-1 .305E-1
.146E+3 -.319E+0 .228E+0
-.107E-1 .464E-1
.195E+3 -.370E+0 .171E+0
.252E-1 .344E-1
.260E+3 -.319E+0 .211E+0
-.499E-1 .533E-1
.346E+3 -.324E+0 .230E+0
.154E-1 .750E-1
.462E+3 -.276E+0 .176E+0
-.118E+0 .983E-1
.616E+3 -.148E+0 .321E+0
.333E-1 -.149E+0

VER 584260. 108025.
.577E+0 .173E-1 .366E+0
.635E-1 .286E-1
.770E+0 -.499E-1 .321E+0
-.702E-1 .102E+0
.103E+1 .893E-1 .296E+0
.143E-1 .178E+0
.137E+1 .115E+0 .166E+0
-.425E-1 .288E+0
.183E+1 .751E-1 -.237E-1
-.156E+0 .356E+0
.243E+1 .620E-1 -.396E-1
-.123E+0 .375E+0
.325E+1 -.200E+0 -.119E+0
-.422E-1 .393E+0
.433E+1 -.101E+0 -.203E+0
-.143E+0 .402E+0
.462E+1 -.101E+0 -.324E+0
-.453E-1 .401E+0
.577E+1 -.152E+0 -.234E+0
.329E-1 .426E+0
.616E+1 -.126E-1 -.317E+0
-.109E+0 .433E+0
.770E+1 -.171E+0 -.329E+0
-.867E-1 .409E+0
.821E+1 -.887E-1 -.334E+0
-.779E-1 .394E+0
.103E+2 -.267E+0 -.368E+0
-.147E+0 .430E+0

.109E+2 -.107E+0 -.374E+0
.416E-1 .380E+0
.137E+2 -.330E+0 -.464E+0
.449E-1 .414E+0
.146E+2 -.116E+0 -.404E+0
-.442E-1 .376E+0
.183E+2 -.349E+0 -.477E+0
.158E+0 .358E+0
.195E+2 -.295E-1 -.433E+0
-.131E+0 .339E+0
.244E+2 -.375E+0 -.487E+0
.403E-1 .282E+0
.260E+2 .149E-1 -.421E+0
-.132E+0 .264E+0
.325E+2 -.193E+0 -.578E+0
.317E+0 .352E+0
.346E+2 -.141E+0 -.531E+0
-.734E-1 .310E+0
.433E+2 -.968E-1 -.540E+0
.378E+0 .323E+0
.462E+2 .172E+0 -.476E+0
-.240E-1 .234E+0
.577E+2 .308E+0 -.430E+0
-.677E-1 .274E+0
.616E+2 .329E-1 -.480E+0
.140E+0 .180E+0
.770E+2 -.295E+0 -.394E+0
.243E+0 .149E+0
.821E+2 .306E+0 -.356E+0
-.201E+0 .173E+0
.110E+3 .388E+0 -.189E+0
.126E+0 .485E-1
.137E+3 -.146E+0 -.433E+0
-.413E+0 .114E+0
.146E+3 .149E+0 -.942E-2
.265E+0 .485E+0
.195E+3 -.552E-1 -.281E+0
-.243E+0 -.230E+0
.260E+3 .343E+0 -.221E+0
.331E-1 .554E-1
.346E+3 .312E+0 -.366E+0
-.838E-1 .362E-1
.462E+3 .155E+0 -.405E+0
.291E+0 .652E-1
.616E+3 .479E+0 .266E+0
.196E+0 .351E+0
.110E+4 .405E+0 -.893E-1
.358E+0 .368E+0

MAV 594090. 88310.
.577E+0 .556E+0 .348E+0
-.103E+0 .819E-1
.770E+0 .158E-1 .115E+0
.176E+0 .141E+0
.103E+1 -.212E+0 .181E+0
.199E+0 -.396E-1
.137E+1 -.258E+0 .201E+0
.184E+0 -.110E+0
.183E+1 -.368E+0 .251E+0
.285E+0 -.194E+0
.243E+1 -.443E+0 .269E+0
.285E+0 -.172E+0
.325E+1 -.503E+0 .225E+0
.261E+0 -.107E+0
.433E+1 -.552E+0 .202E+0
.245E+0 -.709E-1
.462E+1 -.572E+0 .109E+0
.202E+0 -.782E-1
.577E+1 -.600E+0 .222E+0
.238E+0 -.881E-1
.616E+1 -.623E+0 .952E-1
.235E+0 -.927E-1
.770E+1 -.672E+0 .282E+0
.231E+0 -.255E-1
.821E+1 -.687E+0 -.342E-2
.202E+0 .201E+0
.103E+2 -.710E+0 -.708E-1
.191E+0 .298E+0
.109E+2 -.694E+0 -.166E+0
.197E+0 -.861E-1
.137E+2 -.714E+0 -.166E+0
.150E+0 -.280E+0
.146E+2 -.664E+0 -.844E-1
.166E+0 -.198E+0
.183E+2 -.673E+0 -.846E-1
.159E+0 -.336E+0
.195E+2 -.661E+0 -.106E+0
.105E+0 -.154E+0
.244E+2 -.665E+0 .121E+0
.598E-1 -.199E+0
.260E+2 -.664E+0 .153E+0
.658E-1 -.553E-1
.325E+2 -.651E+0 .209E+0
.298E-1 -.171E+0
.346E+2 -.639E+0 .159E+0
.442E-1 -.800E-1
.433E+2 -.651E+0 .275E+0
-.168E-1 -.150E+0
.462E+2 -.558E+0 .177E+0
-.272E-1 -.107E+0
.577E+2 -.579E+0 .294E+0
-.322E-1 -.114E+0
.616E+2 -.521E+0 .185E+0

-.571E-1 -.149E+0
.770E+2 -.558E+0 .370E+0
-.188E-1 -.953E-1
.821E+2 -.447E+0 .247E+0
-.759E-1 .138E-2
.110E+3 -.434E+0 .227E+0
-.762E-1 -.122E+0
.137E+3 -.544E+0 .314E+0
-.467E-1 -.155E+0
.146E+3 -.529E+0 .262E+0
-.524E-1 -.192E+0
.195E+3 -.401E+0 .215E+0
-.889E-1 -.504E-1
.260E+3 -.411E+0 .189E+0
-.844E-1 .696E-2
.346E+3 -.509E+0 .146E+0
-.107E+0 -.351E+0
.462E+3 -.387E+0 .113E+0
-.189E+0 -.178E+0
.616E+3 -.320E+0 .324E+0
-.191E+0 .191E-1
.110E+4 -.227E+0 .156E+0
-.112E+0 .262E+0

PRA 574790. 88760.
.577E+0 -.148E+0 -.584E+0
-.240E-1 .969E-1
.770E+0 -.190E+0 -.622E+0
-.848E-1 .181E+0
.103E+1 -.154E+0 -.669E+0
-.141E+0 .194E+0
.137E+1 -.115E+0 -.714E+0
-.225E+0 .208E+0
.183E+1 -.289E-1 -.768E+0
-.268E+0 .231E+0
.243E+1 -.913E-2 -.846E+0
-.324E+0 .276E+0
.325E+1 -.456E-1 -.872E+0
-.335E+0 .310E+0
.433E+1 -.281E+0 -.100E+1
-.330E+0 .322E+0
.462E+1 -.122E+0 -.101E+1
-.187E+0 .232E+0
.577E+1 -.347E+0 -.106E+1
-.433E+0 .306E+0
.616E+1 -.149E+0 -.104E+1
-.615E-1 .244E+0
.770E+1 -.406E+0 -.109E+1
-.568E+0 .229E+0
.821E+1 -.301E+0 -.105E+1
-.187E+0 .159E+0
.103E+2 -.821E+0 -.115E+1
.944E-1 .119E+0
.109E+2 -.162E+0 -.979E+0
-.135E+0 .503E-1
.137E+2 -.548E+0 -.104E+1
-.321E+0 -.417E-1
.146E+2 -.354E+0 -.926E+0
-.198E+0 .157E+0
.183E+2 -.284E+0 -.769E+0
-.275E+0 -.235E-1
.195E+2 -.191E+0 -.503E+0
-.304E+0 -.109E+0
.244E+2 -.285E+0 -.630E+0
-.266E+0 -.353E-1
.260E+2 -.187E+0 -.477E+0
-.152E+0 -.886E-1
.325E+2 -.288E+0 -.610E+0
-.248E+0 -.104E+0
.346E+2 -.100E+0 -.597E+0
-.173E+0 -.145E+0
.433E+2 -.322E+0 -.663E+0
-.219E+0 -.112E+0
.462E+2 -.764E-1 -.381E+0
-.450E-1 -.137E+0
.577E+2 -.238E+0 -.534E+0
-.156E+0 -.199E+0
.616E+2 -.109E+0 -.415E+0
-.148E+0 -.229E+0
.770E+2 -.244E+0 -.468E+0
-.202E+0 -.328E+0
.821E+2 -.281E+0 -.479E+0
-.672E-1 -.323E+0
.110E+3 -.271E+0 -.417E+0
-.812E-1 -.278E+0
.137E+3 -.299E+0 -.483E+0
-.497E-1 -.272E+0
.146E+3 -.160E+0 -.377E+0
.183E+0 -.932E-1
.195E+3 -.132E+0 -.245E+0
.124E+0 -.783E-1
.260E+3 .183E+0 -.225E+0
.432E-1 -.850E-1
.346E+3 .162E+0 -.227E+0
.874E-1 -.100E+0
.462E+3 .151E+0 -.217E+0
.640E-1 -.904E-1
.616E+3 .135E+0 -.184E+0
-.185E+0 -.927E-1
.110E+4 .863E-1 -.187E+0
-.249E+0 -.301E-2

SAL 574720. 92500.
.577E+0 .827E+0 -.200E+0
-.731E-1 -.315E-1
.770E+0 .868E+0 -.250E+0
-.111E+0 -.711E-1
.103E+1 .906E+0 -.208E+0
-.995E-1 -.196E+0
.137E+1 .957E+0 -.245E+0
-.124E+0 -.227E+0
.183E+1 .998E+0 -.126E+0
-.155E+0 -.324E+0
.243E+1 .105E+1 -.340E+0
-.212E+0 -.324E+0
.325E+1 .105E+1 -.433E+0
-.273E+0 -.523E+0
.433E+1 .124E+1 -.796E+0
-.325E+0 -.299E+0
.462E+1 .124E+1 -.505E+0
-.345E+0 -.392E-1
.577E+1 .131E+1 -.891E+0
-.383E+0 -.269E+0
.616E+1 .130E+1 -.544E+0
-.344E+0 -.376E-1
.770E+1 .134E+1 -.971E+0
-.259E+0 .693E-1
.821E+1 .136E+1 -.481E+0
-.236E+0 .230E+0
.103E+2 .141E+1 -.123E+1
-.237E+0 .253E+0
.109E+2 .138E+1 -.772E+0
-.272E+0 .388E-1
.137E+2 .138E+1 -.896E+0
-.218E+0 -.145E+0
.146E+2 .113E+1 -.492E+0
-.194E-1 -.319E+0
.183E+2 .104E+1 -.604E+0
-.619E-1 -.143E+0
.195E+2 .784E+0 -.306E+0
.623E-1 -.283E+0
.244E+2 .752E+0 -.410E+0
.772E-2 -.304E+0
.260E+2 .576E+0 -.224E+0
.119E+0 -.192E+0
.325E+2 .736E+0 -.322E+0
.108E+0 -.344E+0
.346E+2 .745E+0 -.238E+0
.145E+0 -.124E+0
.433E+2 .696E+0 -.500E+0
.308E+0 .170E+0
.462E+2 .540E+0 -.118E+0
.201E+0 -.162E+0
.577E+2 .549E+0 -.422E+0
.232E+0 .542E-1
.616E+2 .523E+0 -.589E-1
.189E+0 .238E+0
.770E+2 .516E+0 .743E-1
.308E+0 -.359E+0
.821E+2 .514E+0 -.294E+0
.203E+0 -.148E-1
.110E+3 .587E+0 -.345E+0
.127E+0 -.175E+0
.137E+3 .439E+0 .412E+0
.273E+0 -.152E+0
.146E+3 .440E+0 .610E-1
.263E+0 -.337E+0
.195E+3 .403E+0 -.181E+0
.164E+0 .112E+0
.260E+3 .253E+0 -.128E+0
.158E+0 -.186E+0
.346E+3 .107E+0 .277E+0
.189E+0 -.224E-1
.462E+3 .866E-1 .834E-1
.704E-1 -.299E+0
.616E+3 .122E+0 .127E+0
.156E+0 -.150E+0
.110E+4 .313E-1 .583E-1
.197E+0 -.182E+0

ZER 618260. 94630.
.577E+0 -.587E-1 .253E+0
.178E-1 -.479E-1
.770E+0 -.751E-1 .297E+0
.362E-1 -.118E+0
.103E+1 -.963E-1 .400E+0
-.329E-2 -.187E+0
.137E+1 -.118E+0 .477E+0
.732E-2 -.246E+0
.183E+1 -.127E+0 .565E+0
-.468E-1 -.293E+0
.243E+1 -.158E+0 .637E+0
.274E-1 -.333E+0
.325E+1 -.207E+0 .696E+0
.724E-1 -.340E+0
.433E+1 -.227E+0 .804E+0
.118E+0 -.369E+0
.577E+1 -.281E+0 .900E+0
.170E+0 -.382E+0
.770E+1 -.356E+0 .945E+0
.165E+0 -.378E+0
.103E+2 -.415E+0 .895E+0
.641E-1 -.389E+0
.137E+2 -.456E+0 .810E+0
-.125E-1 -.356E+0
.183E+2 -.570E+0 .868E+0
.443E-2 -.365E+0
.244E+2 -.525E+0 .942E+0
.831E-1 -.315E+0
.325E+2 -.456E+0 .829E+0
-.796E-2 -.235E+0
.433E+2 -.445E+0 .832E+0
-.697E-2 -.134E+0
.577E+2 -.286E+0 .765E+0
-.518E-1 -.994E-1
.770E+2 -.241E+0 .632E+0
-.144E+0 -.580E-1
.137E+3 -.205E+0 .584E+0
-.172E+0 -.313E-1
.195E+3 -.100E+0 .456E+0
.126E+0 .125E+0
.260E+3 -.161E+0 .432E+0
-.380E-1 .143E+0
.346E+3 .149E+0 .223E+0
.115E+0 .132E+0
.462E+3 .225E+0 .116E+0
.906E-2 .120E+0
.616E+3 .230E+0 .969E-1
.534E-1 .134E+0
.110E+4 .134E+0 .746E-1
.110E+0 .922E-1

TAS 629340. 100210.
.577E+0 -.189E+0 .505E+0
-.532E-2 .220E-1
.770E+0 -.190E+0 .508E+0
-.355E-1 .100E-1
.103E+1 -.191E+0 .667E+0
-.153E+0 -.108E+0
.137E+1 -.298E+0 .808E+0
-.111E+0 -.212E+0
.183E+1 -.254E+0 .931E+0
-.652E-1 -.256E+0
.243E+1 -.278E+0 .102E+1
.333E-1 -.286E+0
.325E+1 -.353E+0 .111E+1
.157E+0 -.298E+0
.433E+1 -.363E+0 .120E+1
.248E+0 -.303E+0
.577E+1 -.371E+0 .136E+1
.352E+0 -.336E+0
.770E+1 -.398E+0 .142E+1
.312E+0 -.337E+0
.103E+2 -.462E+0 .138E+1
.454E-1 -.397E+0
.137E+2 -.472E+0 .134E+1
.132E+0 -.467E+0
.183E+2 -.552E+0 .122E+1
.249E-1 -.519E+0
.244E+2 -.704E+0 .137E+1
.992E-1 -.472E+0
.325E+2 -.516E+0 .124E+1
-.672E-1 -.343E+0
.433E+2 -.417E+0 .106E+1
-.137E+0 -.247E+0
.577E+2 -.380E+0 .848E+0
-.759E-1 -.211E+0
.770E+2 -.426E+0 .659E+0
-.195E-1 -.132E+0
.137E+3 -.426E+0 .590E+0
-.483E-1 -.366E-1
.195E+3 -.115E+0 .463E+0
-.145E+0 .205E+0
.260E+3 -.161E+0 .847E-1
-.295E+0 .196E+0

BUR 631290. 124280.
.577E+0 .322E+0 .477E+0
-.234E+0 -.257E-3
.770E+0 .413E+0 .321E+0
-.397E+0 -.249E+0
.103E+1 .384E+0 .369E+0
-.493E+0 -.659E+0
.137E+1 .900E-1 -.126E+0
-.472E+0 -.105E+1
.183E+1 .239E+0 -.870E+0
-.378E+0 -.834E+0
.243E+1 -.297E+0 -.946E+0
.230E+0 -.886E+0
.325E+1 -.230E+0 -.686E+0
-.360E-1 -.115E+1
.433E+1 -.648E-1 -.775E+0
.207E+0 -.727E+0
.577E+1 -.189E+0 -.411E+0
.164E+0 -.693E+0
.770E+1 -.125E+0 .114E-1
.802E-1 -.771E+0
.103E+2 -.123E+0 .479E+0
.557E-1 -.278E+0
.137E+2 -.140E+0 .485E+0
.384E-1 -.123E+0
.183E+2 -.140E+0 .393E+0
.508E-1 -.177E+0
.244E+2 -.122E+0 .337E+0
.139E-1 -.674E-1
.325E+2 -.108E+0 .349E+0
.100E-1 -.291E-1
.433E+2 -.113E+0 .388E+0
.158E-1 -.826E-2

.577E+2 -.121E+0 .338E+0
.291E-2 -.871E-2
.770E+2 -.138E+0 .405E+0
.170E-2 .728E-2
.137E+3 -.141E+0 .392E+0
-.261E-2 .690E-3
.195E+3 -.199E+0 .213E+0
-.477E-1 .705E-1
.260E+3 -.134E+0 .278E+0
.203E-2 -.529E-1
.346E+3 .154E+0 .312E+0
-.183E+0 .183E+0
.462E+3 -.254E+0 .379E+0
.120E+0 -.838E-1
.616E+3 -.230E+0 .159E-1
.157E+0 .369E+0
.110E+4 .606E-1 .464E-1
.324E+0 .463E+0

GAS 629650. 113440.
.577E+0 -.500E+0 .111E+1
-.360E-2 .655E-1
.770E+0 -.593E+0 .867E+0
-.892E-2 .221E-2
.103E+1 -.633E+0 .923E+0
-.230E-1 -.130E+0
.137E+1 -.542E+0 .902E+0
.121E-1 -.214E+0
.183E+1 -.484E+0 .976E+0
.519E-1 -.266E+0
.243E+1 -.463E+0 .110E+1
.878E-1 -.284E+0
.325E+1 -.521E+0 .112E+1
.148E+0 -.241E+0
.433E+1 -.577E+0 .115E+1
.207E+0 -.188E+0
.577E+1 -.622E+0 .121E+1
.177E+0 -.172E+0
.770E+1 -.664E+0 .116E+1
.244E+0 -.137E+0
.103E+2 -.809E+0 .111E+1
.163E+0 -.207E+0
.137E+2 -.906E+0 .105E+1
-.746E-2 -.395E+0
.183E+2 -.969E+0 .962E+0
-.921E-1 -.516E+0
.244E+2 -.917E+0 .960E+0
-.393E-1 -.397E+0
.325E+2 -.860E+0 .939E+0
.319E-1 -.201E+0
.433E+2 -.845E+0 .929E+0
.998E-1 -.140E+0
.577E+2 -.857E+0 .878E+0
.882E-1 -.159E+0
.770E+2 -.936E+0 .727E+0
-.353E-1 -.187E+0
.137E+3 -.979E+0 .698E+0
-.498E-1 -.159E+0
.195E+3 -.722E+0 .888E+0
-.670E-1 -.118E+0
.260E+3 -.982E+0 .947E+0
-.315E+0 -.878E-1
.346E+3 -.880E+0 .637E+0
-.195E+0 .775E-1
.462E+3 -.658E+0 .405E+0
-.115E+0 .213E+0
.616E+3 -.597E+0 .397E+0
.358E+0 .772E-1
.110E+4 -.503E+0 .489E+0
-.339E+0 .699E-1

NAN 640810. 117990.
.577E+0 .621E+0 .882E+0
.602E-1 -.136E+0
.770E+0 .589E+0 .100E+1
.447E-1 -.367E+0
.103E+1 .443E+0 .116E+1
.935E-1 -.690E+0
.137E+1 .304E+0 .136E+1
.139E+0 -.886E+0
.183E+1 .228E+0 .152E+1
.192E+0 -.930E+0
.243E+1 .799E-1 .153E+1
.287E+0 -.875E+0
.325E+1 -.343E-1 .155E+1
.310E+0 -.812E+0
.433E+1 -.151E+0 .156E+1
.281E+0 -.712E+0
.577E+1 -.264E+0 .158E+1
.292E+0 -.623E+0
.770E+1 -.341E+0 .154E+1
.238E+0 -.511E+0
.103E+2 -.472E+0 .133E+1
.242E+0 -.383E+0
.137E+2 -.589E+0 .121E+1
.207E+0 -.377E+0
.183E+2 -.650E+0 .966E+0
.152E+0 -.485E+0
.244E+2 -.610E+0 .902E+0
.955E-1 -.309E+0
.325E+2 -.680E+0 .777E+0
.102E+0 .176E-1
.433E+2 -.733E+0 .752E+0

.608E-1 .547E-1
.577E+2 -.751E+0 .610E+0
.285E-1 -.750E-1
.770E+2 -.779E+0 .550E+0
.454E-1 -.197E+0
.137E+3 -.799E+0 .536E+0
.307E-1 -.135E+0
.195E+3 -.672E+0 .446E+0
-.142E+0 -.224E+0
.260E+3 -.657E+0 .424E+0
.161E+0 -.300E+0
.346E+3 -.522E+0 .317E+0
.578E-1 -.280E+0
.462E+3 -.446E+0 .300E+0
.133E+0 -.233E+0
.616E+3 -.600E+0 .335E+0
.255E+0 -.183E+0
.110E+4 -.467E+0 -.183E+0
.148E+0 -.366E+0

NES 642520. 122780.
.577E+0 -.474E+0 .141E+1
.203E+0 -.431E+0
.770E+0 -.732E+0 .110E+1
.399E+0 -.627E+0
.103E+1 -.110E+1 .838E+0
.554E+0 -.885E+0
.137E+1 -.134E+1 .103E+1
.500E+0 -.782E+0
.183E+1 -.142E+1 .113E+1
.476E+0 -.550E+0
.243E+1 -.152E+1 .116E+1
.463E+0 -.389E+0
.325E+1 -.166E+1 .112E+1
.307E+0 -.252E+0
.433E+1 -.170E+1 .107E+1
.210E+0 -.278E+0
.577E+1 -.170E+1 .108E+1
.151E+0 -.372E+0
.770E+1 -.174E+1 .101E+1
.864E-1 -.387E+0
.103E+2 -.166E+1 .115E+1
.145E+0 -.148E+0
.137E+2 -.162E+1 .119E+1
.916E-1 -.247E+0
.183E+2 -.160E+1 .107E+1
.269E-1 -.871E+0
.244E+2 -.145E+1 .116E+1
.997E-2 -.440E+0
.325E+2 -.154E+1 .904E+0
.622E-1 .341E-1
.433E+2 -.152E+1 .733E+0
.832E-2 .142E+0
.577E+2 -.150E+1 .834E+0
.423E-1 -.934E-1
.770E+2 -.142E+1 .858E+0
.468E-1 -.566E+0
.137E+3 -.117E+1 .969E+0
-.279E-1 -.303E+0
.195E+3 -.146E+1 .964E+0
-.619E-1 -.455E+0
.260E+3 -.133E+1 .563E+0
.481E-1 -.563E+0
.346E+3 -.929E+0 .112E+0
-.403E+0 -.885E+0
.462E+3 -.821E+0 -.360E+0
.125E+0 -.742E+0
.616E+3 -.673E+0 .234E-1
.305E+0 -.782E+0
.110E+4 -.698E+0 -.393E+0
-.740E-2 .134E+0

SIM 646660. 116860.
.577E+0 -.642E+0 -.777E+0
.258E+0 .147E-1
.770E+0 -.701E+0 -.730E+0
.317E+0 -.574E-1
.103E+1 -.717E+0 -.598E+0
.661E+0 -.300E+0
.137E+1 -.605E+0 -.714E+0
.706E+0 -.756E+0
.183E+1 -.690E+0 -.364E+0
.110E+1 -.152E+1
.243E+1 -.705E+0 .488E+0
.120E+1 -.171E+1
.325E+1 -.103E+1 .547E+0
.114E+1 -.139E+1
.433E+1 -.179E+1 .954E+0
.129E+1 -.130E+1
.577E+1 -.195E+1 .113E+1
.112E+1 -.117E+1
.770E+1 -.219E+1 .140E+1
.121E+1 -.108E+1
.103E+2 -.280E+1 .119E+1
.716E+0 -.112E+1
.137E+2 -.274E+1 .116E+1
.362E+0 -.143E+1
.183E+2 -.209E+1 .137E+1
.279E+0 -.150E+1
.244E+2 -.187E+1 .136E+1
.137E+0 -.123E+1
.325E+2 -.223E+1 .148E+1
.121E+0 -.356E+0

.433E+2 -.218E+1 .104E+1
.193E+0 -.117E+1
.577E+2 -.203E+1 .777E+0
.273E+0 -.108E+1
.770E+2 -.193E+1 .906E+0
.415E+0 -.963E+0
.137E+3 -.196E+1 .978E+0
.450E+0 -.943E+0
.195E+3 -.173E+1 .340E+0
-.633E+0 -.109E+1
.260E+3 -.134E+1 -.726E+0
.155E+0 -.475E+0
.346E+3 -.127E+1 .409E+0
-.426E+0 .421E+0
.462E+3 -.970E+0 .650E+0
-.250E+0 .126E+0
.616E+3 -.362E+0 -.617E+0
-.975E+0 -.205E+0
.110E+4 .236E+0 -.387E+0
-.541E+0 .274E+0

MAS 601000. 116800.
.577E+0 -.129E+0 .211E+0
.162E-1 -.315E-1
.770E+0 -.153E+0 .245E+0
-.992E-2 -.520E-1
.103E+1 -.155E+0 .261E+0
-.611E-1 -.460E-1
.137E+1 -.143E+0 .272E+0
-.253E-1 -.230E-1
.183E+1 -.129E+0 .245E+0
-.383E-1 .740E-2
.243E+1 -.132E+0 .213E+0
-.320E-1 .900E-2
.325E+1 -.145E+0 .172E+0
-.297E-1 .237E-2
.433E+1 -.148E+0 .161E+0
-.271E-1 .541E-2
.462E+1 -.152E+0 .103E+0
-.114E-1 .332E-1
.577E+1 -.160E+0 .159E+0
-.295E-1 .211E-1
.616E+1 -.173E+0 .475E-1
-.111E-1 .402E-1
.770E+1 -.177E+0 .161E+0
-.134E-1 .443E-1
.821E+1 -.181E+0 .560E-1
-.978E-3 .416E-1
.103E+2 -.198E+0 .145E+0
-.147E-1 .512E-1
.109E+2 -.188E+0 .483E-1
-.111E-1 .798E-1
.137E+2 -.209E+0 .152E+0
-.343E-1 .430E-1
.146E+2 -.192E+0 .834E-1
-.273E-1 .284E-1
.183E+2 -.180E+0 .185E+0
-.547E-1 .956E-2
.195E+2 -.157E+0 .124E+0
-.396E-1 .159E-1
.244E+2 -.166E+0 .196E+0
-.471E-1 .701E-1
.260E+2 -.153E+0 .136E+0
-.555E-1 .366E-1
.325E+2 -.174E+0 .202E+0
-.477E-1 .408E-1
.346E+2 -.133E+0 .158E+0
-.472E-1 .387E-1
.433E+2 -.144E+0 .260E+0
-.998E-1 .394E-1
.462E+2 -.101E+0 .193E+0
-.612E-1 .614E-1
.577E+2 -.156E+0 .210E+0
-.685E-1 .508E-1
.616E+2 -.123E+0 .188E+0
-.925E-1 .966E-2
.770E+2 -.165E+0 .233E+0
-.996E-1 .261E-1
.821E+2 -.956E-1 .202E+0
-.141E+0 .322E-1
.110E+3 -.731E-1 .232E+0
-.192E+0 .932E-1
.137E+3 -.182E+0 .277E+0
-.141E+0 .945E-2
.146E+3 -.192E+0 .207E+0
-.910E-1 -.582E-1
.195E+3 -.203E+0 .248E+0
-.761E-1 .382E-2
.260E+3 -.223E+0 .313E+0
-.155E+0 -.155E-2
.346E+3 -.269E+0 .403E+0
-.366E+0 -.630E-1
.462E+3 -.584E-1 .532E+0
-.399E+0 .240E-1
.616E+3 -.351E+0 .419E+0
-.821E-1 .379E+0
.110E+4 -.228E+0 .590E+0
-.261E+0 .111E+0

REC 605575. 118725.
.577E+0 -.215E+0 .119E+0
.230E-1 -.635E-1
.770E+0 -.193E+0 .146E+0
.374E-1 -.946E-1
.103E+1 -.201E+0 .162E+0
.353E-2 -.121E+0
.137E+1 -.171E+0 .179E+0
.525E-2 -.155E-1
.183E+1 -.142E+0 .164E+0
-.241E-1 -.954E-2
.243E+1 -.143E+0 .132E+0
-.373E-1 -.389E-1
.325E+1 -.149E+0 .115E+0
-.289E-1 -.387E-2
.433E+1 -.145E+0 .118E+0
-.204E-1 .184E-1
.462E+1 -.133E+0 .684E-1
-.211E-1 .178E-1
.577E+1 -.136E+0 .130E+0
-.386E-1 .226E-1
.616E+1 -.137E+0 .635E-1
-.252E-1 .147E-1
.770E+1 -.146E+0 .134E+0
-.356E-1 .527E-2
.821E+1 -.142E+0 .547E-1
-.350E-1 .207E-1
.103E+2 -.144E+0 .116E+0
-.435E-1 .690E-1
.109E+2 -.141E+0 .555E-1
-.395E-1 .406E-1
.137E+2 -.155E+0 .143E+0
-.474E-1 .437E-1
.146E+2 -.136E+0 .398E-1
-.524E-1 .450E-1
.183E+2 -.144E+0 .153E+0
-.595E-1 .675E-1
.195E+2 -.126E+0 .796E-1
-.522E-1 .251E-1
.244E+2 -.112E+0 .151E+0
-.643E-1 .807E-1
.260E+2 -.113E+0 .857E-1
-.576E-1 .448E-1
.325E+2 -.115E+0 .190E+0
-.100E+0 .440E-1
.346E+2 -.118E+0 .108E+0
-.843E-1 .615E-1
.433E+2 -.123E+0 .163E+0
-.105E+0 .146E+0
.462E+2 -.915E-1 .113E+0
-.698E-1 .721E-1
.577E+2 -.102E+0 .189E+0
-.106E+0 .939E-1
.616E+2 -.903E-1 .155E+0
-.928E-1 .820E-1
.770E+2 -.943E-1 .205E+0
-.115E+0 .593E-1
.821E+2 -.101E+0 .942E-1
-.117E+0 .101E+0
.110E+3 -.663E-1 .180E+0
-.185E+0 .144E-1
.137E+3 -.993E-1 .231E+0
-.132E+0 -.187E-1
.146E+3 -.910E-1 .228E+0
-.129E+0 -.313E-1
.195E+3 -.677E-1 .184E+0
-.141E+0 .709E-1
.260E+3 -.145E+0 .208E+0
-.117E+0 .462E-1
.346E+3 -.834E-1 .210E+0
-.278E+0 .127E+0
.462E+3 -.792E-2 .188E+0
-.257E+0 .209E+0
.616E+3 -.261E+0 -.249E+0
-.257E+0 .188E+0
.110E+4 -.298E-1 -.155E+0
-.354E+0 .165E+0

THO 594380. 75820.
.554E+0 .690E-1 .196E+0
-.400E-1 -.772E-1
.739E+0 .111E+0 .267E+0
-.670E-1 -.172E+0
.986E+0 .133E+0 .310E+0
-.473E-1 -.202E+0
.131E+1 .145E+0 .353E+0
.269E-2 -.224E+0
.175E+1 .183E+0 .445E+0
.896E-2 -.248E+0
.234E+1 .229E+0 .483E+0
.272E-1 -.314E+0
.312E+1 .175E+0 .561E+0
.185E+0 -.371E+0
.416E+1 .223E+0 .628E+0
.156E+0 -.403E+0
.443E+1 .144E+0 .632E+0
.133E+0 -.371E+0
.554E+1 .418E-1 .720E+0
.328E+0 -.443E+0
.591E+1 -.102E-1 .692E+0
.209E+0 -.430E+0
.739E+1 -.176E+0 .764E+0
.387E+0 -.503E+0
.789E+1 -.220E+0 .722E+0
.105E+0 -.416E+0
.986E+1 -.406E+0 .813E+0
.200E+0 -.416E+0
.105E+2 -.223E+0 .746E+0
.929E-1 -.353E+0
.131E+2 -.427E+0 .781E+0
.215E+0 -.340E+0
.140E+2 -.207E+0 .696E+0
.202E-1 -.271E+0
.175E+2 -.411E+0 .809E+0
-.135E-1 -.307E+0
.187E+2 -.142E+0 .733E+0
-.167E+0 -.308E+0
.234E+2 .358E+0 .797E+0
-.985E-1 -.204E+0
.249E+2 .144E+0 .746E+0
-.186E+0 -.207E+0
.312E+2 .958E-1 .849E+0
-.311E+0 -.255E+0
.333E+2 .202E+0 .765E+0
-.483E-2 -.122E+0
.416E+2 .252E+0 .848E+0
-.235E+0 -.173E+0
.443E+2 -.176E+0 .845E+0
.146E+0 -.395E-1
.554E+2 .453E-1 .817E+0
-.290E+0 -.606E-1
.591E+2 -.101E+0 .772E+0
.192E+0 -.602E-2
.739E+2 -.398E+0 .800E+0
.107E+0 .944E-1
.789E+2 .339E-2 .676E+0
.264E+0 .117E+0
.105E+3 -.295E+0 .665E+0
.135E+0 .138E+0
.131E+3 -.299E+0 .730E+0
.193E+0 .183E-1
.140E+3 -.454E+0 .597E+0
.174E+0 .651E-1
.187E+3 -.184E+0 .521E+0
-.306E+0 .140E+0
.249E+3 -.462E+0 .411E+0
-.269E+0 .978E-1
.333E+3 -.302E+0 .410E+0
.838E-1 .325E-1
.443E+3 -.152E+0 .406E+0
-.240E+0 -.901E-2
.591E+3 .410E+0 .518E+0
-.426E+0 .604E-2
.105E+4 .518E+0 .454E+0
-.736E-1 .184E+0

BAR 589280. 80050.
.554E+0 .281E+0 .205E+0
.133E-2 -.127E+0
.739E+0 .277E+0 .250E+0
.323E-1 -.199E+0
.986E+0 .253E+0 .316E+0
.479E-1 -.213E+0
.131E+1 .221E+0 .374E+0
.646E-1 -.202E+0
.175E+1 .188E+0 .442E+0
.739E-1 -.204E+0
.234E+1 .156E+0 .509E+0
.885E-1 -.226E+0
.312E+1 .105E+0 .552E+0
.134E+0 -.223E+0
.416E+1 .135E-1 .583E+0
.177E+0 -.229E+0
.443E+1 -.125E+0 .581E+0
.809E-1 -.209E+0
.554E+1 -.203E+0 .602E+0
.148E+0 -.225E+0
.591E+1 -.165E+0 .617E+0
.711E-1 -.241E+0
.739E+1 -.292E+0 .625E+0
.185E+0 -.222E+0
.789E+1 -.257E+0 .624E+0
.812E-1 -.224E+0
.986E+1 -.375E+0 .655E+0
.157E+0 -.203E+0
.105E+2 -.268E+0 .662E+0
.116E+0 -.206E+0
.131E+2 -.320E+0 .668E+0
.120E+0 -.202E+0
.140E+2 -.190E+0 .657E+0
.898E-2 -.195E+0
.175E+2 -.233E+0 .666E+0
-.667E-1 -.154E+0
.187E+2 -.129E+0 .680E+0
-.108E+0 -.168E+0
.234E+2 -.930E-1 .686E+0
-.182E+0 -.146E+0
.249E+2 .118E+0 .701E+0
-.135E+0 -.148E+0
.312E+2 .128E+0 .714E+0
-.175E+0 -.989E-1
.333E+2 .128E+0 .735E+0
-.721E-1 -.520E-1
.416E+2 .190E+0 .738E+0
.138E+0 -.626E-1
.443E+2 .114E+0 .746E+0
-.511E-1 -.300E-1
.554E+2 .219E+0 .722E+0
.336E-1 -.116E-1
.591E+2 -.120E+0 .711E+0
-.802E-1 .123E-1
.739E+2 -.199E+0 .693E+0
-.186E+0 .399E-1
.789E+2 -.568E-2 .626E+0
.185E+0 .486E-1
.105E+3 .321E-1 .641E+0
.252E+0 .119E+0
.131E+3 -.251E+0 .671E+0
-.139E+0 .470E-1
.140E+3 -.270E+0 .657E+0
-.455E-1 .143E+0
.187E+3 .949E-1 .633E+0
-.196E+0 .130E+0
.249E+3 .184E+0 .531E+0
-.111E+0 .152E+0
.333E+3 .109E+0 .454E+0
-.210E+0 .427E-1
.443E+3 .144E+0 .394E+0
-.818E-1 .111E+0
.591E+3 .204E+0 .376E+0
-.104E+0 .229E+0
.105E+4 .189E+0 .236E+0
.220E-1 .154E+0

OYA 596890. 78790.
.554E+0 .464E+0 -.187E+0
-.106E+0 -.738E-1
.739E+0 .216E+0 -.133E-1
-.210E-1 -.276E+0
.986E+0 .162E+0 .921E-1
.248E-1 -.303E+0
.131E+1 .104E+0 .198E+0
.976E-1 -.321E+0
.175E+1 .152E+0 .305E+0
.673E-1 -.389E+0
.234E+1 .135E+0 .370E+0
.141E+0 -.388E+0
.312E+1 .949E-1 .471E+0
.202E+0 -.431E+0
.416E+1 .281E-1 .549E+0
.259E+0 -.447E+0
.443E+1 -.111E+0 .596E+0
.186E+0 -.408E+0
.554E+1 -.191E+0 .614E+0
.277E+0 -.453E+0
.591E+1 -.209E+0 .638E+0
.151E+0 -.453E+0
.739E+1 -.341E+0 .683E+0
.261E+0 -.437E+0
.789E+1 -.300E+0 .686E+0
.867E-1 -.413E+0
.986E+1 -.556E+0 .735E+0
.176E+0 -.355E+0
.105E+2 -.344E+0 .707E+0
.536E-1 -.392E+0
.131E+2 -.557E+0 .746E+0
.168E+0 -.368E+0
.140E+2 -.423E+0 .748E+0
.581E-1 -.367E+0
.175E+2 -.576E+0 .766E+0
.191E+0 -.300E+0
.187E+2 -.421E+0 .776E+0
.170E-1 -.324E+0
.234E+2 -.548E+0 .801E+0
.107E-1 -.296E+0
.249E+2 -.360E+0 .785E+0
-.722E-2 -.229E+0
.312E+2 -.552E+0 .844E+0
.128E+0 -.168E+0
.333E+2 -.443E+0 .835E+0
-.301E-1 -.200E+0
.416E+2 -.644E+0 .809E+0
.113E+0 -.630E-1
.443E+2 -.383E+0 .848E+0
.175E-1 -.197E+0
.554E+2 -.557E+0 .822E+0
.690E-1 -.433E-1
.591E+2 .228E+0 .777E+0
-.125E+0 .198E-1
.739E+2 -.598E+0 .738E+0
.522E-1 -.736E-2
.789E+2 -.246E+0 .761E+0
-.161E+0 .535E-1
.105E+3 -.290E-1 .671E+0
-.352E+0 .272E-1
.131E+3 -.146E+0 .742E+0
.519E+0 .127E-1
.140E+3 -.937E-1 .586E+0
-.286E+0 -.198E-1
.187E+3 .229E+0 .612E+0
-.132E+0 .876E-1
.249E+3 .226E+0 .559E+0
.165E+0 .953E-1
.333E+3 .284E+0 .502E+0
.204E-1 .606E-1
.443E+3 .262E+0 .387E+0
-.973E-1 .678E-1
.591E+3 .290E+0 .376E+0
-.146E-1 .472E-2
.105E+4 .311E+0 .379E+0
.121E+0 .406E-1

REFERENCES

Andrieux, P., Clerc, G. and Tort, P. (1974): Capteur magnétométrique triaxial pour la prospection magnétotellurique artificielle entre 4 Hz et 4 kHz. Rev. Physique Appliquée, **9** : 757-759.

Argand, E. (1911): Les nappes de recouvrement des Alpes Pennines et leurs prolongements structuraux. Matériaux pour la carte géologique de la Suisse. Nouvelle série, **31** : 1-26.

Burkhard, M. (1988): L'Helvétique de la bordure occidentale du massif de l'Aar (évolution tectonique et métamorphique). Eclogae geol. Helv., **81/1** : 63-114.

Egbert, G.D., Booker, J.R. (1986): Robust estimation of geomagnetic transfer functions. Geophys. J. R. astr. Soc., **87** : 173-194.

ERCEUGT-Group (1992): An electrical resistivity crustal section from the Alps to the Baltic Sea (Central Segment of the EGT). Tectonophysics, **207** (1-2): 123-39.

Escher, A., Hunziker, J.C., Marthaler, M., Masson, H., Sartori, M. and Steck, A. (1997): Geologic framework and structural evolution of the Western Swiss-Italian Alps. In: O.A. Pfiffner, P. Lehner, P. Heitzman, S. Mueller and A. Steck (Editors), Results of NRP 20; deep structure of the Swiss Alps. Birkhaeuser Verlag, Basel, pp. 205-221.

Escher, A., Masson, H. and Steck, A. (1988): Coupes géologiques des Alpes occidentales suisses, Service hydrol. et géol. national suisse.

Filloux, J. (1973): Techniques and instrumentation for study of natural electromagnetic induction at sea. Phys. Earth Planet. Inter., **7** : 323-338.

Fischer, G. and Le Quang, B.V. (1981): Topography and minimization of standard deviation in one-dimensional magnetotelluric inversion scheme. Geophys. J. R. astr. Soc., **67** : 279-292.

Glover, P.W.J. and Vine, F.J. (1992): Electrical conductivity of carbon-bearing granulite at raised temperatures and pressures. Nature, **360** : 723-726.

Glover, P.W.J. and Vine, F.J. (1994): Electrical conductivity of the continental crust. Geophys. Res. Let., **21** (22): 2357-60.

Jeanbourquin, P. and Burri, M. (1989): La zone de Sion-Courmayeur dans la région du Simplon, Serv. hydrol. et géol. national suisse.

Jödicke, H. (1992): Water and graphite in the earth's crust - an approach to interpretation of conductivity models. Surveys in Geophysics, **13** : 381-407.

Jones, A.G. (1992): Electrical conductivity of the continental lower crust. In: D.M. Fountain, R.J. Arculus and R.W. Kay (Editors), Continental Lower Crust. Elsevier, pp. 81-143.

Jones, A.G. (1993): Electromagnetic images of modern and ancient subduction zones. Tectonophysics, **219** : 29-45.

Mackie, R.L., Madden, T.R. and Wannamaker, P.E. (1993): Three-dimensional magnetotelluric modeling using difference equations - theory and comparison to integral equation solutions. Geophysics, **58** : 215-226.

Mackie, R.L., Smith, J.T. and Madden, T.R. (1994): Three-dimensional electromagnetic modeling using finite difference equations: the magnetotelluric example. Radio Science : 923-935.

Mancktelow, N. (1992): Neogene lateral extension during convergence in the Central Alps: evidence from interrelated faulting and backfolding around the Simplonpass (Switzerland). Tectonophysics, **215** : 295-317.

Marchant, R. (1993): The Underground of the Western Alps. Mémoires de Géologie Thesis, Université de Lausanne, Lausanne.

Mareschal, M., Fyfe, W.S., Percival, J. and Chan, T. (1992): Grain-boundary graphite in Kapuskasing gneisses and implications for lower-crustal conductivity. Nature, **357** : 674-676.

Mareschal, M., Kellett, R.L., Kurtz, R.D., Ludden, J.N., Ji, S. and Bailey, R.C. (1995): Archean cratonic roots, mantle shear zones and deep electrical anisotropy. Nature, **375** : 134-137.

Masero, W., Fischer, G. and Schnegg, P.-A. (1997): Crustal deformation in the region of the Araguainha impact, Brazil. Phys. Earth Planet. Inter., **101** : 271-289.

Mugnier, J.L., Guellec, S., Ménard, G., Roure, F., Tardy, M. and Vialon, P. (1990): A crustal scale balanced cross-section through the external Alps deduced from the ECORS profile. In: F. Roure, P. Heitzmann and R. Polino (Editors), Deep structure of the Alps. Mém. Soc. géol. suisse, Zürich, pp. 203-216.

Pfiffner, O.A., Lehner, P., Heitzmann, P., Mueller, S. and Steck, A. (1997): Deep Structure of the Swiss Alps, results of the NRP 20. Birkhäuser, Basel, 380 pp.

Schnegg, P.-A. (1993): An Automatic Scheme for 2-D Magnetotelluric Modelling, Based on Low-Order Polynomial Fitting. J. Geomag. Geoelectr., **45** (9): 1039-1043.

Schnegg, P.-A. (1996): Comparison of 2D modelling methods: rapid inversion vs polynomial fitting. In: K. Bahr and A. Junge (Editors), Elektromagnetische Tiefenforschung. Deutsche Geophysikalische Gesellschaft, Burg Ludwigstein, pp. 74-79.

Schnegg, P.-A. (1998): Scheme for 3D MT modelling using polynomials. In: K. Bahr and A. Junge (Editors), Elektromagnetische Tiefenforschung. Deutsche Geophysikalische Gesellschaft, Neustadt a. W.

Stanley, W.D. (1989): Comparison of geoelectric/tectonic models for suture zones in the western U.S.A. and eastern Europe: are black shales a possible source of high conductivities? Phys. Earth Planet. Inter., **53** : 228-238.

Steck, A., Epard, J.L., Escher, A., Marchand, R., Masson, H. and Spring, L. (1989): Coupe tectonique horizontale des Alpes centrales. Mémoires de Géologie (Lausanne), **5** .

Valasek, P., Müller, St. (1997): A 3D crustal model of the Swiss Alps based on an integrated interpretation of seismic refraction and NRP 20 seismic reflection data, Deep structure of the Swiss Alps. Birkhäuser Verlag.

Vozoff, K. (1986): Magnetotelluric Methods. Geophysics reprint series. SEG.

Wehrli, L. (1925): Das Produktive Karbon der Schweizeralpen. Beiträge zur Geologie der Schweiz. Geotechnische Kommission.

Winckler, G., Lutz, R.A. and Orange, D. (1998): Fluid venting in the eastern Aleutian subduction zone. J. Geophys. Res., **103** (B2): 2597-2614

Beiträge zur Geologie der Schweiz
Matériaux pour la Géologie de la Suisse
Contributions to the Geology of Switzerland
Contributi alla Geologia Svizzera

Geophysik - Géophysique - Geophysics - Geofisica

No.		Fr.
1	**H. Röthlisberger.** Zur seismischen und petrographischen Charakterisierung einiger Molassegesteine, einschliesslich der Beschreibung von Methoden der Korngrössenbestimmung in Festmaterial, 91 Seiten, 31 Figuren. 1957	20.-
2	**O. Friedenreich.** Eine grossräumige Widerstandskartierung nordwestlich von Zürich und ihre geologische Deutung. 47 Seiten, 22 Texftiguren, 9 Karten. 1959.	24.-
3	**F. Gassmann.** Schweremessungen in der Umgebung von Zürich. 70 Seiten, 24 Texftiguren, 2 Tafeln. 1962.	30.-
4	**E. Poldini.** Les Anomalies Gravifiques du Canton de Genève. Avec 63 pages, 25 figures et 3 planches. 1963.	30.-
5	**L. Rybach.** Refraktionsseismische Untersuchungen im Raum Aare-, Limmat- und Surbtal. 49 Seiten, 42 Figuren. 1962	20.-
6	**O. Gonet.** Etude gravimétrique de la plaine du Rhône. Région St Maurice - Lac Léman. 50 pages, 30 figures, 2 planches. 1965.	20.-
7	**C. Meyer de Stadelhofen.** Carte des résistivités de la Plaine du Rhône. 8 pages, 2 figures, 2 planches. 1966	10.-
8	**O. Gonet.** *Etude gravimétrique du Lac Léman à bord du mésoscaphe Auguste Piccard. 50 pages, 8 figures,* 1 planche. 1969	10.-
9	**J. -J. Wagner.** Elaboration d'une carte d'anomalie de Bouguer. Etude de la vallée du Rhône de St Maurice à Saxon (Suisse). 91 pages, 32 figures, 2 planches. 1970	27.-
10	**H. Lazreg.** Etude géophysique, géologique et hydrogéologique de la région de Concise à Pompaples (Pied du Jura vaudois). 51 pages, 16 figures, 2 planches. 1971.	27.-
11	**M. Petch.** Contribution à l'étude hydrogéologique de la plaine de l'Orbe. 95 pages, 23 figures, 15 planches. 1970.	27.-
12	**P.-A. Gilliand.** Etude Géoélectrique du Klettgau (Suisse), Canton de Schaffhouse. 85 pages, 47 figures, 10 annexes, 5 planches.1970.	27-
13	**P. Corniche.** Application des méthodes géophysiques à la recherche hydrogéologique. 65 pages, 25 figures. 1973.	27.-
14	**F. Heller.** Magnetische und petrographische Eigenschaften der granitischen Gesteine des Albignagebietes (Nördliches Bergeller Massiv). 66 Seiten, 24 Textfiguren. 1972.	27.-
15	**E. Klingelé.** Contribution à l'étude gravimétrique de la Suisse romande et des régions avoisinantes. 94 pages, 6 figures, 35 planches. 1972.	27.-
16	**W. Sigrist.** Contribution à l'étude géophysique des fonds du Lac Léman. 56 pages, 28 figures, 1 planche. 1974.	27.-
17	**R. Olivier.** Elaboration d'un système de traitement gravimétrique géré par l'ordinateur. Etude gravimétrique du plateau romand de Versoix (GE) à Concise (VD). 56 pages, 21 figures, 10 planches. 1974.	27.-
18	**H. Buchli, R. Paquin, A. Donzé.** Etude géoélectrique et gravimétrique du Chablais entre Anières et Evian. 170 pages, 81 figures, 4 planches. 1976.	38.-
19	**G. Fischer, P.-A. Schnegg, J. Sesiano.** A new geomagnetic survey of Switzerland. 44 pages, 15 figures, 8 tables, 10 cartes. 1979.	34.-
20	**E. Klingelé, R. Olivier.** La nouvelle carte gravimétrique de la Suisse (Anomalies de Bouguer). 96 pages, 9 figures, 4 tables, 1 carte. 1980.	34.-
21	**J.-J. Wagner, St. Müller.** Geomagnetic and gravimetric studies of the Ivrea zone. 64 pages, 44 figures. 1984.	32.-
22	**Ph. Bodmer, L. Rybach.** Geothermal map of Switzerland (Heat flow density). 48 pages, 21 figures, 6 tables. 1984.	42.-
23	**G. Schwarz.** Methodische Entwicklungen zur Aerogammaspektrometrie. 160 Seiten, 56 figuren. 1991.	42.-
24	**U. Schärli, L. Rybach.** Geothermische Detailkartierung der zentralen Nordschweiz (1:100'000). 59 Seiten, *13 Figuren, 2 Karten. 1991.*	48.-
25	**G. Schwarz, E. Klingelé, L. Rybach.** Airborne radiometric mapping in Switzerland. 74 pages, 12 figures, 17 tables, 14 maps, 1992.	48.-
26	**K. Risnes, B. Dumont, R. Olivier & J.-J. Wagner.** Etude des anomalies magnétique et gravimétrique de la région du Chasseral. 42 pages,14 figures et 3 tables.1993.	26.-
27	**G. Fischer, P.-A. Schnegg.** Up-dating the geomagnetic survey of Switzerland. 8 pages, 5 figures, 3 tables, 6 maps. 1994.	30.-
28	**S. Sellami.** Propriétés physiques de roches des Alpes suisses et leur utilisation à l' analyse de la réflectivité de la croûte alpine. 160 pages, 59 figures, 16 tables. 1994.	45.-
29	**E. Rüttener.** Earthquake hazard evaluation for Switzerland. 150 pages, 88 figures, 12 tables, 1995.	45.-
30	**F. Medici, L. Rybach.** Geothermal map of Switzerland 1995 (Heat flow density). 36 pages, 11 figures, 1 table, 1 carte.	55.-
31	**E. Klingelé, M. Cocard, M. Halliday, H.-G. Kahle.** The airborne gravimetric survey of Switzerland. 104 pages, 66 figures, 10 tables, 1996.	55.-

Imprimeries Centrales Neuchâtel S.A. - CH-2001 Neuchâtel
1998